PHYTOCHEMICAL STUDIES ON TRADITIONAL MEDICINAL PLANTS WITH ANTIMALARIAL ACTIVITIES

by Dianne (Tzu-hsiu) Chen

Thesis presented for the Degree of

MASTER OF SCIENCE

in the Department of Chemistry

University of Cape Town

Supervisors: Dr D W Gammon
Mr W E Campbell

March 1997

Abstract

The active antimalarial principles of three traditional medicinal plants, *Passerina obtusifolia* (Thymelaeaceae), *Tetradenia riparia* (Labiatea) and *Xerophyta retinervis* (Velloziaceae) were investigated by employing bioassay guided fractionation. Two novel compounds and five known constituents were isolated from the active fractions of these three plants.

The types of compounds isolated included: three triterpenoids (20(29)-Lupene-3α,28-diol (**30**), 20(29)-Lupene-3α,16β,28-triol (**32**) and 3β-Hydroxy-20(29)-Lupen-28-oic acid (**42**)); two diterpenoids (8-Abietene-7β,13β-diol (**45**) and cariocal (**51**)); one flavonoid (5-Hydroxy-4′,6,7-trimethoxyflavone (**44**)) and one flavonolignan (11-O-acetyl hydnocarpin (**62**)). In addition, one analogue of 7α-hydroxyroyleanone (**41**) (which was previously isolated from *T. riparia* and was found to be the active antimalarial principle of the plant) was prepared.

Flash chromatography and column chromatography techniques were central in the isolation of the compounds. Structural elucidation included the use of HREIMS and various 1D and 2D NMR spectroscopy such as ^{1}H, ^{13}C, COSY, HMQC, HMBC and NOESY spectroscopy. Complete and unambiguous assignments of the ^{1}H and ^{13}C NMR spectra were possible for all the compounds isolated. In addition, antimalarial activity was tested for all the compounds isolated and prepared. IC_{50} values were reported for all these compounds.

Acknowledgements

I would like to thank Dr D.W. Gammon for his interest, guidance and encouragement throughout this project.

Thanks also to Mr W.E. Campbell for all the helpful suggestions, Dr J.J. Nair for all the supports and helpful discussions, Dr B.M. Sehlapelo for valuable suggestions and Dr P. Smith for antimalarial tests on extracts and compounds.

The following people are also gratefully acknowledged:

Dr K. Dimitrova, Ms M. Nair and Mr N. Hendricks in the NMR unit
Mr P. Benincasa for elemental analysis and mass spectra
Dr S. Bourne for x-ray crystal structure determination
The help of Dr P. Boshoff (Cape Technicon) for his high resolution mass spectra and Prof. H. Parolis and Dr L. Parolis (Rhodes University) for their NMR spectra are also gratefully acknowledged.

Special thanks to Devric Dodds for passing on his results to make this project more complete. Thanks also to all those of the steroid research group, specially Anthony and Camielah. Finally, to my parents and my sisters for all their supports.

List of Tables and Figures

page

List of Tables

List of Figures **page**

Appendix

CONTENTS

CHAPTER 1

INTRODUCTION

1.1. Objectives

The objectives of this project were to isolate, purify and identify the active antimalarial principles from the extracts of three traditional medicinal plants: *Passerina obtusifolia*, *Tetradenia riparia* and *Xerophyta retinervis*, using a bioassay guided fractionation procedure.

The rest of the introduction section will be divided into three sections: in the first section, the reasons for studying natural products and in particular those from traditional medicinal plants, as well as the general approach in the search for bioactive plant constituents will be briefly discussed. In the second section, the techniques used in this study for identifying the structure of various compounds isolated from the plants will be briefly discussed with emphasis on the Nuclear Magnetic Resonance (NMR) Spectroscopy and the strategy for analysing the various 1D and 2D NMR spectra in the identification of structure. Finally, in the third section, the disease, malaria, with historical background, the various drugs used as treatment for the disease and the urgency for developing new antimalarial drugs will be discussed. Also, the approaches in the search for new antimalarials in recent years will be demonstrated with examples. In addition, there will be a short summary on the bioassays employed in this study for evaluating the antimalarial activity.

1.2. Traditional Medicine, Plant Natural Products and the Search for New Drugs

The plant kingdom has in the past been referred to as "the sleeping giant of drug development". Chinese medicine makes a great use of natural products with some 5600 plant-derived medicines listed in the Chinese Pharmacopoeia. In India, Ayurvedic, Siddha and Unani medicine is likewise dependent on plants, to the extent of about 2300 species. It has been estimated that about 80 % of the world's population

population rely on various traditional medical systems, all of which use plant-derived remedies. In South Africa, it appears that 70 - 80 % of African people visit traditional doctors on a regular basis and use the locally available herbal preparations prescribed[1].

The plant derived pharmaceuticals that constitute 30 % of prescription drugs used in the western medical systems are obtained from only about 120 plant species. The potential of higher plants as sources for new drugs is still largely unexplored. Among the estimated 250 000 - 500 000 plant species, only a small percentage have been investigated phytochemically and the fraction submitted to biological or pharmacological screening is even smaller[2].

Natural products provide the oldest source for new medicine. Natural selection during evolution and competition between the species, has produced powerful biologically active natural products which can serve as chemical leads, to be refined by the chemist to give more specifically active drugs. For example, moulds and bacteria produce substances that prevent other organisms from growing in their vicinity. The famous *Penicillium* mould led to the considerable range of semisynthetic penicillins, and gave rise to the concept of seeking naturally occurring antibiotics[3].

Another fruitful means of identifying pharmacologically active natural products has been the traditional remedies, which are mainly plant products. The wealth of information from African traditional healers provides a meaningful starting point. It has been shown that plants used in traditional medicine are more likely to yield pharmacologically active compounds: for example, in the field of anticancer activity, a correlation between confirmed biological activity and use in traditional medicine has been demonstrated[4, 5].

The following are a few examples of important medicines that are derived from plants[6]:

1) alkaloids, such as codeine (**1**), for example, which is a common ingredient of syrups used to suppress an irritating cough or of analgesic preparations taken to relieve various aches and pains. This compound is isolated from the opium poppy, *Papaver somniferum*. Morphine (**2**), also from the same plant, is a more potent analgesic than codeine, with additional sedative properties;

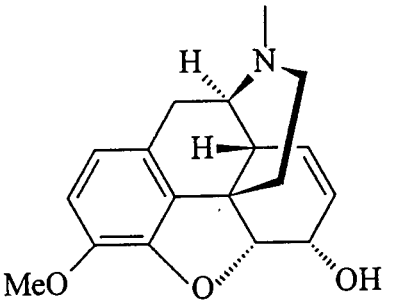

1

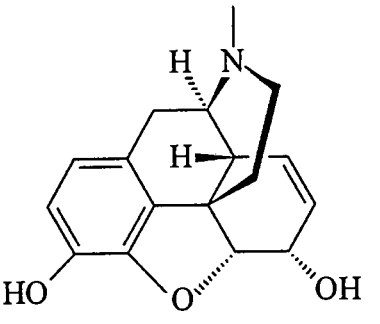

2

2) The steroid diosgenin (**3**), a starting material for the snythesis of the first contraceptive pill, was discovered in wild yams from Mexico and Guatemala. Today, more than 3000 other plants derivatives are used around the world for birth control;

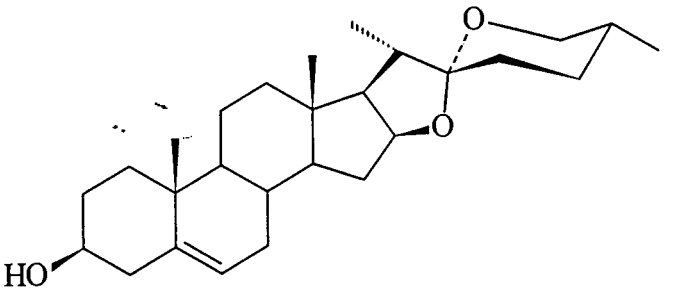

3

3) Reserpine (**4**) has been used as a treatment for hypertension for nearly 30 years in the West but the shrub that produces it has been used in herbal tranquillisers for millennia;

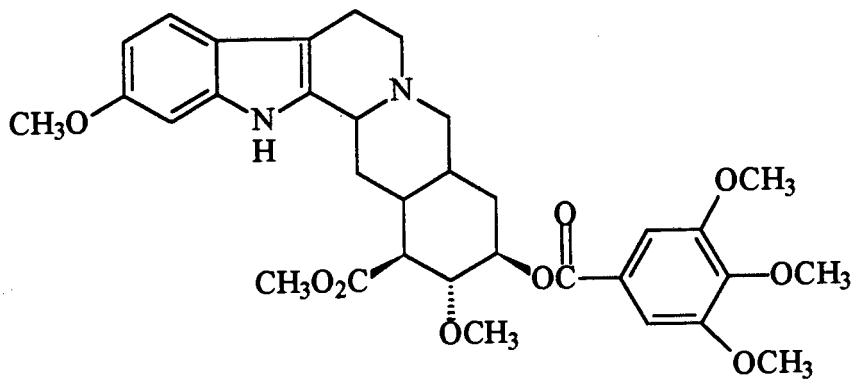

4

4) Sodium cromoglycate (**5**), the active component of Intal, the most commercially successful drug for treating asthma, was developed from substances extracted from a Mediterranean plant used since ancient times for the treatment of colic;

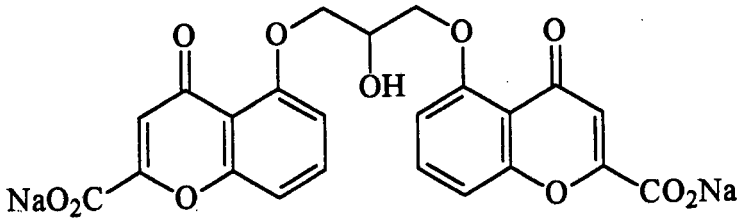

5

5) Pilocarpine (**6**) is an alkaloid which comes from *Pilocarpine jaborandi*. It is used in the treatment of glaucoma;

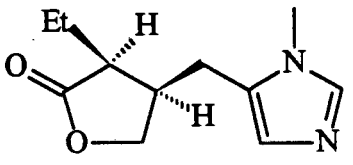

6

6) Nabilone (7) is an antiemetic derived from *Cannabis sativa* (marijuana);

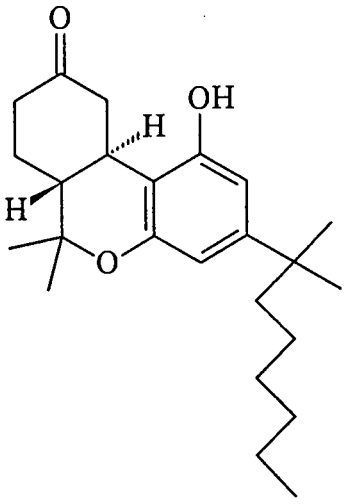

7

7) Quinine (**8**), isolated from an extract of bark of the cinchona tree, was the original treatment for malaria and remains the drug of choice for celebral and other complicated forms of malaria.

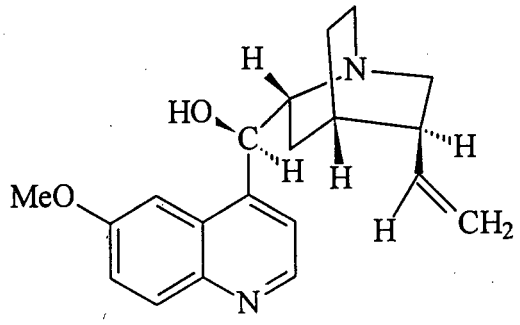

8

Amongst various research efforts in this field, a systematic evaluation of the southern African flora was initiated at Noristan (Pty, Ltd) in 1974 with the aim of isolating and identifying pharmacologically useful compounds. To preserve this rapidly disappearing knowledge, more than 40 000 reports on the medicinal uses of plants have been collected and stored in a computer data base[7].

1.3. Strategy in the Search for Bioactive Plant Constituents

The following steps are normally involved in the process that leads from the plant to a pharmacologically active pure constituent[8]:

1. collection, proper botanical identification and drying of the bio-active plant material: the selection of plants is based on the leads from traditional medicine or information from databases and field work may also be useful;

2. preparation of appropriate extracts in which water, dichloromethane, petroleum ether and ethanol are the solvents commonly used;

3. biological and pharmacological screening of crude extracts in order to identify active extracts for further evaluation;

4. chemical screening of crude extracts by combined analytical techniques such as LC/UV, LC/MS and LC/NMR where available. These hyphenated techniques allow the early recognition of common compounds in the extract and at the same time, the localization of interesting new ones;

5. several consecutive steps of chromatographic separation, where each fraction obtained has to be submitted to bioassay in order to follow the activity (bioassay-guided fractionation);

6. verification of the purity of the isolated compounds;

7. structure elucidation of pure compounds by chemical and physicochemical methods;

8. partial or total synthesis as to confirm structures;

9. preparation of derivatives/analogues for the investigation of structure-activity relationships;

10. large-scale isolation of the pure compound for further pharmacological and toxicological tests.

1.4. Structure Determination

After a plant constituent has been isolated and purified, it should be subjected to various tests in order to determine the class of compound and then to find out which particular compound it is within that class. First of all, its homogeneity must be carefully checked by means of TLC. The class of compound is often obvious from its response to colour tests, its solubility, R_f properties and UV spectral characteristics. Biochemical tests may also be applied.

Other properties of the compound have to be measured in order to identify its structure completely. These properties include melting point (for solid compounds), boiling point (for liquid compounds), $[\alpha]_D$ and R_f. Also, its spectroscopic data, including UV, IR, NMR and MS measurements are useful when compared with those in the literature. A known compound can usually be identified on the above basis. If authentic material is available, direct comparison can be carried out in order to confirm the structure. Otherwise, careful comparison with literature data may be sufficient for its identification. In the case of identifying new compounds, chemical degradation and synthesis can be used to confirm the identification. When a known compound is isolated, it is necessary to confirm the agreement of its spectroscopic assignments with the literature data, particularly where newer high-resolution instruments and techniques allow for unambiguous assignments.

X-ray crystallography has also become widely used in identification of new plant compounds. This technique can be employed when the compound is obtained in sufficient amount and in crystalline form. It is particularly useful in determining the relative, and in some cases absolute stereochemistry of complex natural products[9].

1.4.1. Nuclear Magnetic Resonance Spectroscopy (NMR)

The first commercial NMR spectrometer was made in 1953. Because of the need for higher resolution and sensitivity, 200 - 500 MHz instruments are now routinely used[10], and 800 MHz instruments are also available. NMR spectroscopy is of vital importance in the study of natural products chemistry. By careful investigation of one- and two-dimensional NMR spectra, it is now possible to assign the complete structures of complex molecules based only on NMR. The advantage of NMR spectroscopy is that the sample can be recovered completely and non-destructively after the experiment. With the modern high resolution instruments and techniques, sample amounts of less than 1 mg can produce well defined spectra within reasonable time-spans.

Some of the NMR experiments commonly employed in the study of natural products will be briefly discussed[11,12,13]:

One-Dimensional Techniques

The most widely used nuclei utilized in 1-D NMR spectroscopy in organic chemistry are ^{1}H and ^{13}C. The positions of the signals, i.e. chemical shift δ values, in the 1-D spectra are dependent on the chemical environment of the respective nucleus while spin-spin coupling between neighbouring nuclei gives rise to characteristic splitting of signals, the magnitude of which provides information on connectivities between nuclei and dihedral angles. Therefore the identity of any functional group present can readily be deduced, together with bonding patterns in molecular fragments.

^{13}C NMR spectrometry has been available on a practical basis only since the early 1970's. The ^{12}C nucleus has a spin number (I) of zero, and only the ^{13}C nucleus (I=1/2) can be observed in NMR spectrometry. Since the natural abundance of ^{13}C is only 1.1% that of ^{12}C, NMR experiments involving excitation of ^{13}C nucleus require many more scans in order to obtain a useful spectrum than are necessary in the ^{1}H NMR experiments. Several techniques which enhance the sensitivity of ^{13}C NMR spectrometry are available. One example is the removal of ^{13}C-^{1}H coupling which

simplifies the ^{13}C spectrum and also improves the sensitivity of the nucleus through Nuclear Overhauser Enhancement (NOE).

Trends in chemical shifts (δ) of ^{13}C are somewhat parallel to those of ^{1}H. The ^{13}C shifts are related mainly to hybridization and substituent electronegativity, whereas in ^{1}H NMR spectroscopy, electronegativity (inductive effects), electron delocalization and diamagnetic anisotropy are the main factors to be considered.

The ^{13}C spectrum normally gives better signal separation due to the wider range of chemical shifts involved and the spectrum is also much simpler to interpret. Usually, the total number of carbons present in a molecule can be obtained by simply counting the number of signals in ^{13}C spectrum unless overlapping signals are encountered.

Besides the conventional one-dimensional ^{13}C NMR spectroscopy, a number of multiple pulse experiments which enable distinction between quaternary, tertiary, secondary and primary carbons have been developed. Two of the most commonly used techniques are the APT (Attached Proton Test) and DEPT (Distortionless Enhancement by Polarisation Transfer).

Two-Dimensional Techniques

One-dimensional NMR spectrometry alone can not afford sufficient information for characterising an unknown compound completely. Two-dimensional spectra play an important role in structure elucidation as they yield a large number of spin correlations present within one molecule. Many 2D experiments are available, and a brief discussion will be given for those most frequently used:

COSY (^{1}H-^{1}H Homonuclear Shift Correlation Spectroscopy)

This is the most commonly used 2-D experiment. This experiment yields two 1-D ^{1}H spectra which can be plotted at right angles to each other to give a COSY contour plot. The diagonal of this plot represents the ^{1}H NMR spectrum. Cross-peaks are observed for scalar coupled protons with significant coupling constants. It is therefore possible to trace a spin system and obtain sub-structures. ^{1}H-^{1}H COSY not only provides information for unambiguous ^{1}H NMR assignments but also helps in ^{13}C NMR assignments via ^{1}H-^{13}C COSY spectrum. Other variants of COSY are also useful, for example: the phase sensitive COSY (PS-COSY) is used in establishing remote connectivities, as the COSY cross-peaks display the entire coupling information concerning the protons involved. Double-quantum filtered COSY (DQF-COSY) spectra are used for visualisation of cross-peaks which are close to diagonal. Triple-quantum filtered COSY (TQF-COSY) spectra eliminate all the spin systems that contain less than three or more mutually coupled spins. The shortcoming of COSY is that cross-peaks cannot be seen if the coupling constants between scalar coupled protons are too small (usually less than 1 Hz). Although it is sometimes possible to observe long-range coupling (i.e. W coupling), meta-coupling (in an aromatic ring), and allylic coupling.

NOESY (2D Nuclear Overhauser)

The NOESY experiment is a useful assignment aid which detects NOE's between nearby protons (3Å or closer) in a molecule. Therefore through space relationships can be recognized. This is very useful in confirming the stereochemistry in a complex molecule. In a 2D NOESY spectrum, cross-peaks are observed between proton pairs that are close in space. However, care must be taken when interpreting the results of a NOESY spectrum as due to inappropriate choice of parameters, deceptive results can

be obtained. In addition, NOE peaks are often not observed for rapid tumbling molecules of intermediate size.

COSY and NOESY are both homonuclear correlation techniques as they both only show the relationships between protons in a molecule. Several heteronuclear correlation spectroscopic techniques are available, and a brief discussion to some of these techniques will be given here.

HETCOR (Heteronuclear Correlation Spectroscopy)

It is the ^{13}C-^{1}H correlated spectroscopy which provides connectivities between ^{13}C and ^{1}H signals and therefore allow the number of hydrogen atoms attached to each individual ^{13}C atom to be deduced. In a HETCOR spectrum, cross-peaks are observed between the frequencies of the carbons and their directly attached protons, thus allowing information from one spectrum to help in the assignment of the other spectrum. In the axis where the ^{13}C spectrum is displayed only the protonated carbon signals are detectable.

Long Range HETCOR

The long range HETCOR experiment detects connectivities mediated by two- or three-bond couplings and therefore provides information about the connectivity patterns of protonated carbons and their neighbours.

HMQC (Heteronuclear Multiple Quantum Coherence)

HMQC is equivalent to HETCOR which is the basic ^{13}C-detected heteronuclear correlation experiment. However, HETCOR suffers from the disadvantage of low sensitivity due to the low natural abundance of ^{13}C. HMQC is an inverse-detection 2D NMR technique where heteronuclear chemical shift correlation is achieved via proton detection, therefore requiring a much smaller sample size to produce a useful spectrum within shorter experiment time. Both HETCOR and HMQC experiments

result in a two-dimentional data matrix, where the cross-peaks show correlations between carbon and protons which are linked.

HMBC (Heteronuclear Multiple Bond Correlation)

HMBC is the ^{1}H-detected alternative of Long-Range HETCOR. The contour plot of the 2D matrix obtained shows two-, three- or four-bond correlations between protons and carbons, therefore the linkage positions in a molecule can be determined.

The applications of the above mentioned 1-D and 2-D techniques will be illustrated in the following strategy.

1.4.2. Strategy in NMR Spectroscopic Analysis

The following steps are often involved in the elucidation of structures:

1) the chemical shift data from the ^{1}H and ^{13}C NMR spectra allows the identification of certain functional groups present, and in addition, the number of signals in the ^{13}C spectrum gives the total number of carbons present in the molecule;

2) the DEPT spectrum gives proton-carbon coupling patterns and therefore confirms the pattern of proton substitution;

3) the COSY spectrum aids the analysis of the ^{1}H NMR spectrum from which coupling information reveals through-bond connectivities between protons. Mainly two- and three-bond couplings and occasionally four- or five-bond couplings can be observed, and the magnitude of couplings gives information on the relative spatial orientation of protons. Therefore, the relationship between protonated carbons can be established, this leads to the establishment of spin systems and postulating of sub-structures;

4) the HMQC spectrum reveals one-bond proton-carbon connectivities which leads to the assignment of all the protonated carbons;

5) the HMBC spectrum gives information on two-, three- or four-bond couplings, and therefore confirms the relationships established by the ^{1}H and COSY spectra, the various sub-structures can also be connected by analysing the HMBC spectrum. It is particularly useful in establishing connectivities of protonated carbon atoms to quaternary centres, and the relationship between isolated ^{1}H-^{1}H spin systems in molecules;

6) finally, the NOESY spectrum reveals through space interactions present in a molecule, enabling the assignment of relative stereochemistry.

1.5. Malaria: A Background

Malaria is an infectious disease transmitted by female mosquitoes of the genus *Anopheles*. It is caused by minute parasite protozoa of the genus *Plasmodium*, which infect human and insect hosts alternately[14].

Four species of *Plasmodium* infect man. Three may cause severe illness, as the parasite destroys red blood cells in peripheral capillaries, thus causing anaemia, but are rarely fatal. These are the types of malaria which cause distinctive intermittent fevers, and a patient's temperature chart is a reliable guide to diagnosis. The bouts of fever correspond to the reproductive cycle of the parasite. These three species are: 1. *Plasmodium vivax*; 2. *Plasmodium ovale* and 3. *Plasmodium malariae*. The most dangerous is the fouth species, *Plasmodium falciparum*. In this case, the infected red blood cells become sticky and form clumps in the capillaries of the deep organs of the body and cause microcirculatory arrest. This results in brain delirium, coma and convulsion, and death may ensue within a few days[15].

Plasmodium falciparum is the most common malaria parasite in Africa. It is particularly dangerous to children between the age of one to five, and to travellers from temperate areas. Indigenous adults are protected by a form of partial immunity called premunition, which limits *Plasmodium* multiplication but does not clear the body of parasites: the infected person and the parasite achieve a fragile equilibrium. This develops slowly and only in response to continuous exposure to infection by a specific species of *Plasmodium*.

Malaria exists throughout most of Africa and in a wide range of environments. Transmission of malaria is extremely intensive in Africa with high rates of re-infection and super-infection. In some parts of Tanzania people receive as many as 300 infective bites a year from parasite-carrying mosquitoes[16].

Debilitation, malnutrition, enlargement of the spleen and anaemia are the expected complications of repeated attacks of malaria. The majority of schoolchildren in some endemic areas can be found to have enlargement of the spleen. The risks of chronic malaria are greatest for children, whose growth and development may be seriously and irreversibly impaired. Chronic malaria is more than a threat to individuals, as serious genetic blood disorders increase in populations stressed by endemic malaria. Sickle-cell disease and thalassaemia are the most common.

Malarial Parasite and the Mosquitoes as Vectors

The vital discovery that mosquitoes transmit malaria was made at the end of the nineteenth century. Alphonse Laveran, a young doctor in the French army in Constantine, in Algeria, discovered that the condition is due to members of a family of protozoal parasites named *Plasmodium* which enter red blood corpuscles when in the human blood stream. Later, Sir Patrick Manson, a leading specialist in tropical diseases in London, while working in China, found evidence that this parasite was carried by mosquitoes and that people became infected when bitten. These ideas were confirmed by Ronald Ross, a doctor in the Indian Medical Service, and announced in 1898. In 1902, he received the Nobel prize.

Quinine and Other Quinoline and Acrodine Derivatives as Antimalarial Agents

The first important event in the history of malaria was the discovery of the "Peruvian fever tree", Cinchona. The bark of the Cinchona tree was used in South America by the indigenous people for the treatment of fevers. In the early seventeenth century, an Augustinian monk who had lived in Peru, Father Antonio de la Calancha introduced Cinchona bark into Europe and it proved to be very effective in the treatment of malaria. Cinchona bark must be one of the most successful of all herbal remedies and illustrates the value of traditional medicine. In 1820, Pelletier and Caventou isolated the active antimalarial principle: quinine (**8**), from Cinchona bark and found it to be more potent than the powdered Cinchona bark. The chemical structure of quinine was

elucidated in 1908, and Woodward and Doering achieved the key steps in its total synthesis in 1944[17].

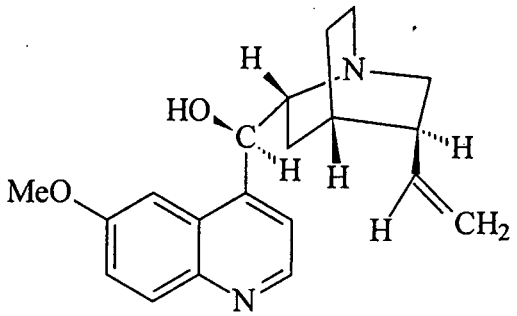

8

All other antimalarials have come from pharmacological research in this century, often stimulated by the medical problems of war. During 1920s a synthetic quinoline derivative, pamaquin (**9**) was found to be more effective than quinine in killing malarial parasite lodged in the liver. Also mepacrine (**10**) was developed as a synthetic alternative to quinine. Further research led to the production of chloroquine (**11**) which has fewer side effects. Primaquine (**12**) is another quinoline derivative with antimalarial activity particularly effective against *P. vivax,* the cause of benign tertian fever. A biquinidine compound proguanil (**13**) also has powerful antimalarial properties but is more generally used as a prophylactic. A pyrimidine derivative, pyrimethamine (**14**), is used for suppression when used alone, for treatment it is used in combination with other antimalarials[15]. Mefloquine (**15**) is another effective synthetic antimalarial compound.

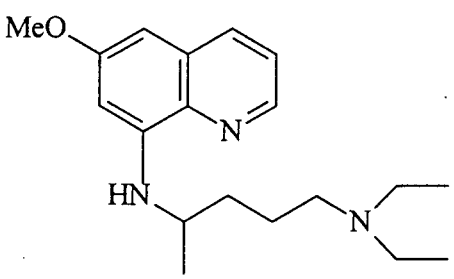

9

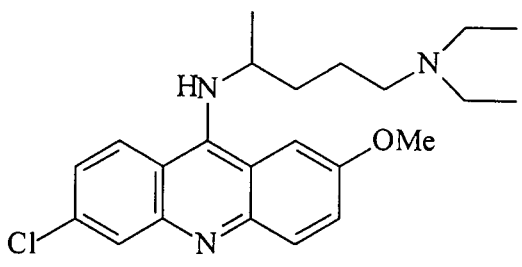

10

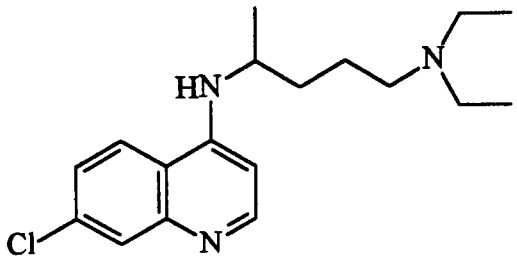

11

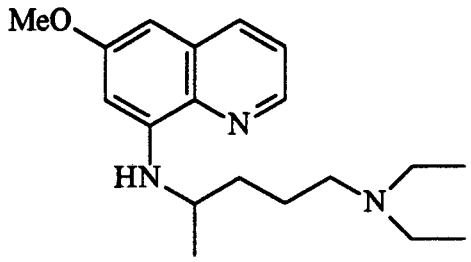

12

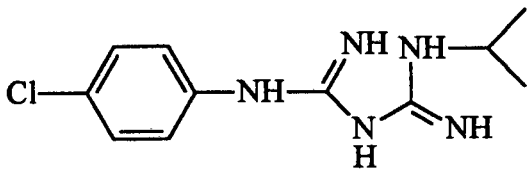

13

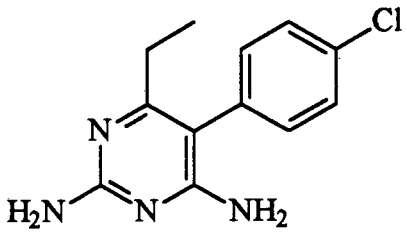

14

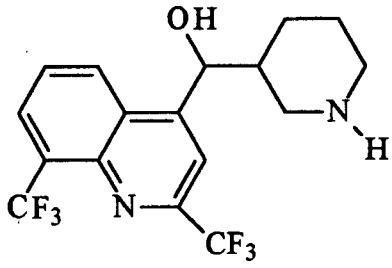

15

During the Second World War only the penicillin project had greater investment than the development of antimalarials. The number of compounds synthesized and tested as antimalarials exceeded a quarter of a million, and at least the same number of compounds has been tested since 1945[14]. Unfortunately, only those mentioned above proved suitable for general use.

Proguanil, pyrimethamine and related drugs act by inhibiting folic acid metabolism much more strongly in the parasite than in the host. The development of the parasite is inhibited by these drugs, which arrest maturation, producing large, non-viable organisms. The effect is exactly the same as folic acid or vitamin B_{12} deficiency has on human erythrocyte maturation. The mechanism of action of other groups of antimalarials is obscure. Chloroquine forms complexes with the heamatin of malaria pigment, causing it to aggregate into coarse granules. Quinine and related drugs cause some clumping of pigment, also producing nuclear and cytoplasmic degeneration. Some of these drugs can interact with *Plasmodium* nucleic acids by intercalation where the drug molecules slide between the stacked bases of the nucleic acid therefore distorting its structure[14].

Most drugs for the treatment of malaria are derivatives of quinoline and acridine, and until recently, there was no alternative chemotherapy. Unfortunately, none of the drugs mentioned above is particularly effective against *P. falciparum*, the most serious form of the infection. Recently, a new lead compound, Artemisinin (**16**), has appeared and early prospects are quite promising.

Artemisinin as Antimalarial Agent

Artemisinin (Qinghaosu in Chinese) is derived from the plant Qinghao, *Artemisia annua* L. (sweet wormwood or annual wormwood), a weedlike plant growing over large parts of China. Qinghao had been used to treat fevers and malaria in China and Vietnam for 2000 years. In the Bencao Gangmu (or "Systematic Materia Medica") it is stated rather concisely that Qinghao "can cure malaria, fever and cold". It was not until 1972 that Chinese scientists isolated the active ingredient in the herb and began research that found it to be extremely effective in treating *P. falciparum*.

The structure of artemisinin, as well as its absolute configuration was determined by X-ray diffraction as **16**.

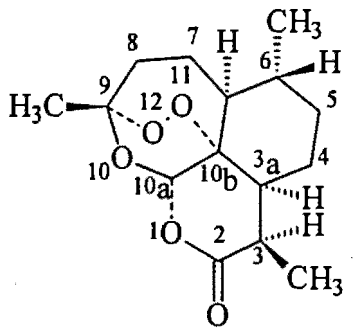

16

The lactone ring has a trans configuration. The most unusual feature of the chemical structure is the 1,2,4-trioxane ring which may also be viewed as a bridging peroxide group. Artemisinin is the only known 1,2,4-trioxane occuring in nature, although compounds with peroxide bridges are common, particularly in marine organisms.

Derivatives of artemisinin are only a couple of years away from widespread use. Artemether (**17**) is an oil-soluble injectable that is currently being produced in France and which was likely to be approved and registered in France and a number of other countries in the near future. The ether derivative, arteether (**18**), is a similar oil-soluble injectable. Arteether is a better antimalarial agent than artemisinin itself and is the form of artemisinin which is also currently under commercial development in the Netherlands under World Health Organization (WHO) guidance. Esters (**19**) are generally as effective as artemisinin but the parent acids are much less so, and this may be a consequence of their lower solubility in lipids. Carbonates (**20**) are the least effective of this group of compounds. Sodium artesunate (the sodium salt of artesunic acid) (**21**) is only slightly less effective than artemisinin *in vitro* and has the advantage of water solubility and can be administered orally however it is said to be showing evidence of toxicity. Other highly effective antimalarial compounds have been obtained by replacing the carbonyl group of artemisinin by a substituted amino group.

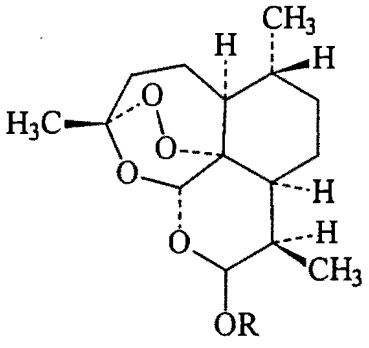

17 R = CH_3

18 R = CH_2CH_3

19 R = COR'

20 R = COOR'

21 R = $OCOCH_2CH_2COONa$

It is almost certain that the crucial structure in artemisinin which gives it its antimalarial activity is the peroxide bridge. Research has been done on modifying other parts of the molecule and it was found that the modified molecules are still active antimalarial agents. Many compounds not obviously related to artemisinin but which contain a peroxide group are antimalarial agents *in vitro* although none is active *in vivo*. This suggests that the remainder of the artemisinin molecule is responsible for the delivery of the drug to the infected erythrocyte in a still active form where it can excercise its toxicity towards malarial parasites.

The action of artemisinin on the malarial parasites appears to be completely different from that of chloroquine and this may be the reason that artemisinin is effective against chloroquine resistant strains of the parasite. Most research suggests that artemisinin acts by an oxidative mechanism and that it affects changes in both red blood cells and the membranes of the malarial parasites. At a molecular level, it is possible that the oxygen-oxygen bond of the peroxide bridge is broken due to an electron transfer with the generation of an oxygen-centred radical (Scheme1). This radical species could be responsible for the destruction of the membranes of the malarial parasites.

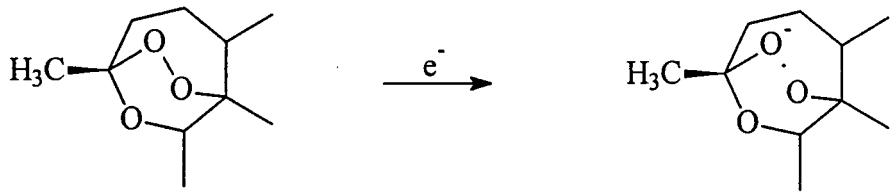

Scheme 1

Shortcomings of artemisinin and its derivatives as antimalarial agents are low solubility in both oil and water. Efficacy by oral administration is poor and administration by injection is a problem in countries where medical facilities are inadequate. Also, there is a high level of recrudescence in treated patients. Therefore, much more work is still waiting to be done in providing the world with a really successful new antimalarial drug[15].

Resistance to Antimalarial Agents

About a decade ago, it was believed that malaria would be successfully eradicated as the insecticide DDT was widely used to successfully eliminate the vector mosquito and the antimalarial drug chloroquine proved effective and relatively inexpensive. In the tropics, chloroquine became a common fixture, although it was sometimes used indiscriminately. In the 1950s, one experiment in Cambodia which was supported by the World Health Organization and the U.S. Agency for International Development (AID), had table salt laced with chloroquine and distributed as a preventive in the Pailin region, one of the most malaria-ridden parts of Indochina. The major resurgence of malaria in that region was due to the outbreak of chloroquine resistant strains of *Plasmodium falciparum*. Resistance to chloroquine was first detected in 1958 in South America and South East Asia. Since then, elsewhere in the world, other strains of the parasite have shown resistance to each successive drug that has been developed to treat the disease. Resistance was first reported from Africa in 1979, from both Kenya and Tanzania. Cambodia is beset by a particularly deadly

strain of the parasite that has proved resistant to all the standard drugs - most likely, as experts said, a result of the earlier experiment in which table salt was laced with chloroquine. The insecticide DDT, although still used in many places, is also losing its effectiveness, as the female Anopheles mosquito, the insects which transmit malaria, are showing resistance to it[16].

Today, fewer tools are available to control malaria than 20 years ago. The parasite adapts to new drugs faster than they can be developed. The parasite develops resistance when it encounters a concentration of a drug that is not potent enough to kill it. This happens when patients fail to take the full course of prescribed treatment or when drugs are used indiscriminately as prophylactics. Therefore in summary, drug resistance results from two factors[14]:

1. The remarkable adaptability of *Plasmodium*;
2. The use of antimalarials for prophylaxis, and for inadequate routine treatment of un-diagnosed fevers in endemic areas.

Although there exist other strategies for malaria prevention, control and erradication, drugs constitute the most convenient and obvious method for the control of malaria. However, up to now there have been only four standard antimalarial drugs available: quinine, chloroquine, mefloquine and halofantrine. All have lost some of their effectiveness, in some cases as much as 50%. Undoubtedly, there is an urgent need for the development of completely new antimalarial drugs and for drugs which may potentiate effects of currently used antimalarials or reverse drug resistance.

The relatively recent discovery of the effective new antimalarial agent artemisinin from extracts of *Artemisia annua* has encouraged the search for other plant-derived compounds which may have similar properties as artemisinin. The importance of artemisinin and its derivatives is that they are believed to act on the parasite in a completely different manner from quinine and its derivatives. The importance of an antimalarial with a completely new mode of action is emphasized by the rapid

development of multi-drug and cross-resistant strains of *Plasmodium falciparum* to quinine and its derivatives. Natural products research has the ability to produce novel compounds with novel modes of action which cannot be achieved by synthetic approach which is currently favoured by pharmaceutical companies.

1.6. Approaches in the Development of New Antimalarial Drugs

Two approaches have been undertaken recently in the development of new antimalarial drugs. One approach is to modify the existing active drugs in ways which retain the antimalarial activity but where the modified drugs are not recognized by the proteins involved in resistance. The other approach is to search for novel compounds with antimalarial activity from medicinal plants or other natural sources. Examples will be illustrated for each approach.

Modifying of the Existing Drugs

Chloroquine had always been a mainstream antimalarial drug, however, due to the development of resistant parasites, it gradually looses its efficacy. By following the approach of modifying drugs, there is interest in this regard in bisquinolines, as the bulky bisquinoline structure may be less efficiently extruded by chloroquine resistant *Plasmodium falciparum*. A number of bisquinolines have been examined. A typical example is piperaquine **(22)** which has shown *in vitro* activity against strains of *P. falciparum*[18] and activity against *P. berghei* in mice and against *P. falciparum* in humans[19]. Bis-(4-amino-7-chloroquinolines) **(23)** which have been synthesized recently, where R is a series of alkane bridges of varying length, were shown to be very effective antimalarial agents with significantly lower resistance index than chloroquine[20]. Another series of bisquinolines **(24)** where the aminoquinoline part of chloroquine is retained and the two units are joined by bisamide links from the carbocyclic ring have been prepared and some antimalarial activity was shown[21].

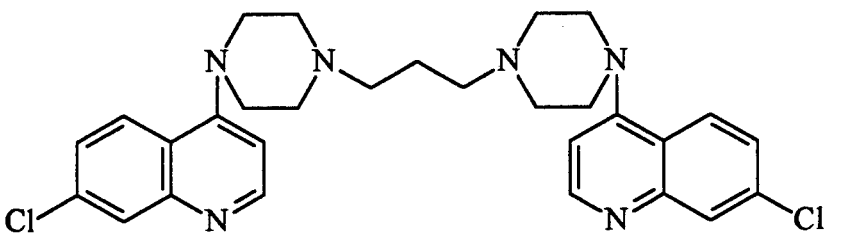

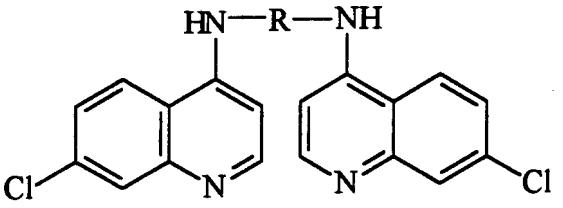

23

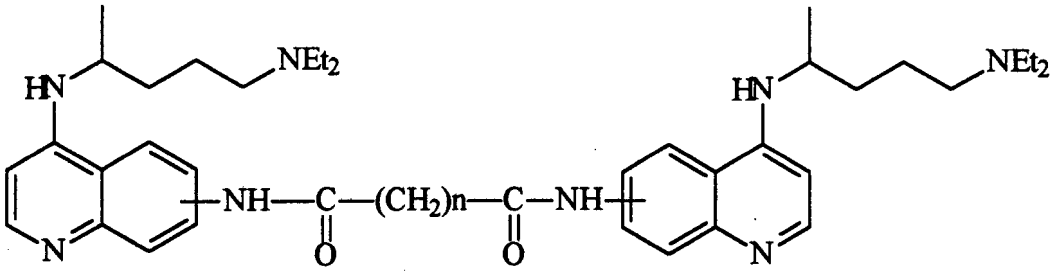

24

Searching for Novel compounds with Antimalarial activity

Two of the mainstay clinically active antimalarial agents, quinine and artemisinin were both originally isolated from plants, and some other classes of compound including the quassinoids and selected limonoids, have demonstrated activity against *Plasmodium falciparum* in culture. Recognizing this potential, many researches have investigated plants for the treatment of malaria or fevers. A comprehensive review on the progress made in the search for antimalarial agents from plants has been published[22]. Some illustrative examples are provided below.

From *Stephania erecta*, (+)-2-N-Methyltelobine (**25**), together with twelve other bisbenzylisoquinoline alkaloids were isolated, which inhibited the growth of cultured *Plasmodium falciparum* strains D-6 and W-2 and displayed nonselective cytotoxicity

with a battery of cultured mammalian cells. However, these bisbenzylisoquinoline alkaloids do not appear to be promising clinical candidates[23].

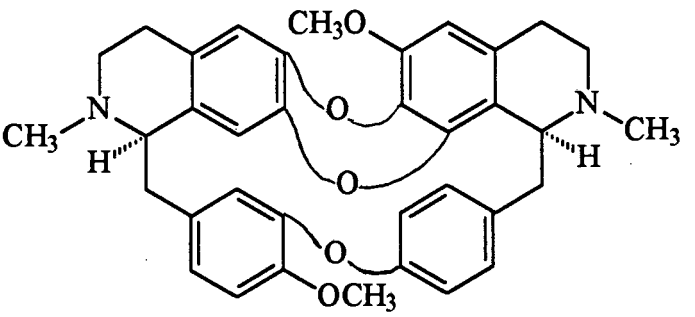

25

The same group of researchers have investigated another plant in the same family, *Stephania pierrei*, after biological evaluation of extracts prepared from the tubers of it revealed cytotoxic and antimalarial activity. Two aporphine alkaloids, (-)-asimilobine-2-O-β-glucoside (**26**) and (-)-nordicentrine (**27**) together with twenty-one isoquinoline alkaloids were isolated.

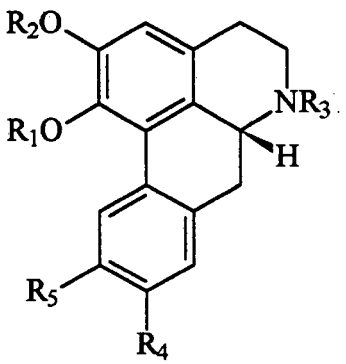

	R_1	R_2	R_3	R_4	R_5
26	Me	Glc	H	H	H
27	$-CH_2-$		H	OMe	OMe

However, none of the isolates showed a degree of selectivity comparable to that of antimalarial drugs such as chloroquine, quinine and artemisinin[24].

Recently, investigation of the two African plants families, the Ancistrocladaceae and the Dioncophyllaceae found that they produce a unique class of natural products: the naphthylisoquinoline alkaloids such as Dioncopeltine A (**28**) and Dioncophylline C (**29**). These compounds consist of a naphthalene and an isoquinoline moiety, linked by a biaryl axis, which due to the steric demand of the two halves, gives rise to restricted rotation and thus to the phenomenon of atropisomerism and axial chirality. Further characteristic structural features are the methyl group at C-3 and the oxygen function at C-8.

One of the presently most exciting biological properties of these alkaloids is their antimalarial activity. Some Ancistrocladus species are used in traditional medicine for the treatment of malaria. Their extracts indeed exhibit high *in vitro* activities against *P. falciparum*, including chloroquine-resistant strains. Compounds **28** and **29** were found to have excellent IC_{50} values (0.021 μg/ml and 0.014 μg/ml respectively)[25].

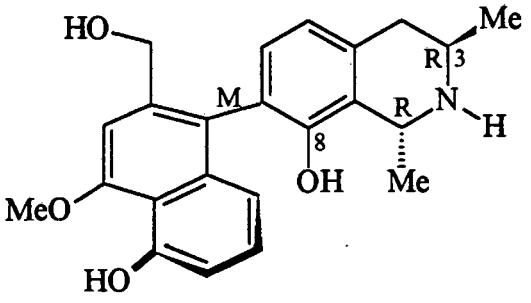

28

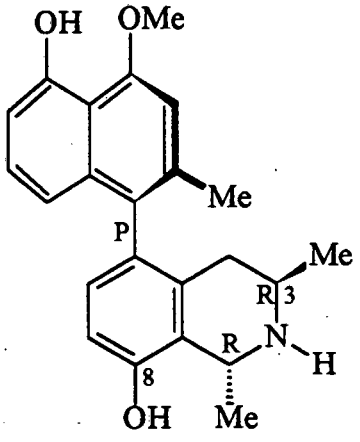

29

1.7. Antimalarial Tests Employed in this Study

Two antimalarial tests were used in this project for evaluating the activity of various extracts and pure compounds. Although the biological details of these two tests are beyond the scope of this project, the basic principles are given briefly as follows:

Parasite Lactate Dehydrogenase Drug Sensitivity Assay

It has been shown that parasite lactate dehydrogenase (pLDH) activity can be distinguished from the host LDH activity using a 3-acetyl pyridine adenine dinucleotide analogue (APAD) of nicotinamide adenine dinucleotide (NADH)[26]. Based on this discovery an enzymatic assay was developed for evaluating antimalarial activity[27]. This method of measuring *P. falciparum* drug sensitivity is based on measuring the parasites survival rate against the various concentrations of drug to which the parasites were exposed. Only living parasites produce APAD and therefore measuring the level of APAD at different drug concentrations is a clear indication of the amount of living parasites.

Parasite LDH can easily be distinguished from host LDH since only parasite LDH converts a substrate, nitroblue tetrazolium to a blue formazan salt. The intensity of this blue formazon salt can be measured spectrophotometrically and is a direct indication of the amount of living parasites.

Inhibition of Tritiated Hypoxanthine Uptake Assay

This assay provides quantitative measurements of the antimalarial activity of compounds. It is based on the inhibition of uptake of a radiolabelled nucleic acid precursor, tritiated hypoxanthine, by the parasites during the short term culture in microtitration plates. The principle of the assay rests on the fact that only living *P. falciparum* parasites have the ability to take up the radiolabelled tritiated hypoxanthine[29, 30].

The effect of a plant extract or compound on the malaria parasites is most conveniently described by the IC_{50} value which is the drug concentration that reduces the density of a culture of parasites to 50 % of the control parasite density.

CHAPTER 2

PASSERINA OBTUSIFOLIA

2.1. Introduction

Passerina obtusifolia belongs to the family Thymelaeaceae. The genus *Passerina* is readily distinguishable from other South African Thymelaeaceae by ericoid leaves with a groove on the upper side lined with hairs, and small wind-pollinated flowers with exerted stamens, dusty pollen and penicillate stigma[30]. In particular, *P. obtusifolia* is an erect shrub up to 2.5 m tall with symmetrically placed leaves and clusters of tiny dark red flowers. It is frequently found in kranses on the Langkloof and the coastal dunes. The flowering season for *P. obtusifolia* is between August to October[31].

P. obtusifolia has been used as a traditional medicine for the treatment of fevers and coughs, although there is no reported literature available on the chemical constituents of the plant. Dried plant material of stems and leaves was supplied by the Department of Pharmacology, UCT.

2.2. Results and Discussion

In order to investigate the antimalarial activity in *P. obtusifolia*, four extracts were prepared:

1. petroleum ether extract of the stems (POSP);
2. ethanol extract of the stems (POSE);
3. petroleum ether extract of the leaves (POLP) and
4. ethanol extract of the leaves (POLE).

The results of *in vitro* tests of activity against *P. falciparum* on these four extracts are summarised in Table 1.

Table 1 The IC_{50} values of the four extracts obtained from *P. obtusifolia*

Extract no.	Extract	IC_{50} (µg/ml)
1	POSP	20 - 40
2	POSE	> 100
3	POLP	> 100
4	POLE	> 1000

It is clear that POSP possessed the highest antimalarial activity, and this fraction was therefore subjected to further fractionation on silica gel columns eluting with petroleum ether and EtOAc. Eleven fractions (fractions A to K) were obtained and the results of the antimalarial test are summarised in Table 2.

Table 2 The IC_{50} values of fractions A to K obtained from the extract POSP

Fraction	IC_{50} (µg/ml)	Fraction	IC_{50} (µg/ml)
A	> 100	G	50 - 100
B	> 100	H	50 - 100
C	> 100	I	> 100
D	> 100	J	10 - 50
E	> 100	K	50 - 100
F	10 - 50		

Fractions F and J were both shown to possess the highest antimalarial activity, and since fraction J was present in larger quantity, it was subjected to further fractionation on silica gel from which two compounds were isolated (compounds **30** and **32**).

2.2.1. Structural Elucidation of Compound 30

Compound **30** was isolated as a white crystalline compound with melting point 210 - 213°C. Analysis of HREIMS, various NMR spectra and literature suggested **30** was a hydroxylated pentacyclic triterpenoid with the structure shown below. This was one of the three related structures encountered in this work, the other two being **32** and **42** described later. Full details of the structural elucidation of **30** are therefore given below to provide a basis for analysis of the other structures.

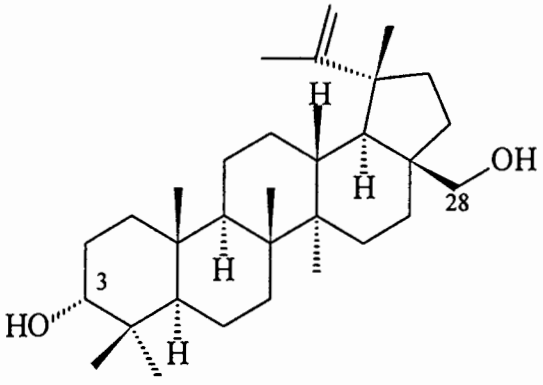

30

HREIMS of **30** showed a molecular ion at m/z = 442.3798, corresponding to the molecular formula $C_{30}H_{50}O_2$, which suggested that **30** is a triterpenoid. A fragmentation peak appeared at m/z = 424 (i.e. $M^+ - H_2O$) indicating that there is at least one hydroxy group present in the molecule. Preliminary analysis of the ^1H NMR spectrum (Appendix, spectrum 1) revealed firstly the presence of 6 methyl groups including one three proton singlet at δ1.67 ppm, which is typical of a vinylic methyl group. Two doublets at δ4.57 and 4.67 ppm, indicated the presence of a terminal methylene group which was shown on the HMBC spectrum to be long range coupled to the vinylic methyl group. Signals in the region δ3.30 to 3.80 ppm integrating for three protons indicated the presence of oxygenated methine or methylene groups. The ^{13}C and DEPT spectra (Appendix, spectra 2 and 3) confirmed the presence of the 6 methyl groups and the terminal olefinic methylene group (δ109.64 and 150.50 ppm), and indicated the presence of one CHOH (δ76.22 ppm) and one CH_2OH group (δ60.55 ppm). The DEPT spectrum also confirmed the presence of, in total, six

methine carbons, 12 methylene carbons, six methyl carbons and, by difference, six quaternary carbons. This was consistent with the presence of the pentacyclic triterpenoid skeleton as shown.

The complete assignment of all the carbon signals, together with all resolved proton signals was possible with the aid of the COSY, HMQC, HMBC and NOESY spectra (Appendix, spectra 4, 5, 6 and 7), and with reference to the literature, in particular the extensive review of ^{13}C data on triterpenoids by Mahato *et. al.*[13]. The correlations observed in the HMBC and NOESY spectra are summarised in Tables 5 and 6 and the most significant of these is discussed below.

As a starting point, the protons in the vicinity of the terminal olefin were readily assignable: from the HMQC spectrum, carbons 20, 29 and 30 could be assigned. The assignment of H-19 (δ2.36 ppm) was confirmed by the HMBC and NOESY spectra: from the HMBC spectrum, H-19 was shown to be long range coupled to C-20, C-29 and C-30 and on the NOESY spectrum, H-19 showed a correlation to H-29a. The shape of the signal for H-19 in the ^{1}H NMR spectrum appeared to be ddd with J = 10.83, 10.83 and 5.87 Hz, which was consistent with two large antiperiplanar (H-19 to H-18 and H-19 to H-21α) and one smaller synclinal (H-19 to H-21β) coupling. From the HMQC spectrum, C-19 could then be assigned to δ47.81 ppm.

From the NOESY spectrum, H-19 showed an NOE to the signal at δ3.32 ppm, which together with the signal at δ3.79 ppm were shown to be doublets and were associated with the same oxygenated carbon at δ60.55 ppm as shown in the HMQC spectrum, indicating that the primary alcohol was at the carbon position 28 and not 27 (from literature, 27-OH and 28-OH are the most commonly occurring in this family of structure).

The HMBC spectrum supported the assignment of the primary alcohol as discussed below: in the HMBC spectrum, H-19 was long range coupled to C-20, C-29, C-30 (which could be readily assigned as discussed above) and the signals at δ48.79 and 30.45 ppm. The signal at δ48.79 ppm was shown by the HMQC spectrum to correlate

with only one proton and confirmed to be a methine carbon by the DEPT spectrum. Therefore, the carbon signal at δ48.79 ppm was assigned to C-18 as it was the closest methine carbon to H-19. Figure 1 shows the sub-structure of rings D and E of the molecule.

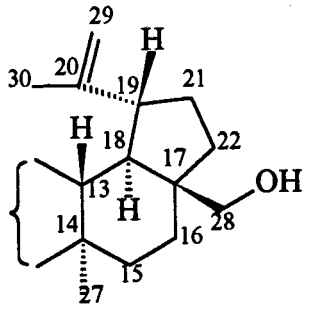

Figure 1

After assigning C-18, H-18 could be easily assigned by the HMQC spectrum to be at δ1.56 ppm. From the HMBC spectrum, H-18 was shown to be long range coupled to the carbon signal at δ60.55 ppm, which is the primary alcohol. This again suggested that the primary alcohol was at the C-28 position as C-27 is too far from H-18 to observe a cross-peak. The assignment of H-18 was also confirmed by the NOESY spectrum where H-18 showed a NOESY to the methyl protons at δ0.99 ppm, which was independently assigned as Me-27 as discussed below.

The methyl groups were then assigned as follows: firstly, the methyl signal at δ0.99 ppm was the only one that did not show NOESY correlation to any of the other methyls, suggesting it was the one at C-27 on the α-face of the molecule. The geminal dimethyl groups, typically at C-4 in triterpenoids, were recognized from the common HMBC correlations observed for signals at δ0.81 and 0.93 ppm, suggesting these were Me-23 and Me-24. Of these two methyl signals, only the signal at δ0.81 ppm showed NOESY connectivity to the methyl signal at δ0.83 ppm, suggesting that these were Me-24 (the β-methyl group at C-4) and Me-25 respectively, and this left the signal at δ0.93 ppm to be assigned as Me-23. Me-25 was in turn correlated to the signal at δ1.01 ppm and this was therefore assigned as Me-26.

These NOESY connectivities are illustrated in Figure 2 below.

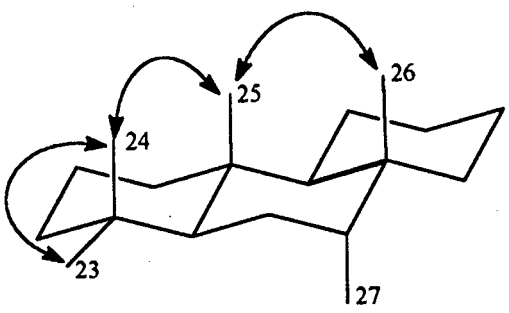

Figure 2

The secondary alcohol was assigned as follows: the proton signal at δ3.37 ppm (which was shown to be associated with the carbon signal at δ76.22 ppm on the HMQC spectrum) showed NOESY correlations to both Me-23 and Me-24, suggesting it was in a gauche relationship to both methyl groups: the proton signal at δ3.37 ppm was therefore concluded to be H-3β. The multiplicity and coupling constant of the signal supported the assignment as it appeared to be a triplet with J = 2.85 Hz, typical of two overlapping vicinal synclinal couplings to adjacent protons (H-3β to H-2α and H-3β to H-2β).

After assigning C-3, C-4, C-18, C-19, C-20, C-28, C-29 and all the methyl groups, the HMQC, HMBC and NOESY spectra were used for the assignment of the methine carbons: C-5 could be identified from the connectivities shown in the HMBC spectrum for Me-23 and Me-24 (C-3, C-4 and C-5); C-13 could be identified from the connectivities shown for Me-27 (C-8, C-13, C-14 and C-15), which also led to the identification of the methylene carbon C-15; C-9 could be identified from the connectivities observed for Me-25 (C-1, C-5, C-9 and C-10), which also led to the identification of the methylene carbon C-1 and the quaternary carbon C-10. C-2 was identified from the connectivities shown for H-1 (C-2 and C-3) and H-3β (C-2 and C-5). The NOESY spectrum confirmed these assignments as Me-26 showed a

correlation to H-13, Me-27 showed a correlation to H-9, H-5 was shown to be correlated to H-1α, and Me-25 and Me-24 were both shown to be correlated to H-2β.

The rest of the carbons were assigned using a combination of the various 2D NMR spectra and the literature data. The complete assignments of the ^{1}H and ^{13}C NMR spectra are shown in Tables 3 and 4.

30, **32** and **42** were found to possess features of the triterpenoid lupeol (**31**).

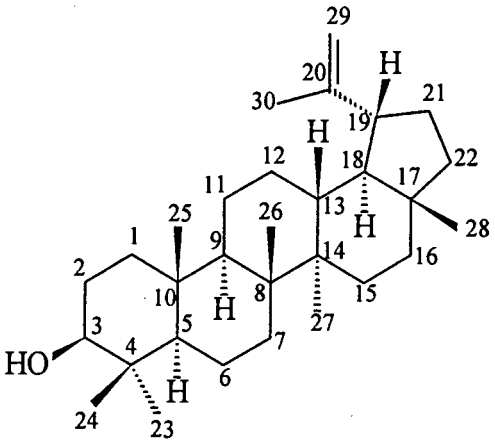

31

Compound **30** was thus concluded to be the known compound epi-betulin[32] (betulin has a β-OH at C-3)[33,34]. Close examination of the literature data for epi-betulin revealed the incomplete assignments of the ^{1}H spectrum and the absence of published ^{13}C NMR data.

Table 3 ^{1}H NMR spectrum assignment of **30**

Proton	δ(ppm), multiplicity* and J(Hz)	Proton	δ(ppm), multiplicity* and J(Hz)
H-1	1.22, 1.37	H-18	1.56
H-2	1.51, 1.92	H-19	2.36, ddd, J = 10.83, 10.83, 5.87 Hz
H-3β	3.37, dd, J = 2.85, 2.85 Hz	H-21	1.39, 1.95
H-5	1.18	H-22	1.02, 1.37
H-6	1.38, 1.39	Me-23	0.93, s
H-7	1.43, 1.84	Me-24	0.81, s
H-9	1.40	Me-25	0.83, s
H-11	1.18, 1.42	Me-26	1.01, s
H-12	1.04, 1.61	Me-27	0.99, s
H-13	1.64	H-28	3.79, d, J = 10.80 Hz; 3.32, d, J = 10.90 Hz
H-15	1.04, 1.69	H-29	4.57, d, J = 1.60 Hz; 4.67, d, J = 1.60 Hz
H-16	1.20, 1.91	Me-30	1.67, s

* indicates multiplets were assumed wherever multiplicities were not stated

Table 4 ^{13}C NMR spectrum assignment of **30**

Carbon	δ(ppm)	Carbon	δ(ppm)
C-1	33.26	C-16	29.20
C-2	25.40	C-17	47.84
C-3	76.22	C-18	48.79
C-4	37.53	C-19	47.81
C-5	49.01	C-20	150.50
C-6	18.26	C-21	30.45
C-7	34.12	C-22	33.98
C-8	41.13	C-23	28.22
C-9	50.19	C-24	22.12
C-10	37.30	C-25	15.90
C-11	20.70	C-26	15.99
C-12	25.22	C-27	14.86
C-13	37.30	C-28	60.55
C-14	42.80	C-29	109.64
C-15	27.01	C-30	19.75

Table 5 HMBC experiment results of **30**

Proton	Connectivities observed	Proton	Connectivities observed
H-1	C-2, C-3	H-22	C-17, C-18
H-2	C-4	Me-23	C-3, C-4, C-5, C-24
H-3β	C-2, C-5	Me-24	C-3, C-4, C-5, C-23
H-5	C-4	Me-25	C-1, C-5, C-9, C-10
H-6	C-5	Me-26	C-7, C-8, C-9, C-14
H-9	C-8, C-10, C-25, C-26	Me-27	C-8, C-13, C-14, C-15
H-16	C-28	H-28	C-16, C-22
H-18	C-13, C-19, C-20, C-28	H-29	C-19, C-30
H-19	C-18, C-20, C-21, C-29, C-30	Me-30	C-19, C-20, C-29
H-21	C-17, C-18, C-19, C-20		

Table 6 lists all the NOESY's observed for **30**. By careful examination of the NOESY spectrum and molecular models, it was possible to distinguish the two diastereotopic protons for all the eleven methylene groups present in the molecule (see Table 6). In particular NOESY's observed for the two diastereotopic protons at C-28 suggested that this methylene group may not experience free rotation. One of the signals (at δ3.79 ppm) showed NOESY's to H-13, H-15β, Me-26 and its geminal partner, whereas the other (at δ3.32 ppm) showed NOESY's to H-19, H-21β and its geminal partner. These results suggested that the signal at δ3.79 ppm was due to $H\text{-}28_R$ and that $H\text{-}28_S$ was at δ3.32 ppm as shown in Figure 3. Also, the two terminal methylene protons at C-29 could be distinguished as H-29a showed NOESY's to H-29b, H-12β and H-19, whereas H-29b showed NOESY's to H-29a and Me-30 only. This suggested that Me-30 was most likely to be anti to H-19. Figure 3 shows the sub-structure of rings D and E of **30** with the various NOESY's observed indicated.

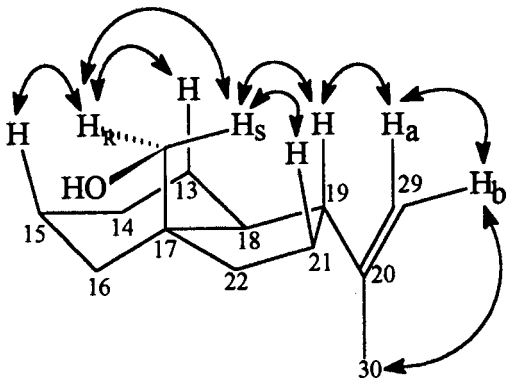

Figure 3

Table 6 NOESY experiment results of **30**

Proton	δ(ppm)	NOESY's observed
H-1α	1.22	H-1β, H-5
H-1β	1.37	H-1α
H-2α	1.51	H-2β
H-2β	1.92	H-2α, H-1β, Me-24, Me-25
H-3β	3.37	H-2α, H-2β, Me-23, Me-24
H-5	1.18	H-1α, H-9, Me-23
H-6α	1.38	H-6β, Me-23
H-6β	1.39	Me-24, Me-25, Me-26
H-7α	1.84	H-15α, Me-27
H-7β	1.43	H-15α
H-9	1.40	H-5, H-12α, Me-27
H-11α	1.42	H-11β, H-12α
H-11β	1.18	H-11α, H-13, Me-25, Me-26
H-12α	1.04	H-12β, Me-27
H-12β	1.61	H-12α, H-13, H-29a
H-13	1.64	H-11β, H-12β, H-19, Me-26
H-15α	1.04	H-15β, H-7β
H-15β	1.69	H-15α, Me-26
H-16α	1.20	H-16β, H-18, H-22α, Me-27
H-16β	1.91	H-16α, H-22β
H-18	1.56	Me-27
H-19	2.36	H-13, H-21β, H-28$_S$, H-29a
H-21α	1.39	H-21β, Me-30
H-21β	1.95	H-21α, H-19, H-28$_S$, H-22β
H-22α	1.02	H-22β, H-18, H-21α
H-22β	1.37	H-22α, H-21β
Me-23	0.93	H-6α, Me-24
Me-24	0.81	H-2β, Me-23, Me-25
Me-25	0.83	H-2β, H-6β, Me-24, Me-26

Table 6 NOESY experiment results of **30**(cont.)

Proton	δ(ppm)	NOESY's observed
Me-26	1.01	H-6β, H-13, H-15β, Me-25
Me-27	0.99	H-9, H-16α
$H\text{-}28_R$	3.79	H-13, H-15β, $H\text{-}28_S$, Me-26
$H\text{-}28_S$	3.32	H-19, H-21β, $H\text{-}28_R$
H-29a	4.67	H-12β, H-19, H-29b
H-29b	4.57	H-29a, Me-30
Me-30	1.67	H-12α, H-29b

2.2.2 Structural Elucidation of Compound 32

Compound **32** was isolated from fraction J as a white crystalline compound with m.p. 215 - 217°C. Analysis results of HREIMS, various 1D and 2D NMR spectra and literature suggested that **32** was a hydroxylated pentacyclic triterpenoid with the structure shown. **32** is one of the three triterpenoids encountered in this study, the other two being **30** and **42**.

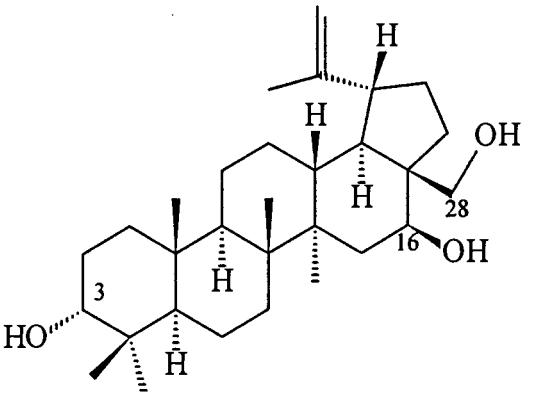

32

HREIMS showed a molecular ion at m/z = 458.3756, which corresponded to the molecular formula $C_{30}H_{50}O_3$ (cal. 458.3760), this suggested that **32** was a triterpenoid. The fragmentation peaks at m/z = 440 (i.e. $M^+ - H_2O$) and 422 ($M^+ - H_2O - H_2O$) indicated that there were at least two hydroxy groups present in the molecule. By comparing the spectroscopic data of **32** with **30**, many similarities were observed, such as the number and chemical shifts of the methyl groups, the presence of a terminal olefinic methylene group and the presence of hydroxyl groups. These led to the conclusion that **32** also possessed a basic lupeol structure (**31**). A full assignment of the ^1H and ^{13}C NMR spectra was carried out in a similar way to that for **30** reported above, and only the significant features of this analysis are reported here.

Examination of the ^{1}H, ^{13}C NMR and the HMQC spectra (Appendix, spectra 8, 9 and 12) of **32** revealed that there were two secondary hydroxyl groups ($^{13}C_{\delta}$ 76.17 and 79.22 ppm) and one primary alcohol ($^{13}C_{\delta}$ 61.18 ppm), confirming that **32** is a triol. The presence of a 3α-hydroxy group was deduced as for **30** from the ^{1}H, HMBC and NOESY data which confirmed a 3β-H at δ3.37 ppm. The presence of a 28-OH was also confirmed by a similar argument to that for **30**. The extra hydroxy group was located at C-16 on the basis of literature data and the HMBC and NOESY spectra (Appendix, spectra 13 and 14), and this and its β-orientation was deduced as follows.

The proton signal at δ3.81 ppm in the ^{1}H NMR spectrum appeared to be dd with J = 11.0 and 4.0 Hz, which implied an axial proton since this would give one large vicinal antiperiplanar coupling and one smaller synclinal coupling. In the HMBC spectrum, the signal at δ3.81 ppm showed long range coupling to C-28; however, there was no NOESY correlation between the signal at δ3.81 ppm and any of the protons on C-28, which suggested that the proton signal at δ3.81 ppm was on the α-face of the molecule. Of the two possible positions, 15α and 16α in ring D, the 16α would be axially oriented and this suggested that the hydroxy group was therefore attatched at C-16 in a β-orientation. This assignment was confirmed by the observation of NOESY correlations between H-16α and Me-27 (methyl groups were assigned by the same strategy as discussed for **30**). The sub-structure for rings D and E of **32** is shown in Figure 4.

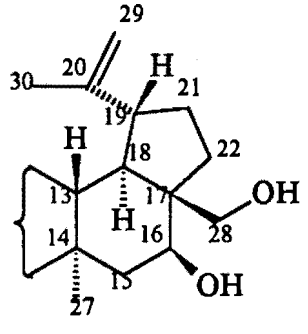

Figure 4

In the NOESY spectrum, H-16α showed further NOESY's to H-15α, H-18 and H-22α. Figure 5 shows the NOESY's observed for H-16α.

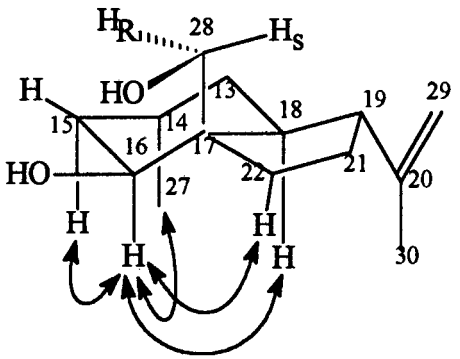

Figure 5

It is interesting to notice that H-18 and H-19 both showed NOESY's to H-29a and Me-30. This implied a free rotation around the C-19 - C-20 bond. Figure 6 illustrates the two alternative orientations for the isopropenyl group with the various NOESY's observed indicated.

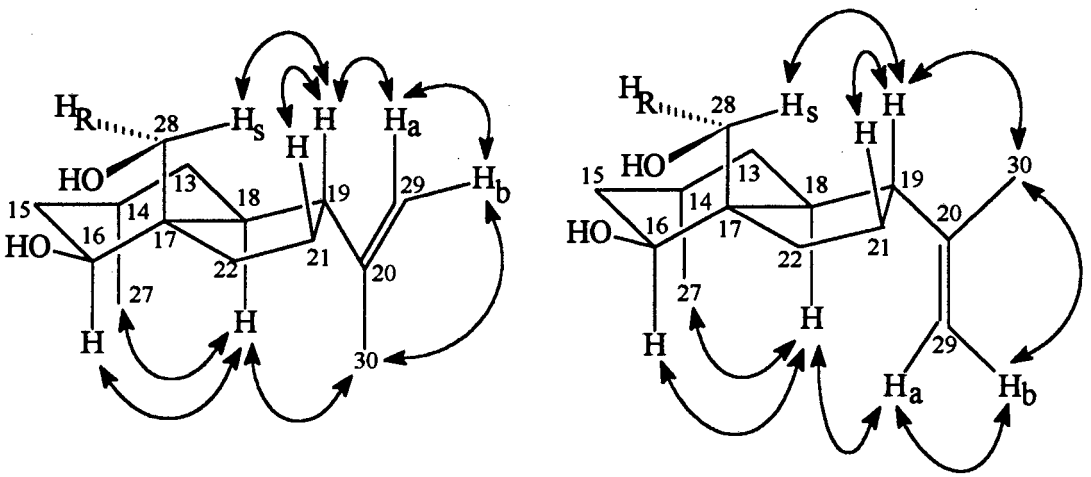

Figure 6

Complete assignment of the ^{1}H and ^{13}C NMR spectra was possible by the aid of the HMQC, HMBC and NOESY spectra. These assignments are shown in Tables 7 and 8, Tables 9 and 10 show the results of the HMBC and NOESY experiments, and it is interesting to notice the almost identical ^{13}C chemical shifts of **30** and **32** for C-1 to C-13 and C-18 to C-30.

Thus, **32** was concluded to be (20)29-lupene-3α,16β,28-triol. This is the first known occurence of this compound, although the epimer, (20)29-lupene-3β,16β,28-triol has been reported before[35, 36].

Table 7 ^{1}H NMR spectrum assignment of **32**

Proton	δ(ppm), multiplicity[#] and J(Hz)	Proton	δ(ppm), multiplicity[#] and J(Hz)
H-1	1.22, 1.37	H-18	1.51
H-2	1.53, 1.92	H-19	2.43, ddd[+]
H-3β	3.37, dd[+]	H-21	1.47, 2.06
H-5	1.20	H-22	1.16, 2.41
H-6	<1.41 >*	Me-23	0.93, s
H-7	< 1.46 >*	Me-24	0.82, s
H-9	1.37	Me-25	0.83, s
H-11	1.16, 1.45	Me-26	1.05, s
H-12	0.97, 1.61	Me-27	1.00, s.
H-13	1.54	H-28	3.37, d[+]
			4.15, d, J = 10.60 Hz
H-15	1.42, 1.86	H-29	4.59, d, J = 1.30 Hz;
			4.68, d, J = 1.30 Hz
H-16	3.81, dd, J = 11.00,	Me-30	1.67, s
	4.00 Hz		

*indicates mean values

[+]indicates multiplicity was deduced from the shape of cross-peaks in the HMQC spectrum and spin coupling considerations as there were peak overlappings in that region and therefore J values were not available

[#] indicates multiplets were assumed wherever mltiplicities were not stated

Table 8 ^{13}C NMR spectrum assignment of **32**

Carbon	δ(ppm)	Carbon	δ(ppm)
C-1	33.30	C-16	79.22
C-2	25.38	C-17	51.42
C-3	76.17	C-18	48.01
C-4	37.53	C-19	47.61
C-5	49.02	C-20	149.62
C-6	18.24	C-21	29.91
C-7	34.11	C-22	32.09
C-8	41.20	C-23	28.22
C-9	49.70	C-24	22.09
C-10	37.25	C-25	16.01*
C-11	20.60	C-26	16.10*
C-12	24.93	C-27	15.90*
C-13	36.59	C-28	61.18
C-14	44.74	C-29	110.01
C-15	37.53	C-30	19.26

* indicates assignments could be interchangeable

Table 9 HMBC experiment results of **32**

Proton	Connectivities observed
H-3β	C-1, C-5
H-5	C-4, C-24
H-9	C-8
H-15(δ1.42 ppm)	C-13, C-14, C-16, C-17, C-27
H-15(δ1.86 ppm)	C-14, C-16, C-27
H-16α	C-28
H-18	C-13, C-19, C-28
H-19	C-13, C-17, C-18, C-21, C-28
H-21	C-19
Me-23	C-4, C-5, C-24
Me-24	C-3, C-4, C-5, C-23
Me-25	C-1, C-3, C-9, C-10
Me-26	C-7, C-8, C-9, C-14
Me-27	C-8, C-13, C-14, C-15
H-28	C-16, C-22
H-29	C-19, C-30
Me-30	C-19, C-20, C-29

Table 10 NOESY experiment results of **32**

Proton	δ(ppm)	NOESY's observed
H-1α	1.22	H-1β, H-9
H-1β	1.37	H-1α
H-2α	1.53	H-2β
H-2β	1.92	H-2α, H-3β, Me-24, Me-25
H-3β	3.37	H-2β, Me-23, Me-24
H-5	1.20	H-9, Me-23
H-6α	1.42	Me-23
H-6β	1.40	Me-23, Me-24, Me-25
H-7α	1.47	H-5, H-9, Me-27
H-7β	1.44	-
H-9	1.37	H-5, H-7α, Me-27
H-11α	1.45	H-11β, H-12α
H-11β	1.16	H-11α, Me-25, Me-26
H-12α	0.97	H-12β
H-12β	1.61	H-12α, H-29a
H-13	1.54	H-19, Me-26
H-15α	1.42	H-15β
H-15β	1.86	H-15α, $H\text{-}28_R$, Me-26
H-16α	3.81	H-15α, H-18, H-22α, Me-27
H-18	1.51	H-16α, H-29a, Me-27, Me-30
H-19	2.43	H-21β, $H\text{-}28_S$, H-29a, Me-30
H-21α	1.47	H-21β, Me-30
H-21β	2.06	H-19, H-21α, H-22β, $H\text{-}28_S$
H-22α	1.16	H-16α, H-18, H-21α, H-22β
H-22β	2.41	H-21β, H-22α
Me-23	0.93	H-3β, H-5, Me-24
Me-24	0.82	H-2β, H-3β, H-6β, Me-23, Me-25
Me-25	0.83	H-2β, H-6β, Me-24, Me-26
Me-26	1.05	H-15β, $H\text{-}28_R$, Me-25

Table 10 NOESY experiment results of **32** (cont.)

Proton	(ppm)	NOESY's observed
Me-27	1.00	H-7α, H-9, H-16α, H-18
$H\text{-}28_R$	4.15	H-13, H-15β, $H\text{-}28_S$, Me-26
$H\text{-}28_S$	3.37	H-19, H-21β, $H\text{-}28_R$
H-29a	4.68	H-18, H-19, H-29b
H-29b	4.59	H-29a, Me-30
Me-30	1.67	H-18, H-21α, H-29b

2.3. Conclusion

Passerina obtusifolia was identified as a potential antimalarial plant on the basis of its traditional usage. Bio-assay-guided fractionation was employed for the isolation of possible antimalarial principle(s). Two triterpenoids (compounds **30** and **32**) were isolated and identified from the active fraction of stems extract of *P. obtusifolia*. The structures of **30** and **32** were deduced from their various 1D and 2D NMR spectra and literature. The ^{1}H and ^{13}C NMR spectra of **30** and **32** were fully assigned by the aid of the COSY, HMQC, HMBC and NOESY spectra. Antimalarial tests showed **30** and **32** to be inactive against malarial parasite *Plasmodium falciparum* (the IC_{50} values for **30** and **32** were >100 and 40 μg/ml respectively).

CHAPTER 3

TETRADENIA RIPARIA

3.1. Introduction

Tetradenia riparia is a deciduous shrub which grows in the shade of other trees and shrubs in dry woods and rocky hillsides. It is easy to propagate when it serves as a garden plant although it cannot withstand frost. The plant loses its leaves in late autumn and flowers bloom soon afterwards[37]. Figures 7 and 8 show the male and female flowers of *Tetradenia riparia*[38]. *Tetradenia riparia* is frequently grown in the Eastern Transvaal and Natal, also to some extent in the Northern Transvaal. It also grows in areas of Zimbabwe, Namibia, Botswana and Swaziland. Several other species grow elsewhere in Africa[39].

In the book " The Medicinal and Poisonous plants of Southern and Eastern Africa" by Watt and Breyer-Brandwijk, it is stated that *Tetradenia riparia* (also known as *Iboza riparia*) possesses many medicinal properties including effectiveness against malaria[40]. Watt and Breyer-Brandwijk describe an infusion of the leaf to be effective against malaria: "the patient taking one dose only at bed-time and is apparently well the next day".

In southern Africa, the Zulu administer an infusion of the leaf for coughs and respiratory troubles. Sometimes it is taken as an emetic to clear the respiratory passages of phlegm. The Lala use an infusion of the young shoots for similar purposes[40]. Githens (in 1949) described how in South Africa the leaf is used as a remedy for diarrhoea and for heamoptysis and is said to contain a volatile oil[41].

Further ethnomedical information and information on the biological activities for extracts of *Tetradenia riparia* has been documented since the first description of the plants and its uses by Watt and Beyer-Brandwijk back in 1939.

Figure 7 Male flowers of *Tetradenia riparia*

Figure 8 Female flowers of *Tetradenia riparia*

Much of the research on *Tetradenia riparia* has been done by van Puyvelde *et. al.* in Rwanda, where it is known under the name Umuravumba. This species is cultivated around almost every house as a remedy against a wide range of illnesses including malaria, diarrhoea and several kinds of fevers and aches[42, 43].

In systematic studies on biologically active substances from medicinal plants of Rwanda, significant chemotherapeutic activity was found in the methanolic extract of *Tetradenia riparia* leaves. Numerous novel compounds have been isolated and identified in *Tetradenia riparia* over the years as well as compounds found in other plants. Some examples are given here: umuravumbolide (**33**), is an α-pyrone isolated in 0.13 % yield from leaf material of *T. riparia*, deacetylumuravumbolide (**34**) was isolated in 0.11 % yield and deacetylboronolide (**35**) was isolated in 0.06 % yield[44]. The search for minor constituents of *T. riparia* resulted in the isolation and structural elucidation of another α-pyrone, 1',2'-dideacetylboronolide (**36**). Three sterols were also isolated: sitosterol (**37**), stigmasterol (**38**) and campesterol (**39**)[45]. A diterpenoid, 8(14),15-sandaracopimaradiene-7α,18-diol (**40**), was isolated from the leaves of *T. riparia*[46] and shown to exhibit significant antimicrobial activity against several bacteria and fungi[47].

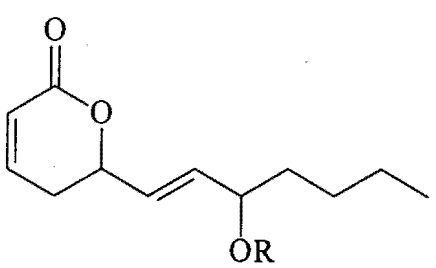

33 R = $COCH_3$

34 R = H

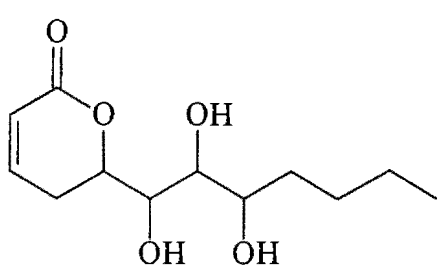

35

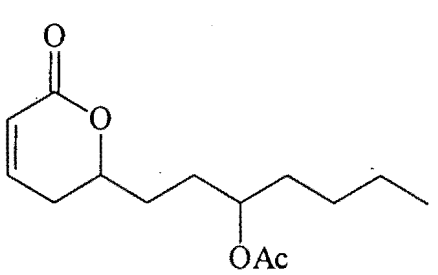

36

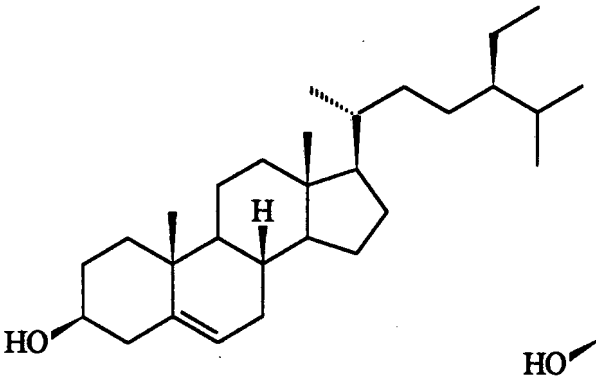

37

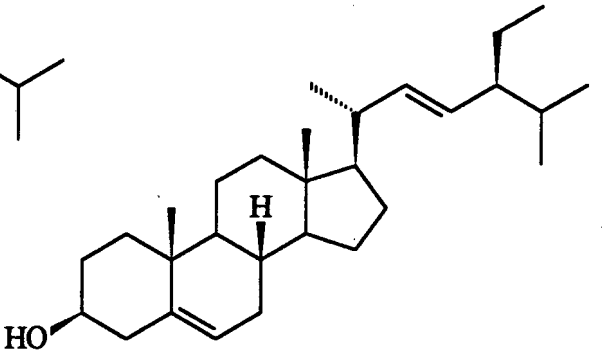

38

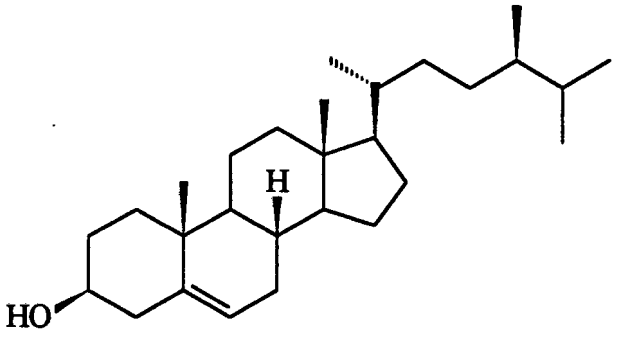

39

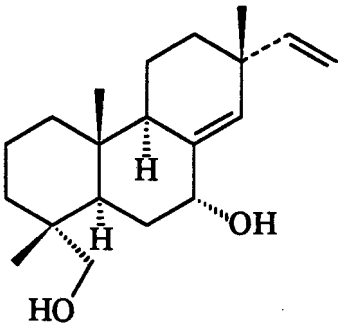

40

Certain references have documented antimalarial activity in *Tetradenia riparia*. In 1988, Hakizamungu *et. al.* performed antimalarial assays on the crude extracts of the leaves of *Tetradenia riparia* and found positive antimalarial activity[48]. Chagnon *et. al.* in 1984 also documented antimalarial activity in *Tetradenia riparia*[49]. However, in spite of these positive results, a detailed examination of the plant extracts and the isolation of possible antimalarial principle(s) had not been pursued until recently.

In a preliminary study initiated in the Department of Pharmacology UCT in 1994[50], the dried plant material of *Tetradenia riparia* was divided into stems, leaves and flowers. Petroleum ether and methanol extracts were prepared for each of these plant parts. Antimalarial tests revealed that the petroleum ether extract of the leaves possessed the

highest activity. This extract was then subjected to fractionation by dry column flash chromatography. From this 29 fractions (fractions A to Zc) were produced and the results of antimalarial tests showed that fractions H and I were the fractions with the highest activity and were both shown by TLC to contain the same compound. This compound was identified as 7α-hydroxyroyleanone (**41**)[51] by MS, IR and NMR spectroscopy. It was found to have an IC_{50} value of 6.9 μg/ml against *P. falciparum in vitro* and showed cytotoxicity with IC_{50} values against WHCO1 and NIH-3T3-MDR 1.41 and 1.51 μg/ml respectively. The other active fractions U and V (IC_{50} values 12.7 and 14.6 μg/ml respectively) were not examined further in the preliminary study and were therefore included in this study in order to complete the analysis of the *T. riparia* extracts. Four compounds were isolated from these two fractions (compounds **42**, **44**, **45** and **51**), and the structural elucidation of these compounds will be presented in this thesis. In addition, a preliminary investigation of the Diels-Alder reactivity of **41** was carried out with a view to preparing analogues for structure-activity studies.

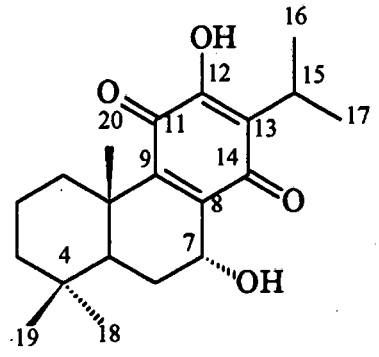

41

3.2 Results and Discussion

3.2.1. Structural Elucidation of Compound 42

Compound **42** was isolated from fraction U as a minor constituent. **42** is an off-white crystalline compound with m.p. 275 - 278°C. Results of HREIMS, various 1D and 2D NMR spectra of **42** and literature data, suggested that **42** is the known compound betulinic acid with the structure shown below. It is one of the three triterpenoids isolated in this study, the other two being **30** and **32**. Full details of the structural elucidation of **30** have been given, therefore only significant differences will be discussed for this compound.

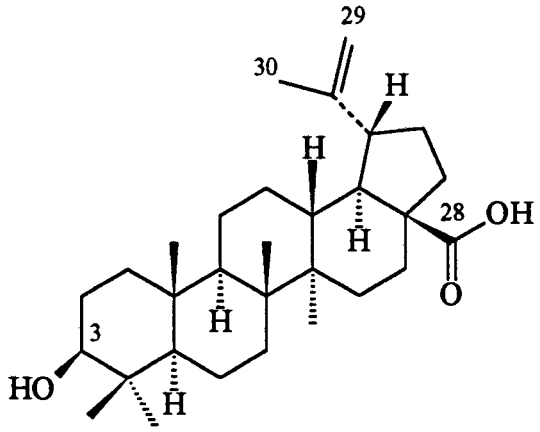

42

HREIMS showed a molecular ion at m/z = 456.3587, which corresponds to the molecular formula $C_{30}H_{48}O_3$ indicating that **42** is a triterpenoid. The ^1H NMR spectrum (Appendix, spectrum 15) of **42** showed a three proton singlet at δ1.68 ppm, which is typical of a vinylic methyl group. Two singlets at δ4.60 and 4.73 ppm were attributed to the terminal methylene protons of an isopropenyl group.

By comparing the spectroscopic data of **42** with literature, it was found that **42** was the known compound betulinic acid which is the C28-COOH product of lupeol (**31**).

A β-OH at C-3 was evident from the dd signal for H-3α at δ3.17 ppm (J = 11.26, 5.04 Hz) in the ^{1}H NMR spectrum, typical of a vicinal antiperiplanar and a vicinal synclinal coupling to adjacent protons. However, on close examination of the HMQC and HMBC spectra (Appendix, spectra 18 and 19) of **42**, some revisions were made on the reported literature data[13].

In particular, the assignments of C-18 and C-19 were found to be reversed on the basis of the following arguments:

In the literature, C-18 and C-19 were assigned to δ46.8 and 49.2 ppm respectively. If these assignments are correct, the HMQC spectrum could identify H-18 and H-19 at δ2.98 and 1.59 ppm respectively. However, H-19 is expected to be further downfield than H-18 as it is an allylic proton. Also, in the ^{1}H NMR spectrum, the multiplicity of the signal at δ2.98 ppm appeared to be a ddd with J = 10.73, 10.73 and 4.40 Hz, this coupling pattern is consistent with two vicinal antiperiplanar (H-19 to H-18 and H-19 to H-21α) and one vicinal synclinal coupling (H-19 to H-21β) to adjacent protons which is typical of H-19 in the lupeol structure (see related compounds **30** and **32**).

In the HMQC spectrum, the shape of the cross-peak for the proton signal at δ1.59 ppm and carbon signal at δ49.31 ppm appeared to be a triplet, which is consistent with an overlapping dd with large coupling, i.e. two vicinal antiperiplanar couplings (H-18 to H-13 and H-18 to H-19) to adjacent protons.

The assignment of C-13 was confirmed by the HMBC spectrum. From the HMBC spectrum, Me-27 (δ0.97 ppm) showed long range couplings to carbon signals at δ40.73, 38.39, 42.47 and 29.71 ppm. The carbon signals at δ40.73 and 42.47 ppm were found to be quaternary carbons from the HMQC spectrum and the carbon signal at δ29.71 ppm was found to be a methylene carbon, whereas the carbon signal at

δ38.39 ppm was found to be a methine carbon. This led the carbon signal at δ38.39 ppm to be assigned to C-13 as it was the closest methine carbon to Me-27. From the HMQC spectrum, H-13 could be found to be at δ2.20 ppm which was a ddd with J = 12.10, 12.10 and 3.06 Hz consistent with two vicinal antiperiplanar (H-13 to H-12α and H-13 to H-18) and one vicinal synclinal coupling to the adjacent protons. The COSY spectrum (Appendix, spectrum 17) gave another indication for the assignment of H-18 as the signal at δ2.20 ppm (H-13) showed a correlation to the signal at δ1.59 ppm (H-18), which correlated to the carbon signal at δ49.31 ppm in the HMQC spectrum.

The HMBC spectrum supported the revised assignments for C-18 and C-19 as the proton at δ1.59 (H-18) showed long range couplings to C-13, C-17, C-19, C-20 and C-28.

Figure 9 shows the sub-structure of rings D and E for **42**.

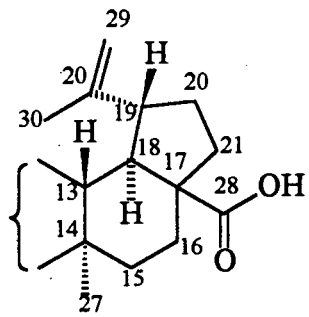

Figure 9

Similarly, the assignments of C-15 and C-21 were found to be reversed in the literature as discussed below.

In the HMBC spectrum, Me-27 (δ0.97 ppm) showed long range coupling to the carbon signals at δ40.73, 38.39 (C-13), 42.47 and 29.71 ppm. The carbon signal at δ29.71 ppm appeared to be a methylene carbon from the HMQC spectrum, which was

most likely to be C-15 rather than the literature assignment, C-21, as a seven bond correlation would be required in the latter case.

C-16 was assigned to δ32.15 ppm on the basis of the literature data. From the HMQC spectrum, the H-16 protons could be assigned to δ1.44 and 2.26 ppm. In the COSY spectrum, the proton signal at δ2.26 ppm showed cross-peaks with the protons at δ1.44, 1.52 and 1.19 ppm. The latter two proton signals were found to be associated with the carbon signal at δ29.71 ppm in the HMQC spectrum. Therefore C-15 was reassigned to δ29.71 ppm.

C-22 was assigned on the basis of the literature data to δ37.01 ppm. From the HMQC spectrum, the H-22 protons could be found to be at δ1.46 and 1.96 ppm. In the COSY spectrum, the proton signal at δ1.96 ppm showed correlations to the proton signals at δ1.46, 1.98 and 1.41 ppm. The latter two protons were found to be associated with the carbon signal at δ30.56 ppm in the HMQC spectrum. Therefore, C-21 was reassigned to δ30.56 ppm. The down field signals of the H-21 and H-22 protons (δ1.98 and 1.96 ppm respectively) could be assigned as H-21β and H-22β on the basis of the carboxylic acid at C-28 causing a deshielding effect on the neighbouring protons.

The only direct evidence from the NMR spectra recorded to confirm the location of the carboxyl group at C-28 was the long range coupling of H-18 to the carboxyl carbon shown by the HMBC spectrum.

The full and revised assignments of ^{1}H and ^{13}C NMR spectra are shown in Table 11 and 12 respectively. The literature data for ^{13}C NMR chemical shifts of betulinic acid was listed for comparison. Table 13 lists the results observed for HMBC experiment.

Recent investigations have revealed interesting bioactivities of betulinic acid. For example, it has been shown to have melanoma specific cytotoxicity *in vivo*. As a result, the compound is undergoing preclinical evaluation for the treatment or

prevention of malignant melanoma. Betulinic acid has also been found to have promising anti-HIV activity, whereby the compound inhibits HIV replication[52,53].

Table 11 ^{1}H NMR spectrum assignment of **42**

Proton	δ(ppm), multiplicity# and J(Hz)	Proton	δ(ppm), multiplicity# and J(Hz)
H-1	0.90, 1.67	H-18	1.59
H-2	<1.58 >*	H-19	2.98, ddd, J = 10.73, 10.73, 4.40 Hz
H-3α	3.17, dd, J = 11.26, 5.04 Hz	H-21	1.41*, 1.98
H-5	0.68	H-22	1.46, 1.96
H-6	1.37, 1.52	Me-23	0.96, s
H-7	<1.37 >*	Me-24	0.75, s
H-9	1.26	Me-25	0.82, s
H-11	1.22, 1.41	Me-26	0.93, s
H-12	1.03, 1.69	Me-27	0.97, s
H-13	2.20, ddd, J = 12.10, 12.10, 3.06 Hz	H-29	4.60, d, J = 1.65 Hz; 4.73, d, J = 1.65 Hz
H-15	1.19*, 1.52*	Me-30	1.68, s
H-16	1.44*, 2.26		

* indicates mean values

# indicates multiplets were assumed wherever multiplicities were not stated

Table 12 ^{13}C NMR spectrum assignment of **42** (in ppm) and literature data

Carbon	**42**	Literature data	Carbon	**42**	Literature data
C-1	38.75	38.7	C-16	32.15	32.1
C-2	27.41	27.4	C-17	56.22	56.3
C-3	78.97	78.9	C-18	49.31	46.8
C-4	38.87	38.8	C-19	46.87	49.2
C-5	55.39	55.3	C-20	150.38	150.3
C-6	18.31	18.3	C-21	30.56	29.7
C-7	34.37	34.3	C-22	37.01	37.0
C-8	40.73	40.7	C-23	27.99	27.9
C-9	50.57	50.5	C-24	15.34	15.3
C-10	37.23	37.2	C-25	16.04	16.0
C-11	20.88	20.8	C-26	16.13	16.1
C-12	25.54	25.5	C-27	14.71	14.7
C-13	38.39	38.4	C-28	179.80	180.5
C-14	42.47	42.4	C-29	109.69	109.6
C-15	29.71	30.5	C-30	19.39	19.4

Table 13 HMBC experiment results of **42**

Proton	Connectivities observed
H-1	C-25
H-5	C-25
H-9	C-26
H-18	C-13, C-17, C-19, C-20, C-28
H-21	C-19
H-22	C-18
Me-23	C-3, C-4, C-5, C-24
Me-24	C-3, C-4, C-5, C-23
Me-25	C-1, C-5, C-9, C-10
Me-26	C-7, C-8, C-9, C-14
Me-27	C-8, C-13, C-14, C-15
H-29	C-19, C-30
Me-30	C-19, C-20, C-29

3.2.2. Structural Elucidation of Compound 44

Compound **44** was isolated from both fractions U and V as a yellow crystalline compound with m.p. 186 - 188°C. The MS of **44** showed a molecular ion at m/z = 328. The ^{1}H NMR spectrum of **44** (Appendix, spectrum 20) appeared to be very simple: 3 singlet methoxy methyl groups were observed at δ3.88, 3.91 and 3.96 ppm, 6 aromatic protons in the region δ6.50 - 7.90 ppm including. an AA'BB' system at δ7.00 and 7.83 ppm (J = 9.00 Hz) and 2 singlets at δ6.53 and 6.57 ppm. The ^{13}C NMR spectrum of **44** (Appendix, spectrum 21) showed 18 peaks including two signals with high intensities, suggesting overlapping of the carbon resonances in each. Together, the MS and ^{1}H NMR data indicated a molecular formula $C_{18}H_{16}O_5$. The UV spectrum of **44** displayed λ_{max} 216 nm, typical of a flavonoid.

From the ^{1}H, ^{13}C, UV and the bright yellow colour of **44**, it was suspected to be a flavone.

From the literature, a compound called cirsimaritin (**43**) which was isolated previously from *Drymis Winteri*[54] was found to be closely related to **44**.

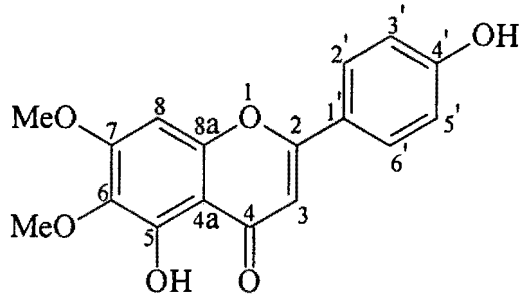

43

Close examination showed that **44** was the known compound salvigenin[55] (5-Hydroxy-4′,6,7-trimethoxyflavone) on the following arguments:

The aromatic AA′BB′ system at δ7.83 and 7.00 ppm, both have J = 9.00 Hz, were each integrated for two protons and shown to be correlated to each other in the COSY spectrum (Appendix, spectrum 22), suggesting they were two chemically equivalent pairs of protons which could be assigned to H-2′/6′ and H-3′/5′. From the NOESY spectrum (Appendix, spectrum 24), the signal at δ7.00 ppm showed a correlation to the methoxy signal at δ3.88 ppm, suggesting the position of this methoxy group was at C-4′ and the proton signal at δ7.00 ppm was assigned H-3′/5′. This left the proton signal at δ7.83 ppm to be assigned to H-2′/6′.

The singlets at δ6.53 and 6.57 ppm showed no correlation to each other nor to any of the other proton signals in the COSY spectrum. The very deshielded -OH singlet at δ12.76 ppm suggested strong hydrogen bonding to the C-4 carbonyl group, thus placing the -OH at C-5. On the NOESY spectrum, the proton signal at δ6.57 ppm showed a correlation to the proton signal at δ7.83 ppm which was assigned H-2′/6. Therefore the proton signal at δ6.57 ppm was assigned H-3 and this left the proton signal at δ6.53 ppm to be assigned H-8. Methoxyls with at least one hydrogen in the *ortho* position resonate at δ55 ppm while those without any *ortho* proton neighbours resonate at δ60 ppm. Hence, from the HETCOR spectrum (Appendix, spectrum 23) the methoxyl signal at δ3.91 ppm (with carbon signal at δ59.90 ppm) was assigned 6-OMe while the one at δ3.96 ppm (with carbon signal at δ56.30 ppm) was assigned as 7-OMe.

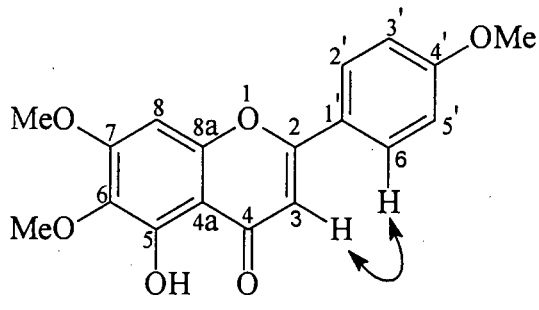

44

Table 14 and 15 show the ^{1}H and ^{13}C NMR spectra assignment of **44**. The ^{13}C NMR spectrum assignments were based on those reported for cirsimaritin[56].

Table 14 ^{1}H NMR spectrum assignment of **44**

Proton	δ(ppm), multiplicity and J(Hz)	Proton	δ(ppm), multiplicity and J(Hz)
H-3	6.57, s	4′-OMe	3.88, s
H-8	6.53, s	6-OMe	3.91, s
H-2′/6′	7.83, d, J = 9.00 Hz	7-OMe	3.96, s
H-3′/5′	7.00, d, J = 9.00 Hz	5-OH	12.76,s

Table 15 ^{13}C NMR spectrum assignment of **44**

Carbon	δ(ppm)	Carbon	δ(ppm)
C-2	164.00	C-8a	153.00
C-3	104.14	C-1′	123.57
C-4	182.66	C-2′/6′	128.00
C-4a	106.14	C-3′/5′	114.51
C-5	153.22	C-4′	162.60
C-6	132.63	OMe-4′	55.54
C-7	158.71	OMe-6	59.90
C-8	99.55	OMe-7	56.30

3.2.3. Structural Educidation of Compound 45

Compound **45** was isolated from fraction V as a white crystalline compound with m.p. 147 - 150°C. By comparing the spectroscopic data of **45** to that of those compounds which had been isolated previously from *Tetradenia riparia*, it was concluded that **45** is the known compound Ibozol[57]. Details of the structural elucidation is given below.

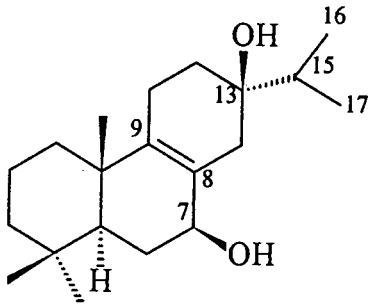

45

MS showed a molecular ion at m/z = 306. The ^{1}H NMR spectrum (Appendix, spectrum 25) revealed the presence of 5 methyl groups including three singlets (δ0.86, 0.88 and 1.05 ppm) and two 3-proton doublets at δ0.91 and 0.93 ppm with J = 1.29 and 1.39 Hz respectively, indicating the presence of an isopropyl group. A carbinol methine signal at δ4.00 ppm accounted for a secondary hydroxyl group. The ^{13}C NMR spectrum (Appendix, spectrum 26) confirmed the presence of the secondary hydroxyl group as a signal at δ72.18 ppm was observed. The other signal at δ72.11 ppm suggested the presence of a tertiary hydroxyl group. In addition, two signals at 126.76 and 141.76 ppm indicated the presence of a double bond. However, from the ^{1}H NMR spectrum, there was no vinyl proton observed and therefore the double bond was tetrasubstituted. In the region δ1.00 - 2.50 ppm, there were many overlapping CH and CH_2 signals. Twenty carbon signals were detected in the ^{13}C spectrum which suggested that **45** is a diterpenoid, and together with MS and ^{1}H NMR data, a molecular formula of $C_{20}H_{34}O_2$ was deduced. From these results an abietane skeleton **46** was inferred. The structure of this compound was deduced as follows:

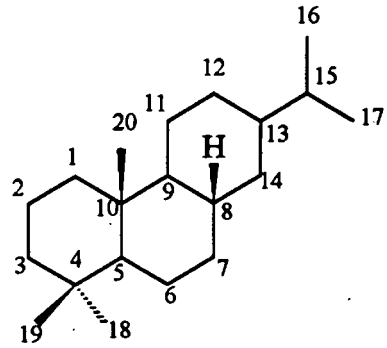

46

The geminal dimethyl groups at C-4 were recognized from the common HMBC correlations observed (see Appendix, spectrum 28) for methyl signals at δ0.86 and 0.88 ppm, and these two signals were therefore assigned as Me-18 and Me-19. Me-18 and Me-19 were shown on the HMBC spectrum to be correlated to the carbon signals at δ41.39, 33.02 and 49.63 ppm, which were found to be a methylene carbon, a quaternary carbon and a methine carbon respectively on the HMQC spectrum (Appendix, spectrum 27). These three carbon signals were assigned to C-3, C-4 and C-5 respectively. The other methyl singlet at δ1.05 ppm could then be assigned to Me-20. From the HMBC spectrum, Me-20 was shown to be correlated to the signals at δ37.05 (a methylene carbon), 141.76 (a quaternary carbon), 38.40 (a quaternary carbon) and C-5, and therefore the double bond could be placed at C-8 and C-9, which were assigned at δ126.76 and 141.76 ppm respectively. Also, C-1 and C-10 could be assigned at δ37.05 and 38.40 ppm respectively.

H-5 showed long-range coupling to C-1, C-4, C-10 and the carbon signals at δ30.06 (a methylene carbon) and 72.18 ppm (the carbinol methine carbon). The signal at δ72.18 ppm was further correlated to C-8 and C-9, this confirmed that the secondary hydroxyl group was most likely to be at C-7. Therefore C-6 and C-7 were assigned at δ30.06 and 72.18 ppm respectively.

In an abietane skeleton, the isopropyl group is typically found at C-13, and the tertiary hydroxyl group was located at C-13 on this basis. C-13, C-15, C-16 and C-17 could be assigned from the cross-peaks observed for Me-16 and Me-17 in the HMBC

spectrum. C-14 could be readily assigned from the HMQC spectrum as the two H-14's were shown to be simple doublets with J_{gem} = 16.67 Hz. C-11 and C-12 could then be assigned from the correlations observed on the HMBC spectrum for H-14.

However, close examination of the literature data revealed the incomplete assignment of the ^{1}H NMR spectrum and some uncertainty about the stereochemistry at C-13. In the literature[57] this was assigned on the basis of comparison of ^{13}C spectral data with that of related structures **47** and **50**, as well as from conformational considerations. Details of the argument presented by these authors are summarised as follows:

The authors first noted that an analysis of the pimaradienes (**47**) suggested that irrespective of the stereochemistry at C-13, ring C adopted a half-chair conformation **48** rather than the alternative **49**. This was deduced *inter alia* from the difference in the ^{13}C chemical shifts for the methyl carbons C-17 in **47a** and **47b** (δ23.5 and 28.2 ppm respective), implying that the one was pseudo-axial and the other pseudo-equatorial. They assumed that this conformation was favoured as it minimizes non-bonded hydrogen interactions between H-1β and H-11β, H-1β and H-11α also C-20 and H-11β[58].

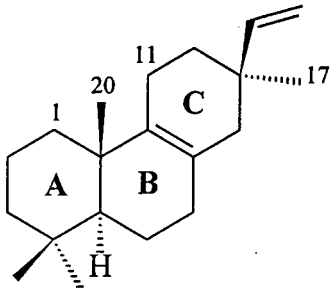

47a

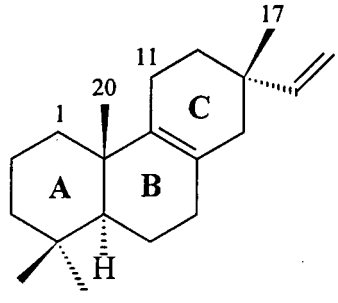

47b

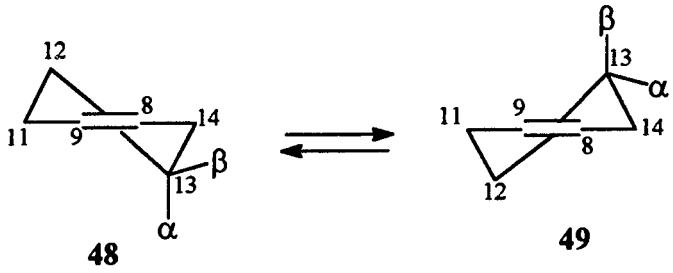

48 **49**

a: $\alpha = Me$; $\beta = C_2H_3$

b: $\alpha = C_2H_3$; $\beta = Me$

They then extended this argument to Ibozol, assuming that ring C would also adopt conformation **48** for similar reasons as discussed for pimaradienes (**47**). Analysis of the ^{13}C chemical shift for the isopropyl methine carbon (C-15) should therefore by analogy reveal the stereochemistry at C-13 in Ibozol, with the pseudo-axial methine carbon further upfield than the pseudo-equatorial one. Since only one stereoisomer of Ibozol was available, they used as a model (4)-terpinenol (**50**) where the isopropyl group was assumed to be mostly equatorial. In this compound the isopropyl methine carbon was found at δ36.6 ppm which was c.a. 2 ppm downfield from the corresponding carbon in Ibozol (C-15, δ34.7 ppm), and this, they suggested, was evidence that C-15 in Ibozol was pseudo-axial and therefore an α-substituent, and the -OH group therefore β. While there is some merit in this argument it did not provide a proof of stereochemistry.

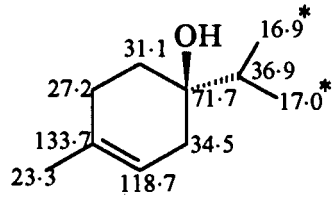

50

* indicates a possible signal reversal

Since a few large crystals of Ibozol were obtained on recrystallization, one suitable crystal was submitted for single crystal x-ray diffraction in order to confirm the stereochemistry. The following results were obtained:

The x-ray crystal structure of **45** clearly showed that the stereochemistry at C-13 was β-OH and α-isopropyl and that it crystallized with the 13β-OH group axially oriented as shown in Figure 10. There are two independent molecules in the asymmetric unit. It is interesting to notice that examination of the bond lengths, bond angles and torsion angles showed that the two molecules are in two slightly, but significantly, different conformations. This is an unusual phenomenon for small molecules, although another example of this unusual characteristic is found in the crystal structure of cholesterol. Table 16 lists all the torsion angles for the two molecules A and B and differences observed between the two molecules. It was clear that significant differences in the torsion angles occur mainly in rings B and the side chains of the two molecules. It was suspected that these two molecules do not have much energy differences, i.e. they are equally stable. The packing diagram, as shown in Figure 11, shows that the molecules pack in sheets, with their hydrophobic faces together. They are held in place by strong hydrogen bonding between hydroxy moieties, which is evident from the following O···O distances (in Å, the numbers in the brackets are the standard deviations). Normally, an O···O distance of 2.6 - 2.8 Å can be regarded as a significant hydrogen bonding, although weak hydrogen bondings can be observed for an O···O distance of up to 3.0 Å.

2.766 (0.010) O7B - O7A
2.734 (0.009) O7A - O13B
2.748 (0.010) O13B - O13A
2.832 (0.010) O13A - O7B*

* indicates a different molecule B

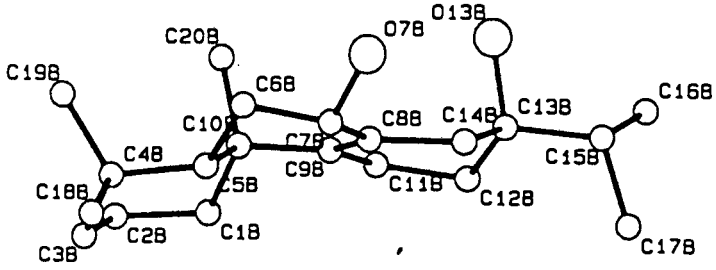

Figure 10 Crystal structure of **45**

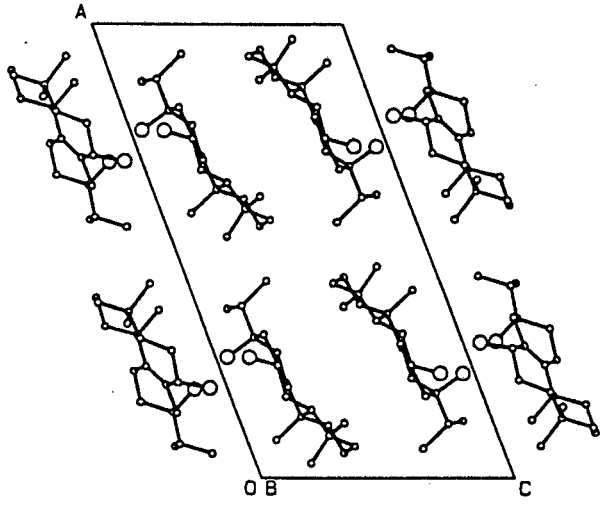

Figure 11 Packing diagram of the crystal of **45**

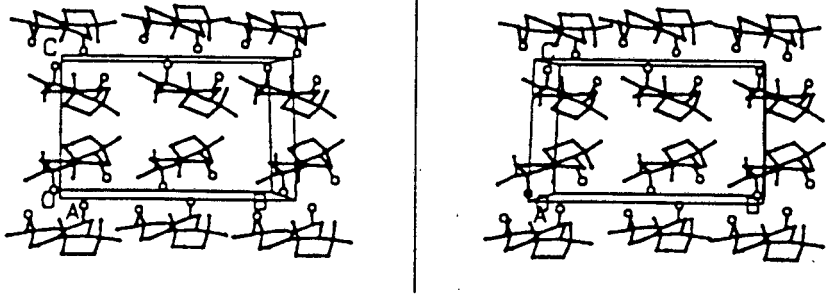

Figure 12 Stereo view of the crystal structure of **45**

Figure 12 shows the stereo view of the crystal which can be seen by any standard stereo viewer.

Table 16 Torsion angles comparison for molecules A and B of **45**

Ring	fragment of molecule	Torsion angle in molecule A	Torsion angle in molecule B	Δ
A	C10-C1-C-2-C3	-59	-60	1
	C1-C2-C3-C4	57	57	0
	C2-C3-C4-C-5	-48	-49	1
	C3-C4-C5-C10	49	49	0
	C4-C5-C10-C1	-51	-56	5
	C5-C10-C1-C2	51	57	6
B	C5-C6-C7-C8	39	40	1
	C6-C7-C8-C9	-15	-9	6
	C7-C8-C9-C10	12	1	11
	C8-C9-C10-C5	-31	-24	7
	C9-C10-C5-C6	54	56	2
	C10-C5-C6-C7	-60	-68	8
C	C8-C14-C13-C12	-48	-47	1
	C14-C13-C12-C11	57	54	3
	C13-C12-C11-C9	-41	-34	7
	C12-C11-C9-C8	12	9	3
	C11-C9-C8-C14	-0.5	-0.4	0.1
	C9-C8-C14-C13	20	20	0
Side Chain	C16-C15-C13-C12	180	-66	246
	C17-C15-C13-C12	56	59	3
	C16-C15-C13-C14	-60	64	124
	C17-C15-C13-C14	176	-171	347

Having established the stereochemistry at C-13, complete assignments of the ^{1}H and ^{13}C NMR spectra were possible with the aid of the HMQC and HMBC spectra. These assignments are shown in Tables 17 and 18.

Table 17 ^{1}H NMR spectrum assignment of **45**

proton	δ(ppm)[#], multiplicity[+] and J(Hz)	proton	δ(ppm)[#], multiplicity[+] and J(Hz)
H-1α	1.05, ddd[□]	H-12	< 1.59 >*
H-1β	1.75	H-14α	2.32, d, J = 16.67 Hz
H-2	1.47, 1.61	H-14β	2.12, d, J = 16.67 Hz
H-3α	1.14, ddd, J = 14.5, 14.5, 4.0 Hz	H-15	1.68, septet, J = 6.91 Hz
H-3β	1.41	Me-16	0.91, d, J = 1.29 Hz
H-5	1.16	Me-17	0.93, d, J = 1.39 Hz
H-6	1.44, 2.12	Me-18	0.88, s
H-7α	4.00	Me-19	0.86, s
H-11	< 2.08 >*	Me-20	1.05, s

[□] indicates multiplicity was deduced from the shape of the cross-peak in the HMQC spectrum and spin coupling considerations, therefore J values were not available in that case

* indicates mean values

[+] indicates multiplets were assumed wherever multiplicities were not stated

[#] indicates the assignments for H-14α and H-14β, Me-16 and Me-17 and Me-18 and Me-19 were interchangeable

Table 18 ^{13}C NMR spectrum assignment of **45** in δ(ppm) and literature data

Carbon	45	Literature data	Carbon	45	Literature data
C-1	37.05	37.2	C-11	21.04	20.9
C-2	18.91	18.9	C-12	31.82	31.7
C-3	41.39	41.4	C-13	72.11	72.3
C-4	33.02	33.0	C-14	35.66	35.3
C-5	49.63	49.6	C-15	34.17	34.7
C-6	30.06	30.1	C-16	16.66	16.7
C-7	72.18	71.4	C-17	16.77	16.8
C-8	126.76	126.8	C-18	33.02	33.0
C-9	141.76	141.7	C-19	21.60	21.6
C-10	38.40	38.4	C-20	20.24	20.2

A challenge in the assignment of the ^{1}H spectrum arose from the overlapping signals in the region δ1.00 - 2.50 ppm. Detailed analysis of the HMQC spectrum revealed the peak shapes and multiplicities of the individual spin systems. For example, Figure 13 shows the sub-spectrum generated for C-3, which resonated at δ41.39 ppm as confirmed by the HMBC spectrum and was associated with the proton signals at δ1.14 and 1.41 ppm. In the sub-spectrum, the signal at δ1.14 ppm was revealed as a ddd with coupling constants 14.5, 14.5, and 4.0 Hz consistent with one geminal coupling, one vicinal antiperiplanar coupling and one vicinal synclinal coupling. By viewing the perspective structure and Newman projection of ring A in Ibozol (shown in Figure 14), it was clear that of H-3α and H-3β, only H-3α meets the requirements. The coupling pattern of H-3α is shown in Figure 15.

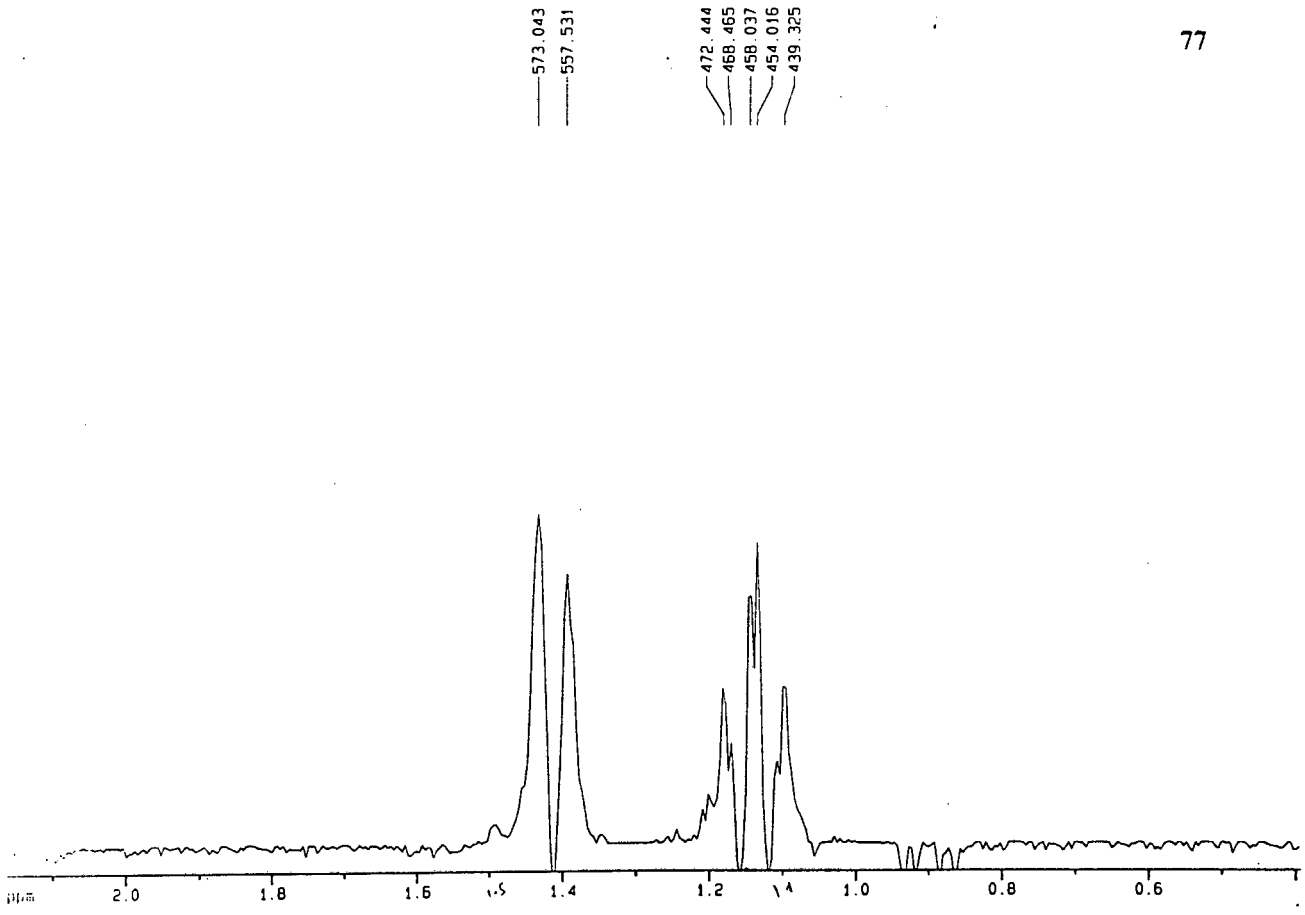

Figure 13 Sub-spectrum of C-3 of **45**

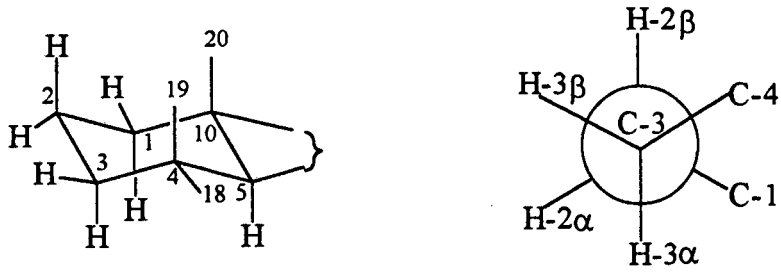

Figure 14 Perspective structure and Newman projection of ring A of **45**

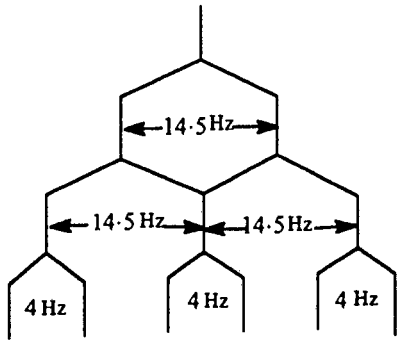

Figure 15 Coupling pattern of H-3α of **45**

Therefore the signal at δ1.14 ppm was assigned as H-3α. The shape of the cross-peak shown on the HMQC spectrum for H-3α and C-3 complemented the assignment, as shown in Figure 16 (right). Having assigned the one signal as H-3α, the other signal shown on the sub-spectrum with δ1.41 ppm would then be H-3β. The signal for H-3β was not as well resolved as that for H-3α. This was consistent with its coupling pattern which arose from a geminal coupling to H-3α and two vicinal synclinal couplings to H-2α and H-2β. The two vicinal synclinal couplings were small as the dihedral angles were *ca* 45°. The shape of the cross-peak for H-3β and C-3 was consistent with an incompletely resolved ddd, with one large coupling constant of c.a. 15.5Hz (see Figure 16, left).

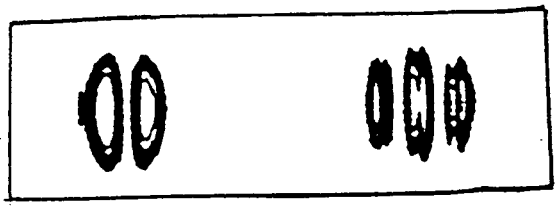

Figure 16 Cross-peaks of H-3α and H-3β of **45**

Using this approach, the two diastereotopic protons on C-1 and C-3 could be distinguished. With the aid of the HMBC spectrum, the assignments of ^{1}H and ^{13}C NMR spectra could be confirmed to be unambiguous. The connectivities of various protons with carbons are listed in Table 19.

Table 19 HMBC experiment results of **45**

proton	Connectivities observed
H-1α	C-2, C-5, C-10
H-1β	C-3, C-5
H-2	C-1, C-3, C-4, C-5
H-3α	C-4, C-5
H-3β	C-1, C-2, C-5, C-10
H-5	C-1, C-4, C-6, C-7, C-10
H-6	C-4, C-5, C-7, C-8, C-10
H-7α	C-8, C-9
H-11	C-8, C-9, C-12
H-12	C-9, C-11, C-13, C-14, C-15
H-14	C-7, C-8, C-9, C-12, C-13, C-15
H-15	C-13, C-14, C-16, C-17
Me-16	C-13, C-15, C-17
Me-17	C-13, C-15, C-16
Me-18	C-3, C-4, C-5, C-19
Me-19	C-3, C-4, C-5, C-18
Me-20	C-1, C-2, C-5, C-9, C-10

3.2.4. Structural Elucidation of Compound 51

Compound **51** was present in both fractions U and V as a minor constituent. However, it persistently eluted together with **44** on silica gel chromatography. After a few attempts at purifying **51** by gravity column failed, HPLC-UV was chosen to separate these two compounds as they both show characteristic absorption properties as shown in Figure 17. By using suitable gradient eluting solvent systems containing H_2O and CH_3CN, it was possible to separate **44** and **51** completely. The HPLC chromatogram is shown in Figure 18. A semi-preparative column was used in order to inject up to 10 mg of sample for each run. By optimising both solvents composition and flow rate, efficient separation could be achieved with minimum time.

51 was obtained as a white crystalline compound with m.p. 187-189°C. Close examination of various spectroscopic data and literature suggested **51** to have the following structure. Details of the structural elucidation are given below.

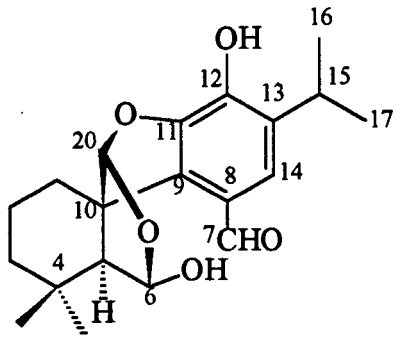

51

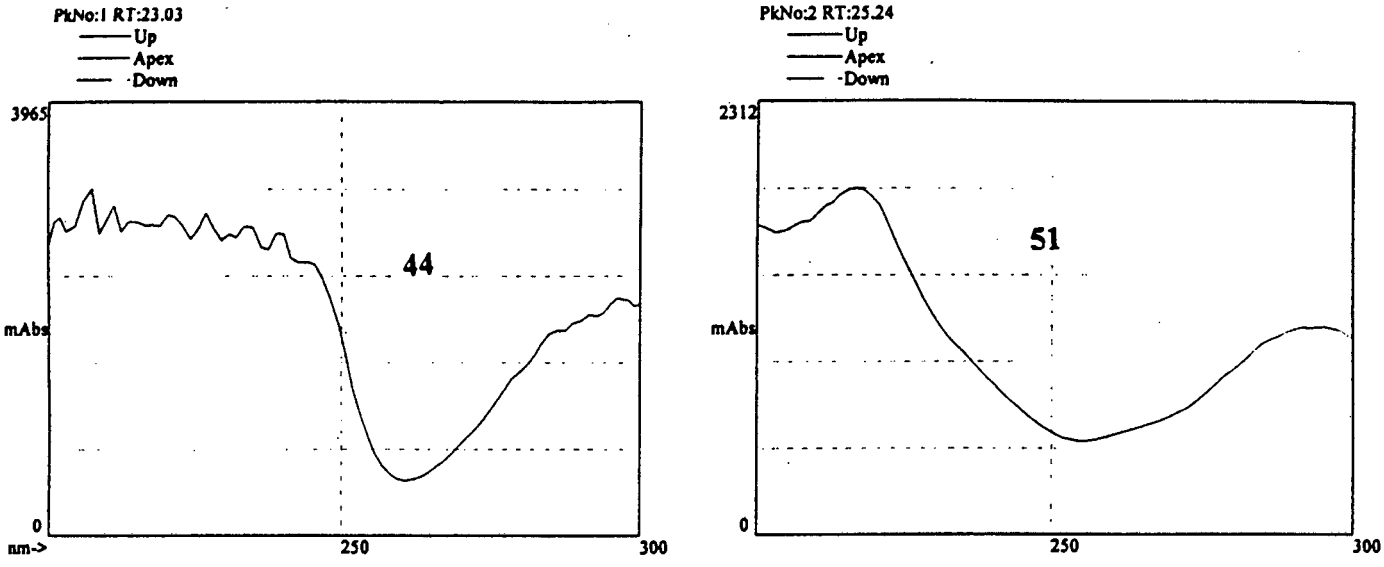

Figure 17 UV spectra of **44** and **51**

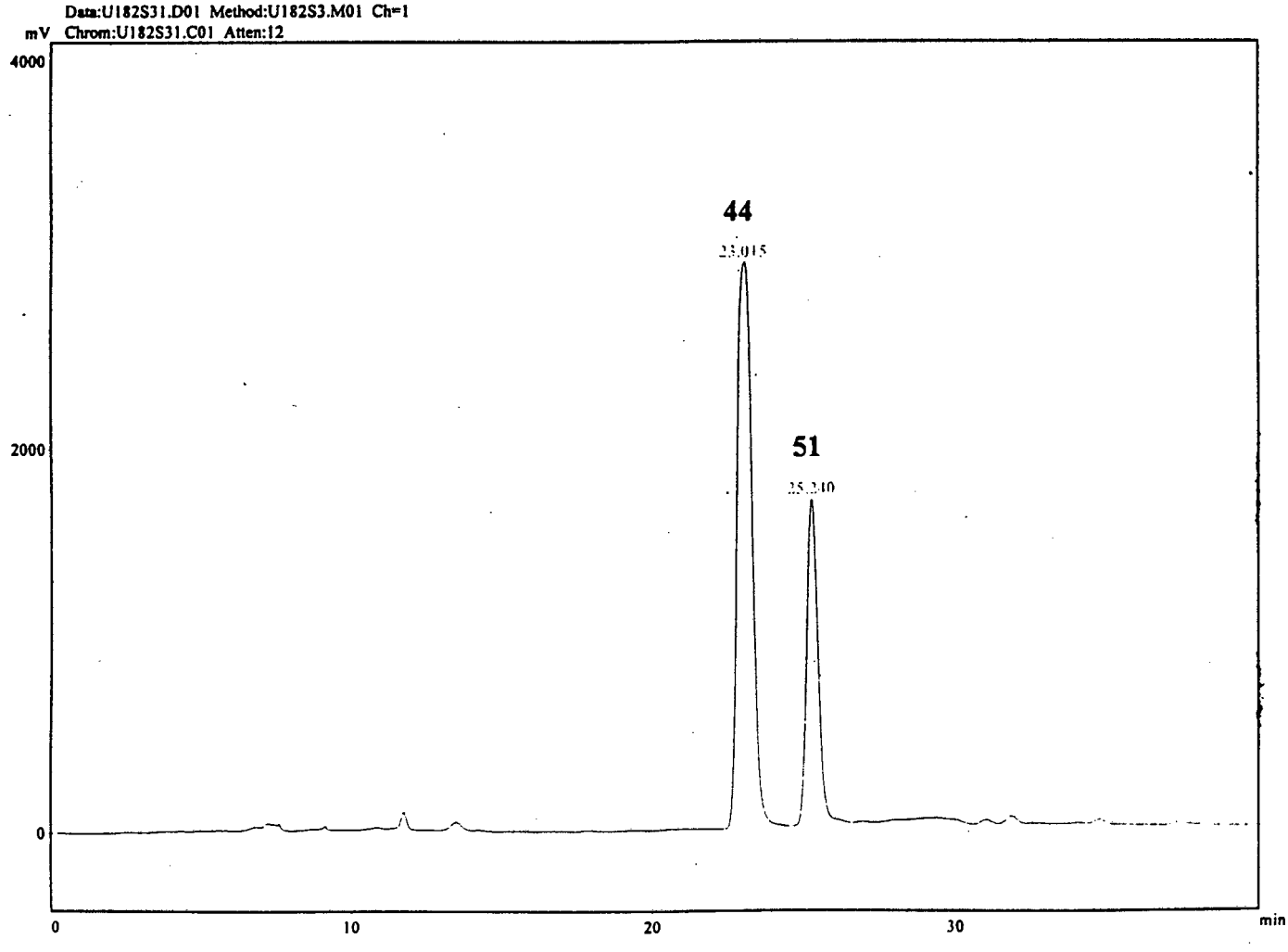

Figure 18 HPLC chromatogram of **44** and **51**

HREIMS of **51** showed a molecular ion at m/z = 346.1794, which corresponded to the molecular formula $C_{20}H_{26}O_5$. A fragmentation peak appeared at m/z 328 (i.e. M^+ - H_2O) indicating that there was at least one hydroxy group present in the molecule. The ^1H NMR spectrum of **51** (Appendix, spectrum 29) showed the presence of 4 methyl groups including an isopropyl group as indicated by the two 3-proton doublets at δ1.26 and 1.28 ppm. Six distinct protons signals appeared in the region δ2.80 - 9.90 ppm including: one methine proton singlet at δ2.80 ppm; two proton singlets at δ5.26 and 5.95 ppm, typical of protons attached to oxygenated carbons; one septet at δ3.30 ppm which could be assigned to the isopropyl methine proton; one aromatic proton singlet at δ7.34 ppm and one aldehyde proton singlet at δ9.88 ppm. By comparing the spectroscopic data of **51** with literature data, **51** was identified as cariocal, a seco-diterpene previously isolated from *Coleus barbatus*[59] which also belongs to the Labiatae family. This is the first time that cariocal is reported to be present in *Tetradenia riparia*.

In the literature, the authors described how they determined the structure of cariocal to be **51** instead of **52**, since by interpreting only ^1H and ^{13}C NMR spectra (Appendix, spectrum 30), there was no direct indication of which was the correct structure. The experimental support for structure **51** came from oxidation of cariocal methyl-ether (**53**) to lactone (**54**) which showed in its ^1H NMR spectrum deshielding effects on H-5, H-20 and Me-18, comparable to those observed on oxidation of acetyl enmein (**55**) to lactone (**56**)[60].

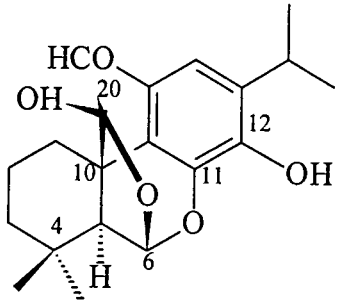

52

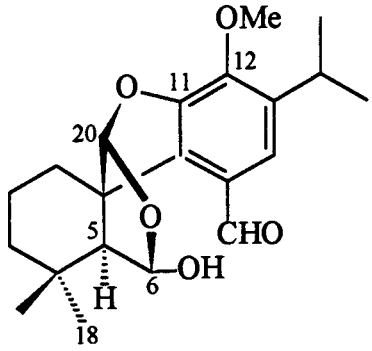

oxidation

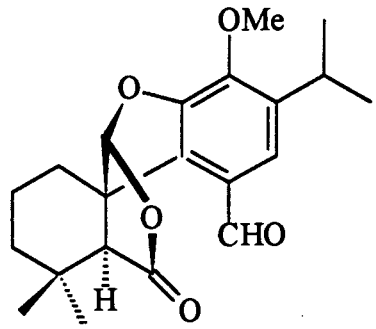

53 **54**

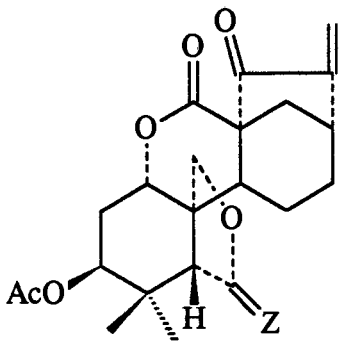

55 Z = 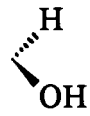

56 Z = O

In this study, the structure, as well as full ^{1}H and ^{13}C NMR spectra assignments were confirmed by the HMQC and HMBC spectra (Appendix, spectra 33 and 34). The cross-peak expected to be observed in order to confirm the structure of **51** rather than **52** was between H-20 and C11 which was a three bond correlation through a heteroatom - oxygen. The results of the HMBC experiment are shown in Table 20.

Table 20 HMBC experiment results of **51**

Proton	Connectivities observed
H-5	C-4, C-6, C-9, C-10, C-18, C-19, C-20
H-7	C-8, C-9
H-14	C-7, C-9, C-12, C-15
H-20	C-6, C-9, C-10, C-11
Me-16	C-13, C-15, C-17
Me-17	C-13, C-15, C-16
Me-18	C-3, C-4, C-5, C-19
Me-19	C-3, C-4, C-5, C-18

From Table 20, it is clear that only H-20 correlates to C11, therefore the structure of cariocal was successfully confirmed to be **51** by spectroscopy. In the literature, there is uncertainty about the assignments of C-9 and C-13. From the HMBC spectrum, it was clear that C-9 (δ133.67 ppm), appeared at higher field than C-13 (δ135.48 ppm) as H-5, H-14 and H-20 all showed correlations to the carbon signal at δ133.67 ppm, whereas Me-16 and Me-17 both showed correlations to the carbon signal at δ135.48 ppm. Also, in the literature, complete ^{1}H assignments were not available, but by performing a HMQC experiment, secondary protons in ring A could be assigned completely. Table 21 lists the full assignment of ^{1}H NMR spectrum and Table 22 shows the ^{13}C NMR spectrum assignment and the literature data is listed for comparison.

Table 21 ^{1}H NMR spectrum assignment of **51**

Proton	δ(ppm), multiplicity and J(Hz)	Proton	δ(ppm), multiplicity and J(Hz)
H-1α	2.00, ddd, J=13.88, 13.88, 5.85 Hz	H-14	7.34, s
H-1β	1.67, m	H-15	3.30, septet, J = 6.87 Hz
H-2	< 1.55 >*	Me-16	1.26, d#
H-3α	1.85, ddd, J=13.16, 13.16, 3.10 Hz	Me-17	1.28, d#
H-3β	1.40, m	Me-18	1.12, s
H-5	2.80, s	Me-19	0.89, s
H-6	5.26, s	H-20	5.95, s
H-7	9.88, s		

* indicates mean values

# indicates J values were not available

Table 22 ^{13}C NMR spectrum assignment (δ in ppm) of **51** and literature data

Carbon	**51**	literature data	Carbon	**51**	literature data
C-1	29.70	29.69	C-11	144.41	145.63
C-2	18.64	19.39	C-12	143.88	144.88
C-3	37.51	38.37	C-13	135.48	135.17*
C-4	30.68	31.08	C-14	129.17	128.55
C-5	56.45	56.72	C-15	26.96	27.47
C-6	101.91	101.82	C-16	22.46+	22.86#
C-7	191.13	191.50	C-17	22.19+	22.58#
C-8	124.15	124.66	C-18	32.06	32.39
C-9	133.67	136.11*	C-19	22.98	23.31
C-10	56.57	56.90	C-20	114.52	114.81

*, # and + indicate assignments interchangeable

3.2.5. Preparation and Structural Elucidation of an Analogue (61) of 7α-Hydroxyroyleanone (41)

In an earlier study of the antimalarial activity of *T. riparia* as discussed at the beginning of the chapter, 7α-hydroxyroyleanone (**41**) was isolated from the active fraction of the stems extract and was found to be the most active compound against *P. falciparum in vitro* (IC_{50} = 3.40 μg/ml) in the plant. It was also found to be cytotoxic (with IC_{50} values against WHCO1 and NIH-3T3-MDR 1.41 and 1.51 μg/ml respectively). Since a significant amount of **41** was available from the extract, it was thought that it would be of interest to prepare structural analogues for evaluation of structure-activity relationships. Apart from the obvious transformations possible such as esterification, oxidation of the secondary alcohol and dehydration to create an additional double bond, the Diels-Alder reactivity was chosen for further study. From the range of possible dienes, cyclopentadiene (**57**) was chosen for the initial study. In theory, eight products would be expected as there are two potential dienophiles present in **41** and each could produce four products i.e. those arising from α- and β-face addition of cyclopentadiene in both exo- and endo- orientations.

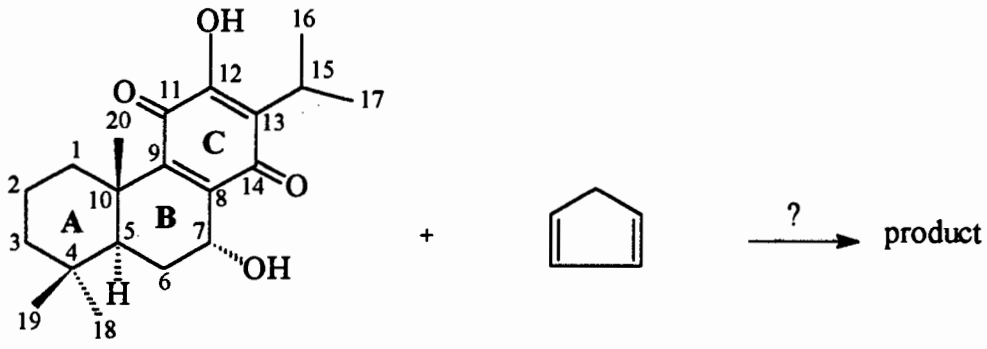

41 **57**

Scheme 2

An interesting precedent is the reaction of the benzoquinone (**58**) and trans-β-ocimene (**59**) which was performed in the context of a total synthesis of (+)-Perovskone (**60**) as shown in Scheme 3[61]:

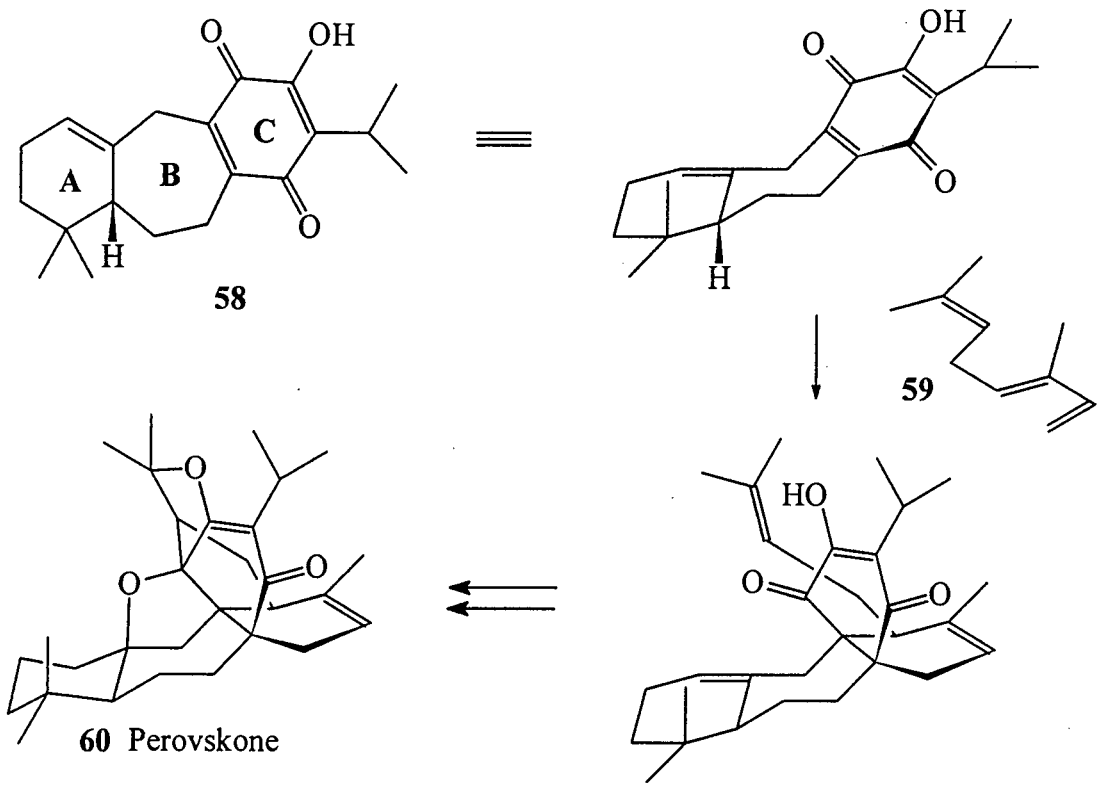

Scheme 3

The authors noted that on the basis of NMR studies of St. Jacques and Vaziri[62], which showed that benzocycloheptenes favour a chair conformation, the preferred conformation of quinone **58** should be cup-shaped with the α-face readily accessible, and therefore the diene would add from the α-face. The bulky isopropyl group was thought to control the regiochemistry of this cycloaddition. While the C rings of **41** and **58** are the same, there are distinct differences in the A and B rings of the two molecules such as the absence of a double bond at the ring A - ring B junction in **41**,

the number of carbons in ring B and the presence of Me-20 and the 7α-OH in **41**. It would therefore be expected that the C-8-C-9 double bond in **41** would be less accessible than the corresponding one in **58**.

The reaction shown in Scheme 2 was therefore attempted. At first, the reaction was carried out at room temperature without the addition of the catalyst, $BF_3.Et_2O$. However, no reaction product was observed. In the second successful attempt the reaction mixture was cooled to 0°C before the addition of the catalyst, and the reaction mixture was then allowed to warm to room temperature with stirring until completion.

Two products were obtained in 80% yield. After purification by column chromatography, the major product (**61**) was isolated as a colourless glassy compound. MS showed a molecular ion at m/z = 398. Significant fragmentation peaks appeared at m/z = 380 (i.e. $M^+ - H_2O$) and m/z = 365 (i.e. $M^+ - H_2O$ - Me) similar to those observed in the parent structure (**41**).

The ^1H and ^{13}C spectra (Appendix, spectra 35 and 37) showed features consistent with a product of cycloaddition at the C-12-C-13 double bond. The most significant feature was the upfield shift (c.a. 0.90 ppm) of the isopropyl methine proton (H-15), suggesting it was no longer attached to an unsaturated carbon. Further evidence came from the upfield shift of the C-12 resonance in the ^{13}C spectrum from δ151.1 ppm to δ62.13 ppm. In contrast, the ^1H chemical shift of H-7β remained virtually unchanged at δ4.70 ppm, suggesting that the C-8-C-9 double bond was intact. In addition, new olefinic signals were observed at δ5.58 and 5.81 ppm. Starting from this preliminary evidence, it was possible to carry out a complete assignment of the ^1H and ^{13}C NMR spectra with the aid of various 2D experiments, which led to the identification of **61** as 7α,12β-dihydroxy-3′β,6′β-methano-3′,4′,5′,6′-tetrahydrobenzo[12,13]-(13α)-abieta-8,4′-diene-11,14-dione with stereochemistry as shown.

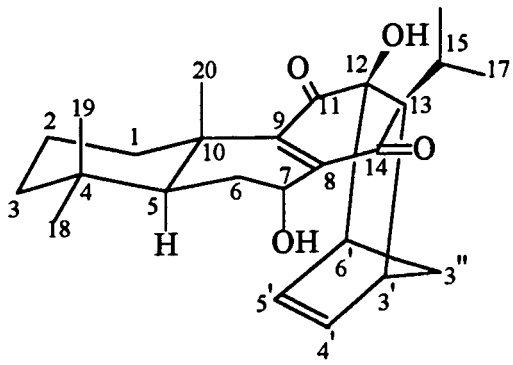

61

The proton and carbon signals in rings A and B were shown to have similar chemical shifts with the starting material. From the signal at δ4.70 ppm for H-7β, the protons H-6α and H-6β could be identified from the COSY spectrum (Appendix, spectrum 38) to be δ1.70 and 2.12 ppm respectively. C-6 could then be identified at δ26.32 ppm from the HMQC spectrum (Appendix, spectrum 39). The geminal dimethyl groups at C-4 were recognized from the common HMBC (Appendix, spectrum 40) correlations observed for signals at δ0.91 and 0.96 ppm, suggesting that these were methyls 18 and 19. Of these only the signal at δ0.91 ppm showed NOESY (Appendix, spectrum 41) correlation to the methyl signal at δ1.16 ppm, suggesting that these were Me-19 and Me-20 respectively. After assigning the methyl groups, C-1, C-3, C-4 and C-5 were readily assignable from the HMBC spectrum, therefore, H-1, H-3 and H-5 could be assigned from the HMQC spectrum. C-2 was assigned by comparing the spectroscopic data of **61** with the starting material. The assignment of H-5 led to the identification of C-9 and C-10 from the HMBC spectrum as H-5 was shown to be long range coupled to these two carbons. This completed the assignment for rings A and B.

A spin system could be identified in the ^{1}H NMR spectrum which corresponded to the new bridge ring system fused at C-12 and C-13. The single methylene group in this system was identified from the fact that the protons resonating at δ2.00 and 2.47 ppm

were correlated in the HMQC spectrum to one carbon at δ35.54 ppm, and this was assigned as the bridge C-3″.

The two olefinic protons appearing at δ5.58 and 5.81 ppm were shown to be multiplets which were assigned as H-4′ and H-5′.

The two protons in the 3″methylene group were shown to be coupled to H-3′ in the COSY spectrum and this in turn had a strong 4-bond coupling (W-coupling) to H-6′.

From the ^{1}H, ^{13}C and COSY data it was not possible to unambiguously distinguish between H-4′ and H-5′, and between methine protons H-3′ and H-6′. However, information from the NOESY spectrum was helpful in this regard. The isopropyl methine proton H-15 showed a correlation to the signal at δ2.90 ppm but not to the signal at δ3.94 ppm, therefore, these two signals were assigned as H-3′ and H-6′ respectively. H-6′ showed a correlation to the signal at δ5.58 ppm which was therefore assigned as H-5′.

These assignments were confirmed by the HMBC correlations in particular, H-3′ showed a correlation to C-15 and H-6′ showed a correlation to C-12.

The remaining issue to be resolved was the relative orientation of the 4′-5′ olefin and the methylene group in the bridged ring D, i.e., whether cycloaddition had taken place in endo- or exo- mode and from the α- or β-face. The NOESY experiment provided evidence for the stereochemistry as discussed below.

A correlation was observed between the 3″ methylene protons and the methyl groups at C-16 and C-17. In addition, correlations between H-5′ and H-5, and H-5′ and H-1α were observed. This suggested that the new ring has formed from the α-face with the olefin oriented towards ring A as shown in the perspective diagram in Figure 19.

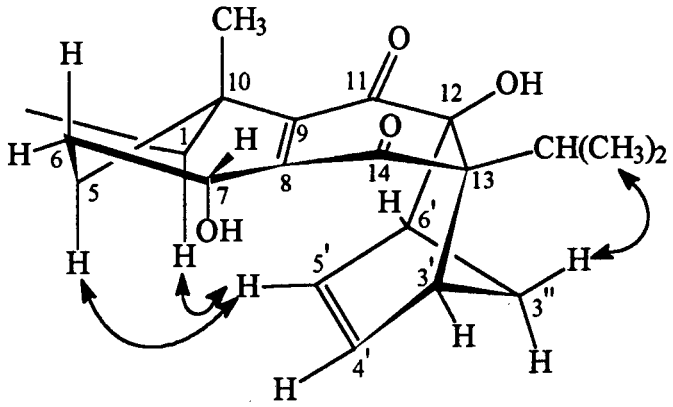

Figure 19

Molecular modelling confirmed that the observed NOE's are possible since the new ring is folded under the original skeleton and is twisted so that only H-5′ is within the range (3Å) for observable through-space interactions.

The observed atomic distances predicted by molecular modelling for selected pairs of atoms is shown below:

H-5′ - H-5	2.85 Å
H-5′ - H-1α	2.28 Å
H-1α - H-5	2.41 Å
H-4′ - H-5	3.67 Å
H-4′ - H-1α	4.46 Å

Tables 23 and 24 summarise the assignments for ^{1}H and ^{13}C NMR spectra, whereas Table 25 lists the HMBC spectrum results. In Table 23, the multiplicities of H-1α, H-3α and H-5 were deduced from the shape of cross-peaks in the HMQC spectrum and spin coupling considerations, therefore J values were not available in those cases.

Table 23 ^{1}H NMR spectrum assignment of **61**

Proton	δ(ppm), multiplicity# and J(Hz)
H-1α	1.23, ddd
H-1β	2.76
H-2	1.48, 1.62
H-3α	1.15, ddd
H-3β	1.42
H-5	1.63, t
H-6α	1.70
H-6β	2.12, ddd, J = 11.34, 13.64, 9.24 Hz
7α-OH	2.35, d, J = 3.60 Hz
H-7β	4.70, ddd, J = 9.24, 9.24, 3.00 Hz
12-OH	6.62, s
H-15	2.21, septet, J = 7.00 Hz
Me-16*	1.14, d, J = 2.00 Hz
Me-17*	1.16, d, J = 2.00 Hz
Me-18	0.96, s
Me-19	0.91, s
Me-20	1.16, s
H-3′	2.90, ddd, J = 9.89, 9.89, 4.73 Hz
H-4′	5.81
H-5′	5.58
H-6′	3.94
H-3″	2.00, 2.47

*indicates assignments were interchangeable

# indicates multiplets were assumed wherever multiplicities were not stated

Table 24 ^{13}C NMR spectrum assignment of **61**

Carbon	δ(ppm)	Carbon	δ(ppm)
C-1	36.75	C-14	206.78
C-2	18.66	C-15	28.78
C-3	41.62	C-16	18.83
C-4	40.64	C-17	18.83
C-5	46.02	C-18	20.97
C-6	26.32	C-19	32.90
C-7	63.64	C-20	20.74
C-8	140.46	C-3′	40.07
C-9	146.12	C-4′	134.58
C-10	34.44	C-5′	130.41
C-11	194.76	C-6′	45.80
C-12	62.13	C-3″	35.54
C-13	71.49		

Table 25 HMBC experiment results of **61**

Proton	Connectivities observed	Proton	Connectivities observed
H-1α	C-4, C-20	Me-16	C-13, C-15, C-17
H-1β	C-3	Me-17	C-13, C-15, C-16
H-2	C-1, C-3, C-4, C-10, C-20	Me-18	C-3, C-4, C-5, C-19
H-3α	C-1, C-4, C-5, C-18, C-19	Me-19	C-3, C-4, C-5, C-18
H-3β	C-1	Me-20	C-1, C-4, C-5
H-5	C-1, C-4, C-6, C-9, C-10, C-18, C-20	H-3′	C-11, C-12, C-13, C-15, C-4′, C-5′, C-6′, C-3″
H-6α	C-4, C-5, C-7	H-4′	C-3′, C-5′, C-6′, C-3″
H-6β	C-5, C-7, C-10	H-5′	C-3′, C-4′, C-6′, C-3″
H-7β	C-5, C-6, C-14	H-6′	C-9, C-12, C-4′, C-5′
12-OH	C-8, C-9, C-11	H-3″	C-4′, C-5′
H-15	C-11, C-13, C-14, C-16, C-17		

Table 26 NOESY experiment results of **61**

Proton	NOESY's observed
H-1α	H-1β, H-2α, H-3α, H-5, H-5′
H-1β	H-1α, H-2α, H-2β, OH-12
H-2α	H-2β, H-3α
H-2β	H-2α, H-3β, Me-19
H-3α	H-1α, H-2α, H-3β, H-5, Me-18
H-3β	H-2β, H-3α, Me-18, Me-19
H-5	H-1α, H-3α, H-5′, Me-18
H-6α	H-6β, H-7β, Me-18
H-6β	H-6α, Me-19
OH-7α	H-7β
H-7β	H-6α, H-6β, Me-20, OH-7α
OH-12	H-1β, Me-16, Me-17
H-15	H-3′, Me-16, Me-17
Me-16	H-15, H-3′, H-3″, OH-12
Me-17	H-15, H-3′, H-3″, OH-12
Me-18	H-3α, H-3β, H-5, H-6α, Me-19
Me-19	H-2β, H-3β, H-6β, Me-18, Me-20
Me-20	H-1β, H-2β, H-6β, Me-19
H-3′	H-15, H-3″, Me-16, Me-17
H-4′	H-5′, H-3′
H-5′	H-1α, H-5, H-4′, H-6′
H-6′	H-5′
H-3″	H-3′, Me-16, Me-17

The formation of the product indicates that the reactivity of dienophile at C-8 and C-9 was lower than that at C-12 and C-13, this might be due to the presence of Me-20 and OH-7α at the β- and α-face respectively of the starting material making the dienophile at C-8 and C-9 less accessible. It is interesting to notice that the molecular modelling of the starting material shows that the C ring was folded upwards, i.e. the two carbonyl groups were pointing up, this might have contributed to the accessibility of the α-face. Also, it is suggested that the $BF_3.Et_2O$ is more likely to form a complex on the β-face which would also favour α-attack of the diene.

The success of the above Diels-Alder reaction has encouraged further modification of the structure which may contribute to the study of structure-activity relationships.

3.3. Conclusion

As a continuation of the previous work done at the Pharmacology Department, UCT[50], fractions identified with antimalarial activity from the traditional plant *Tetradenia riparia* were further fractionated. Fractions U and V were the two fractions identified and subjected to fractionation in order to isolate possible antimalarial principle(s). Four compounds (**42**, **44**, **45** and **51**) were isolated and identified. ^{1}H and ^{13}C NMR spectra of all four compounds have been fully assigned by using the various 1D and 2D NMR techniques.

7α-hydroxyroyleanone (**41**) was previously isolated from an active fraction of *T. riparia* and identified to be the active principle of the plant. One analogue (**61**) was prepared for **41** by reacting **41** with cyclopentadiene (**57**). The structure of **61** was deduced from its various 1D and 2D NMR spectra. The ^{1}H and ^{13}C of **61** were fully assigned by the aid of the COSY, HMQC, HMBC and NOESY spectra.

The IC_{50} values of all the compounds isolated and prepared are listed in Table 27, which shows that Ibozol (**45**) is the most active antimalarial compound present in *T. riparia* extracts.

Table 27 The IC_{50} values of compounds **42**, **44**, **45**, **51** and **61**

Compound	IC_{50}(μg/ml)
42	>100
44	10
45	2.8
51	23
61	17

CHAPTER FOUR

XEROPHYTA RETINERVIS

4.1. Introduction

Apart from the two plants investigated in this project, *Passerina obtusifolia* and *Tetradenia riparia*, one novel flavonolignan was obtained from the methanol extract of *Xerophyta retinervis* which was supplied by Noristan. Records for *X. retinervis* in the Noristan database reveal that the plant has reported antimicrobial, antiulcer, central nervous system and anti-inflammatory activity.

Although there was no immediate access to bioassays for evaluating the reported activity of *X. retinervis*, the extract was subjected to investigation due to the following reasons:

(1) there was a large quantity of material available (c.a. 20g of extract);
(2) the antimalarial activity of this plant had not been investigated previously.

X. retinervis was formerly known as Vellozia, and is also known as: monkey's tail, bobbejaanstert, olifantstert and besembos. "*Xerophyta*" is from the Greek, meaning a plant that loves dry areas, and is structurally adapted for growth with a limited water supply, and *retinervis* is Latin, meaning reticulately nerved[63]. Its interesting to mention that *X. retinervis* is known as a "resurrection plant" because of its desiccation tolerance: it is one of several plants capable of surviving severe drying or desiccation. *X. retinervis* belongs to the family Velloziaceae which consists of fibrous perennials with dwarf and tufted stems covered with numerous leaf-bases[64].

The flowers of *X. retinervis* are usually blue or mauve, rarely white (see Figures 20 and 21) with capsules covered with rough hairs[65]. *X. retinervis* occurs on rocky hills around Pretoria and Johannesburg, as well as in the western and eastern Transvaal and Swaziland[63].

Figure 20 Flowers of *Xerophyta retinervis* (blue or mauve)

Figure 21 Flowers of *Xerophyta retinervis* (white)

The methanol extract contained a major component (**62**) which was obtained as a precipitate from the extract when dissolved in EtOAc later purification and recrystallization gave a yellow, crystalline compound with m.p. 247 - 248°C. HREIMS of **62** showed a molecular ion at m/z = 506.1224 which corresponded to the molecular formula $C_{27}H_{22}O_{10}$ (M^+ = 506.1213).

4.2. Results and Discussion

4.2.1. Structural Elucidation of Compound 62

The proposed structure of **62** resulted from an analysis of a complete set of NMR data, as well as identification of the products of acetylation and deacetylation of **62**.

A preliminary analysis of the ^1H, ^{13}C, DEPT and COSY NMR spectra (Appendix, spectra 42, 43, 44 and 45) revealed the following information: the ^1H NMR spectrum showed four isolated spin systems, three in the downfield region typical of aromatic signals, and the fourth in the region δ4.0 - 5.0 ppm, typical of protons attached to oxygenated aliphatic carbons. Closer examination of the coupling patterns suggested the presence of sub-structures A′, B′, C′ and D′ (Figure 22). The substitution pattern of the aromatic rings (A′, B′ and C′) was deduced from the presence of ortho- (ca. 8.3 Hz) or meta- (ca. 2.0 Hz) couplings (see Table 28).

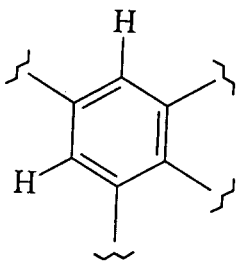

(A')

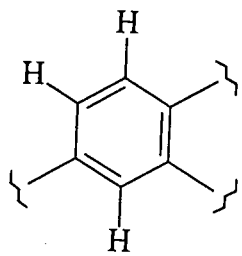

(B')

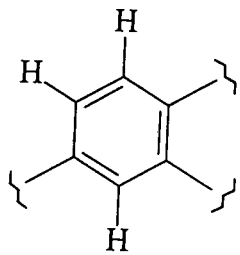

(C')

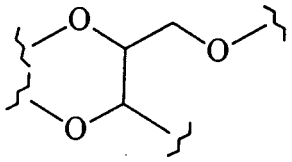

(D')

Figure 22

In addition there were five singlets indicating the presence of a methoxyl group (δ3.78 ppm), an O-acetyl group (δ2.04 ppm), an olefinic proton at a chemical shift typical of an α,β-unsaturated carbonyl system (δ6.82 ppm), and the remaining two in downfield positions (δ9.25 (broad) and 12.86 ppm) suggesting phenolic -OH groups. The ^{13}C NMR and DEPT spectra confirmed the presence of 13 protonated carbons, including two methyl, one methylene and 10 methine carbons. It also confirmed the presence of a carbonyl carbon. At this stage it was necessary to establish the connectivity between the sub-structures shown as well as the nature and location of all 10 oxygen atoms in **62**. The foregoing information accounts for 8 oxygens (1 methoxyl, 1 acetyl, 2 phenolic, 1 carbonyl and the three additional oxygens in sub-structure D').

Acetylation of **62** (see Scheme 4) produced a tetra-acetate (**63**) as judged from the four acetyl proton singlets in the ^{1}H NMR spectrum (Appendix, spectrum 48), confirming the presence of three additional hydroxyl groups. Compound **63** has been prepared previously, the spectroscopic data of **63** compares well with literature[66]. A deacetylation was also carried out (see Scheme 4) to gain further information: this proved difficult by conventional methods due to the poor solubility of **62**, but it was found that it did dissolve in large volumes of dry methanol and so was treated in this solution with methanolic sodium methoxide to achieve the deacetylation. The product (m.p. 261 - 263°C) was found to be identical by comparison of m.p. and spectral data to the known flavonolignan, hydnocarpin (**64**), identified previously in *Hydnocarpus wightiana*[67]. Table 31 shows the ^{13}C NMR spectrum assignment of **64** (see also Appendix, spectrum 49) with literature data listed for comparison. This implied that

62 was a mono-acetate of this compound, and further 2D NMR experiments were carried out to determine the location of the acetate, and to fully assign the ^{1}H and ^{13}C spectra.

The HETCOR spectrum (Appendix, spectrum 46) permitted the full assignment of the protonated carbons in the sub-structures A′, B′, C′ and D′. With these assignments in hand, the HMBC spectrum (Appendix, spectrum 47) could be used to fully assign the remaining carbons in each of the sub-structures from the connectivities listed in Table 30. The way in which the different sub-structures were connected was then established from the following significant correlations in the HMBC spectrum: both H-2′ and H-6′ showed connectivity to C-2 , H-3 showed connectivities to C-2, C-4, C-10 and C-1′, and both H-6 and H-8 showed connectivity to C-10. The following sub-structure (E′) shown in Figure 23 could be obtained from these connectivities:

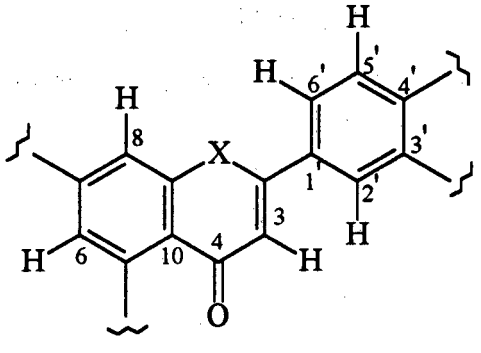

(E')

Figure 23

The other part of the molecule was established as follows: both H-15 and H-19 were shown to be long range coupled to C-13; H-13 showed connectivities to C-12, C-14, C-15 and C-19; the two H-11 protons showed connectivities to C-12 and C-13; finally, the methyl group in OCOMe showed connectivities to C-11 and C-21. The following sub-structure (F′) shown in Figure 24 was then obtained:

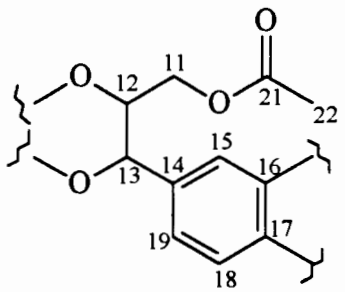

(F')

Figure 24

The two sub-structures E′ and F′ were joined as the chemical shifts of C-3′ and C-4′ (143.02 and 146.89 ppm respectively) suggested that they were connected to oxygens. X in sub-structure (E′) was also assigned to oxygen as indicated by the chemical shifts of C-9 and C-2 (δ157.28, 162.66 ppm respectively). The chemical shifts of carbons 5, 7, 16 and 17 (δ161.35, 164.25, 147.38 and 147.71 ppm respectively) suggested that they are all directly bonded to oxygens which accounted for the presence of three -OH groups and one -OMe group in **62**.

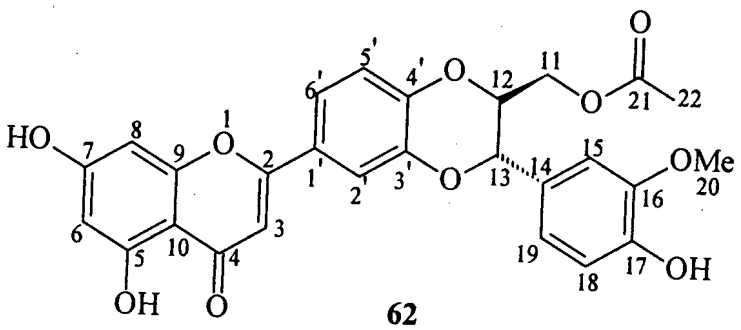

62

Ac_2O, pyridine

NaOMe(cat.) in MeOH

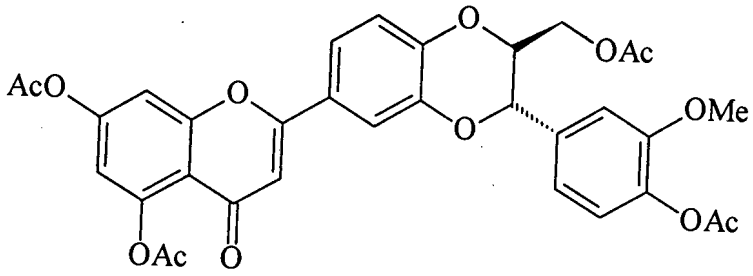

63

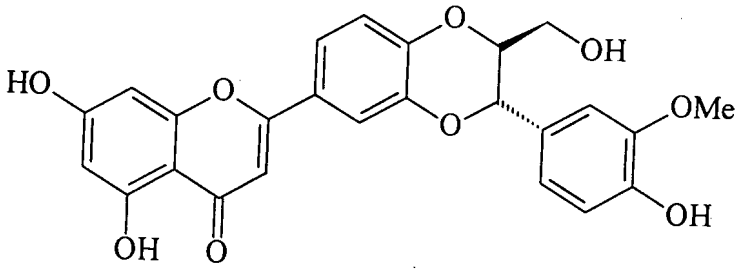

64

Scheme 4

The following are interesting features to notice: aromatic protons of ring C are more deshielded than those of ring E probably due to the adjacent oxygen atoms in ring D; the anti-relative stereochemistry at H-12 and H-13 was indicated by the value of 8.1 Hz for $J_{12\text{-}13}$; and the ^1H signal for H-12 was observed as a multiplet due to additional coupling to the diastereotopic protons at C-11.

Full assignments of the ^1H and ^{13}C NMR spectra of **62** are shown in Tables 28 and 29 respectively. Table 30 lists the resuts for the HMBC experiment.

Table 28 ^1H NMR spectrum assignment of **62**

Proton	δ(ppm), multiplicity and J(Hz)	Proton	δ(ppm), multiplicity and J(Hz)
H-3	6.82, s	H-12	4.6, m
H-6	6.20, d, J = 2.08 Hz	H-13	5.05, d, J = 8.12 Hz
H-8	6.53, d, J = 1.98 Hz	H-15	7.03, d, J = 1.92 Hz
H-2′	7.65, d, J = 2.35 Hz	H-18	6.81, d, J = 8.12 Hz
H-5′	7.07, d, J = 8.54 Hz	H-19	6.87, d, J = 8.12 Hz
H-6′	7.58, dd, J = 8.55, 2.35 Hz	OMe	3.78, s
H-11's	4.03, m	OCOMe	2.04, s

Table 29 ^{13}C NMR spectrum assignment of **62**

Carbon	δ(ppm)	Carbon	δ(ppm)
C-2	162.66	C-6′	120.13
C-3	103.99	C-11	62.41
C-4	181.69	C-12	74.89
C-5	161.35	C-13	76.25
C-6	98.87	C-14	126.01
C-7	164.25	C-15	111.72
C-8	94.07	C-16	147.38*
C-9	157.28	C-17	147.71*
C-10	103.73	C-18	115.42
C-1′	123.89	C-19	120.63
C-2′	114.91	C-20	55.65
C-3′	143.02	C-21	169.98
C-4′	146.89	C-22	20.38
C-5′	117.59		

* indicates assignments interchageable

Table 30 HMBC experiment results of **62**

Proton	Connectivities observed	Proton	Connectivities observed
H-3	C-2, C-4, C-10, C-1′	H-2′	C-2, C-3′, C-4′, C-6′
H-6	C-5, C-7, C-8, C-10	H-5′	C-1′, C-3′, C-4′, C-6′
H-8	C-6, C-7, C-9, C-10	H-6′	C-2, C-2′, C-4′
H-13	C-12, C-14, C-15, C-19	H-11's	C-12, C-13
H-15	C-13, C-16, C-19	OMe	C-16
H-18	C-14, C-16, C-17	OCOMe	C-11, C-21
H-19	C-13, C-15, C-17		

Table 31 ^{13}C NMR assignment (in ppm) of **64** and literature data

Carbon	**64**	Literature data	Carbon	**64**	Literature data
C-2	164.29	164.2	C-5′	117.49	116.7
C-3	103.91	103.8	C-6′	119.88	119.3
C-4	181.74	181.6	C-11	60.05	59.6
C-5	157.32	157.3	C-12	76.34	76.4
C-6	98.91	98.5	C-13	77.98	78.1
C-7	161.40	161.4	C-14	126.93	127.0
C-8	93.69	93.9	C-15	111.83	110.9
C-9	162.89	162.8	C-16	147.62*	147.7#
C-10	103.75	103.8	C-17	147.12*	147.0#
C-1′	123.67	123.6	C-18	115.33	115.4
C-2′	114.53	114.6	C-19	120.58	120.6
C-3′	143.63	143.6	C-20	55.72	55.8
C-4′	147.07	147.2			

* and # indicate assignments interchangeable

4.3. Conclusion

A new flavonolignan, 11-O-acetyl hydnocarpin (**62**) has been isolated from *Xerophyta retinervis* in significant amounts. The fraction of the crude extract containing this component had been shown to inhibit stress-induced ulceration in rats at Noristan. Antimalarial test of **62** showed an IC_{50} value of 12 μg/ml.

CHAPTER 5

EXPERIMENTAL SECTION

5.1. General

5.1.1. Characterisation of Compounds

^{1}H and ^{13}C NMR spectra were recorded at room temperature on one of the following three spectrophotometers: (1) a Varian VXR-200 (200.057 MHz); (2) a Varian Unity (399.951 MHz) or (3) a Bruker AMX-400 (400.136 MHz) in deuteriochloroform unless otherwise stated. The ^{1}H chemical shifts (δ) are given in ppm relative to the signal of tetramethylsilane (TMS, δ = 0.00 ppm) or the residual chloroform (δ = 7.25 ppm) in deuteriochloroform. The ^{13}C spectra were recorded with proton noise decoupling and chemical shifts (in ppm) were assigned relative to the central line of the deuteriochloroform triplet at δ77.09 ppm.

Infrared spectra were recorded in Nujol or dichloromethane using a Perkin Elmer Paragon 1000 FT-IR spectrometer.

All melting points were determined on a Reichert Jung hot stage microscope melting point apparatus and are uncorrected.

Mass spectra were recorded on a VG micromass 16 F mass spectrometry at 70 eV with accelerating voltage of 4KV. High resolution masses and mass spectra were recorded at the Mass-Spectrometry Unit of the Cape Technicon.

All fractionations and reactions were monitored by TLC (see below). Detection was achieved by one of the following methods:

(1) using an ultra-violet lamp (wavelength 254 nm and 365 nm),

(2) by spraying the TLC plates with a 1 % solution of ceric ammonium sulphate in H_2SO_4 followed by heating at *ca* 100°C or

(3) by spraying the TLC plates with a 2.5 % solution of anisaldehyde in H_2SO_4/EtOH followed by heating at *ca* 100°C.

Analytical TLC was performed using Merck TLC aluminium-backed silica gel 60 sheets; layer thickness 0.2 mm, employing one of the following solvent systems (in the appropriate optimized ratios):

Petroleum ether : EtOAc
$CHCl_3$: EtOAc
$CHCl_3$: EtOAc : Petroleum ether

Four different types of column chromatography was employed. Flash chromatography was performed in either a large (10 cm diameter) or a small (4 cm diameter) glass column packed with silica gel 60 (PF_{254} containing gypsum, for preparative layer chromatography, Merck Art. 7749). The third column was a 1.5 cm diameter glass column packed with silica gel 60 (0.040 - 0.053 mm particle size, 230 - 400 mesh ASTM, Merck Art. 9385) in which elution proceed by gravity. The fourth column comprised of a 0.75 mm diameter pasteur pipette packed with silica gel 60 (less than 0.063 particle size, finer than 230 mesh ASTM, Merck Art. 7729). The above solvent systems were also applicable to the column separations.

HPLC was performed on a LC10 (Shimadzu) apparatus with reverse phase C18 silica column and a diode array spectrophotometer (Shimadzu) as detector. Distilled water (Millipore) and HPLC grade Acetonitrile (Merck) in the appropriate optimized ratios were used as eluting solvents.

5.1.2. Solvents

Petroleum ether: CP (chemically pure) grade, distilled
EtOAc: CP (chemically pure) grade, distilled

$CHCl_3$: CP (chemically pure) grade, distilled

C_6H_6: AR (analytical reagent) grade, distilled and dried over Na wire.

5.2. *Passerina obtusifolia*

The ground plant material of *Passerina obtusifolia* was supplied by the Pharmacology Department at UCT. The plant material was divided into two parts, leaves and stems 576.53 g and 703.90 g respectively) which were then subjected to Soxhlet extraction with petroleum ether followed by ethanol. The gums obtained from these four extractions were then subjected to bioassay from which the petroleum ether extract of the stems (18.04 g) was found to have the highest activity. Further fractionation of this active extract by flash chromatography produced 11 fractions (fractions A to K). The one fraction identified with activity (fraction J, 1.20 g) was then chromatographed by flash chromatography, and further purification was achieved by employing the third and fourth column as described above. Two compounds were isolated from this active fraction (compounds **30** and **32**).

20(29)-Lupene-3α,28-diol (**30**)

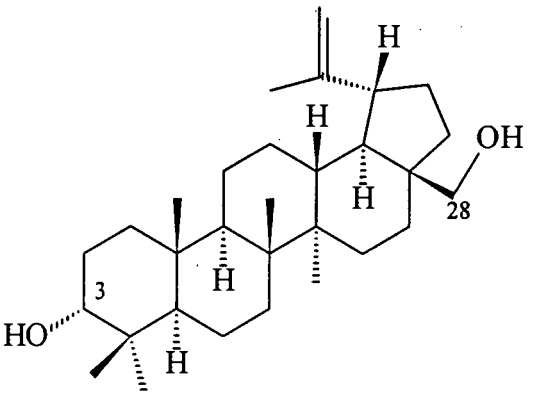

Crystallized from petroleum ether/EtOAc as white crystals (312.5 mg); m.p. 210 - 213°C (lit.[68]C NMR, see Table 4; HREIMS: M^+ 442.3798, $C_{30}H_{50}O_2$ requires 442.3811; EI-MS m/z (rel.int.): 442 (M^+, 29), 424 (M^+ - H_2O, 19), 411 (24), 234 (18), 220 (19), 207 (51), 203 (46), 189 (100), 135 (63).

20(29)-Lupene-3α,16β,28-triol (**32**)

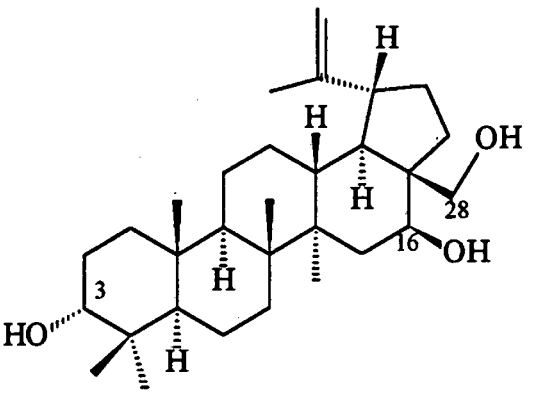

Crystallized from petroleum ether/EtOAc as white crystals (8.7 mg), m.p. 215 - 217°C; IR, ν_{max} 3383, 1617, 1378, 1259; ^{1}H NMR, see Table 7; ^{13}C NMR, see Table 8; HREIMS: M^+ 458.3756, $C_{30}H_{48}O_3$ requires 458.3760; EI-MS m/z (rel.int.): 458 (M^+, 3), 440 ($M^+ - H_2O$, 92), 422 ($M^+ - H_2O - H_2O$, 30), 409 (42), 391 (39), 385 (33), 220 (18), 219 (18), 207 (51), 203 (30), 201 (39), 189 (100), 187 (68).

5.3. *Tetradenia riparia*

Fractions U and V (0.65 and 1.04 g respectively) from *T. riparia* extract were obtained from Mr. D.R. Dodds, Department of Pharmacology, UCT[50]. The fractions were chromatographed by employing flash chromatography on a small glass column, later chromatographic separation of the fractions by employing the third and fourth column yielded four compounds (compounds **42**, **44**, **45** and **51**).

3β-Hydroxy-20(29)-lupen-28-oic acid (**42**)

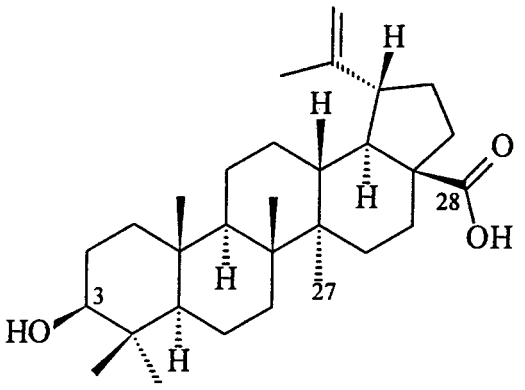

Crystallized from petroleum ether/EtOAc as off-white crystals (4.3 mg), m.p. 274 - 277°C (Lit.[68] 275 - 278°C); ^{1}H NMR, see Table 11; ^{13}C NMR, see Table 12; HREIMS: M^+ 456.3587, $C_{30}H_{48}O_3$ requires 456.3603; EI-MS m/z (rel.int.): 456 (M^+, 5), 438 (M^+ - H_2O, 31), 423 (M^+ - H_2O - Me, 27), 410 (9), 248 (15), 220 (14), 219 (13), 207 (37), 203 (27), 189 (100).

5-Hydroxy-4′,6,7-trimethoxyflavone (**44**)

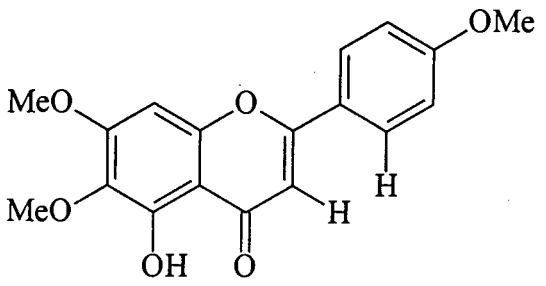

Crystallized from $CHCl_3$ as yellow needles (16.5 mg), m.p. 186 - 188°C (Lit.[68] 188°C) IR, ν_{max} 3439, 1658, 1589, 1511, 1495, 1357, 1126; ^{1}H NMR, see Table 14; ^{13}C NMR, see Table 15; MS: M^+ 328, molecular formula $C_{18}H_{16}O_6$; EI-MS m/z (rel. int.): 328 (M^+, 100), 313 (M^+ - Me, 89), 299 (23), 285 (24), 256 (20), 181 (25), 167 (32), 153 (42).

8-Abietene-7β,13β-diol(**45**)

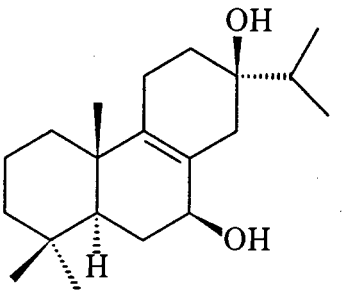

Crystallized from petroleum ether/EtOAc as colourless crystals (150 mg), m.p. 147 - 150°C (Lit.[68] 146 - 150°); ^{1}H NMR, see Table 17; ^{13}C NMR, see Table 18; MS: M^+ = 306, molecular formula $C_{20}H_{34}O_2$; EI-MS m/z (rel.int.): 306 (M^+, 4), 273 (16), 255 (5), 227 (5), 217 (8), 202 (4), 189 (35), 187 (17), 173 (9), 119 (63).

Cariocal (**51**)

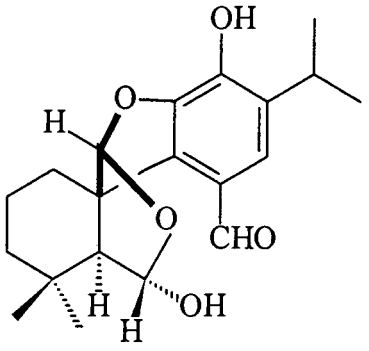

Crystallized from petroleum ether/EtOAc as white crystals (8.0 mg), m.p. 185 - 187°C (Lit.[68] 186 - 189 °C); ^{1}H NMR, see Table 21; ^{13}C NMR, see Table 22; HREIMS: M^+ 346.1794, $C_{20}H_{26}O_5$ requires 346.1780; EI-MS m/z (rel.int.): 346 (M^+, 99), 328 ($M^+ - H_2O$, 73), 313 (16), 300 (56), 285 (59), 271 (28), 257 (40), 149 (46), 69 (61).

Preparation of 7α-Hydroxyroyleanone (**41**) Analogue: 7α,12β-dihydroxy-3′β,6′β-methano-3′,4′,5′,6′-tetrahydrobenzo[12,13]-(13α)-abieta-8,4′-diene-11,14-dione (**61**)

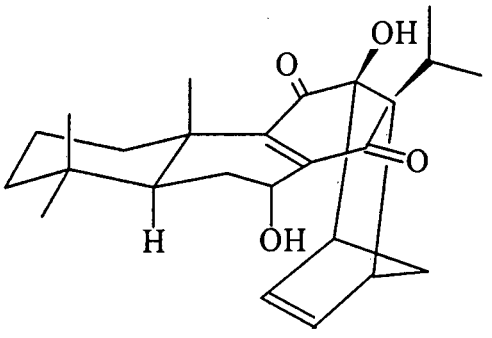

7α-Hydroxyroyleanone (**41**) (100 mg, 0.30 mmol) was dissolved in dry benzene (1 cm^3) with stirring. Once the solids dissolved, the solution was cooled to 0°C. Freshly distilled cyclopentadiene (**57**) (0.25 cm^3, 3.03 mmol) was added dropwise to the solution. One drop of $BF_3.OEt_2$ was added to the reaction mixture as catalyst. The reaction mixture was left stirring for 48 hrs before working-up which was as follows: Sat. $NaHCO_3$ (15 cm^3) was added to the reaction mixture, and the resulting mixture extracted with EtOAc (3 x 10 cm^3). Finally, the resulting EtOAc (30 cm^3) was extracted with $NaHCO_3$ (10 cm^3) and H_2O (2 x 10 cm^3). The organic phase was dried over anhydrous $MgSO_4$ filtered and the volume of solvent reduced *in vacuo* to afford the crude product which was then chromatographed on silica gel (10 g) eluting with EtOAc-petroleum ether (5 : 95) yielding **61** as a colourless glassy compound (73 mg, 73 % yield).

^1H NMR, see Table 23; ^{13}C NMR, see Table 24; MS: M^+ 398, molecular formula: $C_{25}H_{34}O_4$; EI-MS m/z (rel. int.): 398 (M^+, 51), 380 (M^+ - H_2O, 46), 365 (5), 355 (25), 338 (100), 333 (21), 323 (5), 319 (12), 316 (20), 315 (24), 310 (33), 269 (12), 195 (24), 123 (33), 66 (72).

5.4. *Xerophyta retinervis*

The crude leaves methanol extract of *X. retinervis* was obtained from Noristan. Compound **62** was obtained as a precipitate from this extract when dissolved in EtOAc. Later purification gave a yellow crystalline compound.

11-O-acetyl hydnocarpin (**62**)

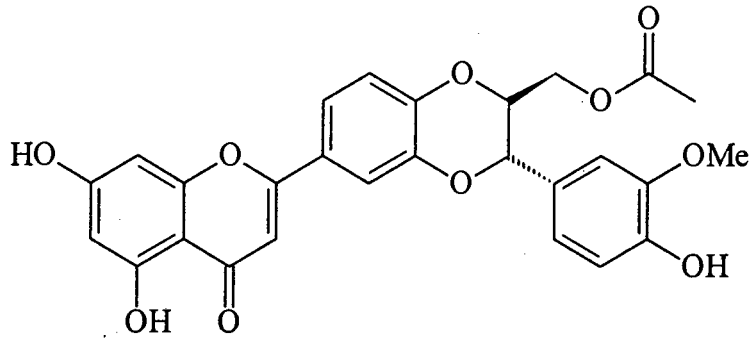

Crystallized from THF as yellow crystals, m.p. 247 - 248°C; IR, ν_{max} 3406 (OH), 2953, 1738 (C=O), 1614, 1585 (C=C), 1305; ^{1}H NMR, see Table 28; ^{13}C NMR, see Table 29; HREIMS: M^{+} 506.1224, $C_{27}H_{22}O_{10}$ requires 506.1213; Microanalysis found: C, 64.01, H, 4.46 %, $C_{27}H_{22}O_{10}$ requires C, 64.03, H, 4.38 %; EI-MS m/z (rel.int.): 506 (M^{+}, 18), 447 (6), 179 (18), 147 (10), 137 (7), 124 (7).

Tetra-acetylated Hydnocarpin (**63**)

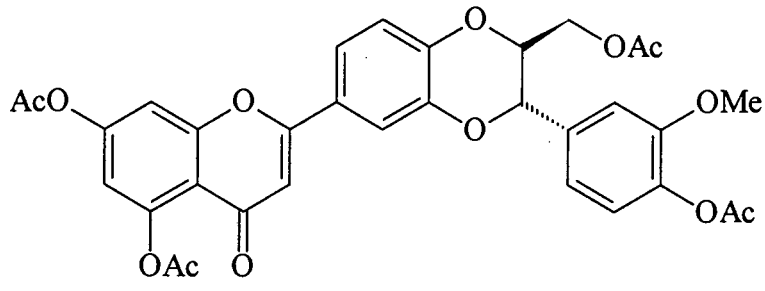

Compound **62** (30 mg, 0.059 mmol) was dissolved in pyridine (2 cm^3) then acetic anhydride (2 cm^3) was added and the mixture refluxed for 2 hrs. Then the reaction mixture was cooled to 0°C, MeOH (5 cm^3) added, then toluene (5 cm^3) before

evaporating off the solvents under reduced pressure. Further portions of toluene (5 cm^3) were added to remove final traces of pyridine and removed under reduced pressure. Finally, portions of MeOH (7 cm^3) were added to remove toluene and solvents removed under reduced pressure. The product was chromatographed on silica gel. Elution of **63** with petroleum ether - EtOAc (50: 50) gave 7 mg of **63**, a yellow crystalline compound with m.p. 195 - 197°C (Lit.[66] 196 - 198°C). ^{1}H NMR (200 MHz): δ7.53 (d, J = 1.93 Hz, H-15); 7.43 (dd, J = 8.54, 2.10 Hz, H-6′); 7.34 (d, J = 2.25 Hz, H-8); 7.10 (d, J = 8.59 Hz, H-19); 7.08 (d, J = 8.50, H-18); 6.99 (H-2′); 6.97 (H-5′); 6.84 (d, J = 2.28 Hz, H-6); 6.58 (s, H-3); 5.00 (d, J = 8.00 Hz, H-13); 4.60 (m, H-12); <4.40>* (m, H-11); 3.86 (s, O<u>CH$_3$</u>); 3 singlets at 2.44, 2.35 and 2.33 ppm corresponded to the 3 Ar-O-CO<u>CH$_3$</u>; 2.09 (s, aliphatic-OCO<u>CH$_3$</u>)

Deacetylated derivative of **62** - **64** (Hydnocarpin)

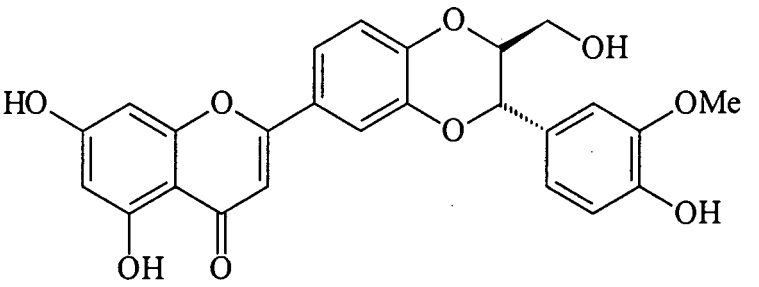

Compound **62** (25 mg, 0.049 mmol) was dissolved in dry MeOH (100 cm^3). A catalytic amount of 0.1 M MeONa was added and the reaction vessel left overnight at room temperature. The solvent was removed by evaporation and the product purified on silica gel to give **64** as a yellow crystalline compound with m.p. 261 - 263°C (Lit.[66] 262 - 264°C). The ^{13}C NMR data of **64** corresponded well with that of the known compound hydnocarpin (see Table 31).

* indicates mean δ value.

References

1. Scott, G., *Veld & Flora*, **1993**, September

2. Hostettmann, K.; Wolfender, J.L.; Rodriguez, S. and Marston, A., *Chemistry, Biological and Pharmacological Properties of African Medicinal Plants,* Proceedings of the first International IOCD-Symposium, Victoria Falls, Zimbabwe, Feb 25-28, **1996**, 21

3. Ganellia, C.R., *Medicinal Chemistry: The Role of Organic Chemistry in Drug Research*, 2nd edition, Chapter 7, Academic Press Limited, **1993**

4. Spjut, R.W. and Perdue, R.E., *Cancer Treatment Reports*, **1976**, *60*, 979

5. Farnsworth, N.R. and Kaas, C.J., *Journal of Ethnopharmacology*, **1981**, *3*, 85

6. Bird, C., *New Scientist*, 17 August **1991**, 34

7. Fourie, T.C.; Swart, I. and Snyckers, F.O., *South African Journal of Science*, **1992**, *88*, 190

8. Hostettmann, K.; Marston, A. and Wolfender, J.L., *Phytochemistry of Plants Used in Traditional Medicine*, **1995**, 17

9. Harbourne J.B., *Phytochemical Methods: A Guide to Modern Techniques in Plant Analysis*, Chapman and Hall, **1984**, 4

10. Silverstein, R.M.; Bassler, G.C. and Morrill, T.C., *Spectrometric Identification of Organic Compounds*, Fifth edition, John Wiley & Sons, Inc., **1991**, 169

11. Leslie, M.R., *Structural Studies on the capsular antigens of some Escherichia coli serotypes*, PhD thesis, Rhodes University, S.A., **1994**, 50

12. Martin, G.E. and Crouch, R.C., *Two-Dimensional NMR in Natural Products and Pharmaceutical Chemistry* in *Two-Dimensional NMR Spectroscopy Application for Chemists and Biochemists*, Croasmun, W.R. and Carlson, R.M.K. (Eds), 2nd edition, VCH publishers, New York, **1994**

13. Mahato, S.B. and Kundu, A.P., *Phytochemistry*, **1994**, *37*, 1517

14. Knell, A.T., *Malaria*, 1st edition, **1991**, Oxford University Press

15. Butler, A.R. and Wu, Y.L., *Chemical Society Review*, **1992**, 85

16. Johnson, M., *Time*, **1993**, May, 31

17. Woodward, R.B. and Doering, W.E., *J. Am. Chem. Soc.*, **1944**, *66*, 849

18. Vennerstrom, J.L.; Ellis, Y.W.; Ager, A.L.; Andersen, S.L.; Gerena, L. and Milhous, W.K., *J. Med. Chem.*, **1992**, *35*, 2129

19. Guan, W-D.; Zhou, Y. and Huang, W., *J. Parasitol. Parasitic D.* **1983**, *1*, 88

20. Chen, L., *Chin. Med. J. (Beijing, Engl. Ed.)*, **1991**, *104*, 161

21. Raynes, K.; Galatic, D.; Cowman, A.F.; Tilley, L. and Deady, L.W., *J. Med. Chem*, **1995**, *38*, 204

22. Nkunya, M.H.H., *Progress in the Search for Antimalarials*, NAPRECA Monograph series No.4. Published by NAPRECA, Addis Ababa University, Addis Ababa, **1992**

23. Likhitwitayawuid, K.; Angerhofer, C.K.; Cordell, G.A. and Pezzuto, J.M., *J. Nat. Prod.*, **1993**, *56*, 30

24. Likhitwitayawuid, K.; Angerhofer, C.K.; Chai, H.; Pezzuto, M.J. and Cordell, G.A., *J. Nat. Prod.*, **1993**, *56*, 1468

25. Bringmann, G., *Chemistry, Biological and Pharmacological Properties of African Medicinal Plants*, Proceedings of the first International IOCD-Symposium, Victoria Falls, Zimbabwe, Feb 25-28, **1996**, 1

26. Malker, M.T. and Hicrichs, D.J., *Am. J. Trop. Med. Hyg.*, **1993**, *48*, 205

27. Makler, M.T.; Reis, J.M.; Williams, J.A.; Bancroft, J.E.; Piper, R.C.; Gibbens, B.L. and Hinrichs, D.J., *Am. J. Trop. Med. Hyg.*, **1993**, *48*, 739

28. Desjardins, R.E.; Canfield, C.J.; Haynes, J.D. and Chulay, J.D., *Antimicrobial Agents and Chemotherapy*, **1979**, 710

29. Geary,T.G.; Divo, A.A. and Jensen, J.B., *J. Parasitol*, **1983**, *69*, 577

30. Thoday, *Kew Bulletin*, **1924**, 146

31. Moriarty, A. *Tsitsikamma and Eastern Little Karoo, South African Wild Flower Guide 2*, Claremont, Botanical Society of South Africa, **1982**

32. Davy, G.S.; Halsall, T.G. and Jones, E.R.H., *J. Chem. Soc.*, **1951**, 2696

33. Das, S.C., *Chemistry and Industry*, **1991**, 1331

34. Herz, W.; Santhanam, P.S. and Wahlberg, I., *Phytochemistry*, **1972**, *11*, 3061

35. Errington, S.G.; Ghisalberti, E.L. and Jefferies, P.R., *Aust. J. Chem*, **1976**, *29*, 1809

36. St. Pyrek, J., *Polish Journal of Chemistry*, **1979**, *53*, 2465

37. National Botanical Gardens of South Africa (Kirstenbosch), *Wild Flowers of South Africa*, **1980**, Struik, 110

38. Onderstall, J., *South Africa Wild Flower Guide 4: Transvaal Lowveld and Escarpment (including the Kruger National Park)*, CTP Book Publishers, **1982**, 170

39. Eliovson,S., *Discovering Wild Flowers in Southern Africa*, Timmins, **1969**, 168

40. Watt, J.M. and Breyer-Brandwijk, M.G., *The Medicinal and Poisonous Plants of Southern and Eastern Africa*, 2nd edition, E. and S. Livingstone, Edinburgh., **1962**, 516

41. Githens,T.S., *Univ. Pa. Afr. Hdbk 8*

42. Van Puyvelde, L. and Kayonga, A., *Afr. Med.*, **1975**, *14*, 925

43. Van Puyvelde, L., *Rapp. Deuxieme Colloq.*, CAMES, **1976**, 60

44. Van Puyvelde, L.; Dube, S.; Uwimana, E.; Uwera, C.; Dommisse, R.A.; Esmans, E.L.; van Schoor, O. and Vlietink, A.T., *Phytochemistry*, **1979**, *18*, 1215

45. Van Puyvelde, L.; De Kimpe, N.; Dube, S.; Chagnon-Dube, M.; Boily, Y.; Borremans, F.; Schamp, N. and Antenuis, M.J.O., *Phytochemistry*, **1981**, *20*, 2753

46. De Kimpe, N.; Schamp, N.; Van Puyvelde, L.; Dube, S.; Chagnon-Dube, M.; Borremans, F.; Antenuis, M.J.O.; Declercq, J-P.; Germain, G. and Van Meerssche, M., *J. Org. Chem.*, **1982**, *47*, 3628

47. Van Puyvelde, L.; Nyirankuliza, S.; Panebianco, R.; Boily, Y.; Geizer, I.; Sebikali, B.A.; De Kimpe, N. and Schamp, N., *Journal of Ethnoparmacology*, **1986**, *17*, 269

48. Hakizamungu, E. and Wery, M., *Bulletin de Liaison ACCT: Médicine Traditionelle et Pharmacopée*, **1988**, *2*, 11

49. Chagnon, M., *Journal of Ethnopharmacology*, **1984**, *12*, 239

50. Dodds, D.R., *Isolation and Characterization of an Active Antimalarial Principle from the Indigenous South African Plant, Tetradenia riparia* (*Labiatea*), Honours Project, Pharmacology Department, UCT, **1995**

51. Hensch, M.; Ruedi, P. and Eugster, C.H., *Helv. Chim. Acta*, **1975**, *58*, 1795

52. Pisha, E.; Chai, H.; Lee, I-S.; Chagwedera, T.E.; Farnsworth, N.R.; Cordell, G.A.; Beecher, C.W.W.; Fong, H.H.S.; Kinghorn, A.D.; Brown, D.M.; Wani, M.C.; Wall, M.E.; Hieken, T.J.; Das Gupta, T.K. and Pezzuto, J.M., *Nature Medicine*, **1995**, *1*, 1046

53. Fujioka, T.; Kashiwada, Y.; Kilkuskie, R.E.; Cosentino, L.M.; Ballas, L.M.; Jiang, J.B.; Janzen, W.P.; Chen, I-S. and Lee, K-H., *J. Nat. Prod.*, **1994**, *57*, 243

54. Cruz, A. and Silva, M., *Phytochemistry*, **1973**, *12*, 2549

55. Silva, M.; Wiesenfeld, A.; Sammes, P.G. and Tyler, T.W., *Phytochemistry*, **1977**, *16*, 379

56. Nair,A.G.R. and Silvakumar, R., *Phytochemistry*, **1992**, *31*, 671

57. Zilnik, R.; Rabenhorst, E.; Matida, A.K. and Gottlieb, H.E., *Phytochemistry*, **1978**, *17*, 1795

58 Wenkert, E. and Buckwalter, B.L., *J. Am. Chem. Soc.*, **1972**, *94*, 4367

59 Kelecom, A. and Dos Santos, T.C., *Tetrahedron*, **1985**, *26*, 3659

60 Kubota, T.; Matsuura, T.; Tsutsui,T.; Uyeo, S.; Irie, H.; Numata, A. and Fujita, T., *Tetrahedron*, **1966**, *22*, 1659

61 Majetich, G. and Zhang, U., *J. Am. Chem. Soc.*, **1994**, *116*, 4979

62. St. Jacques M.and Vaziri, C., *Org. Magn. Reson.*, **1972**, *4*, 77

63. Fabian, A. and Germishuizen, G., *Transvaal Wild Flowers*, Johannesburg: Macmillan South Africa, **1982**

64. Letty, C., *Wild Flowers of the Transvaal*, published by the Trustees: Wild Flowers of the Transvaal Book Fund, **1962**

65. Van Wyk, B.; Malan, S. and Lowrey, T.K., *Field Guide to the Wild Flowers of the Witwatersrand and Pretoria area*, Cape Town, Struik, **1988**

66. Ranganathan, K.R. and Sechadri, T.R., *Tetrahedron Letters*, **1973**, *36*, 3481

67. Parthasarathy, M.R.; Ranganathan, K.R. and Sharma, D.K., *Phytochemistry*, **1979**, *18*, 506

68. Dictionary of Natural Products, Chapman & Hall, **1994**

Appendix

spectrum 1 ^{1}H NMR spectrum of **30**

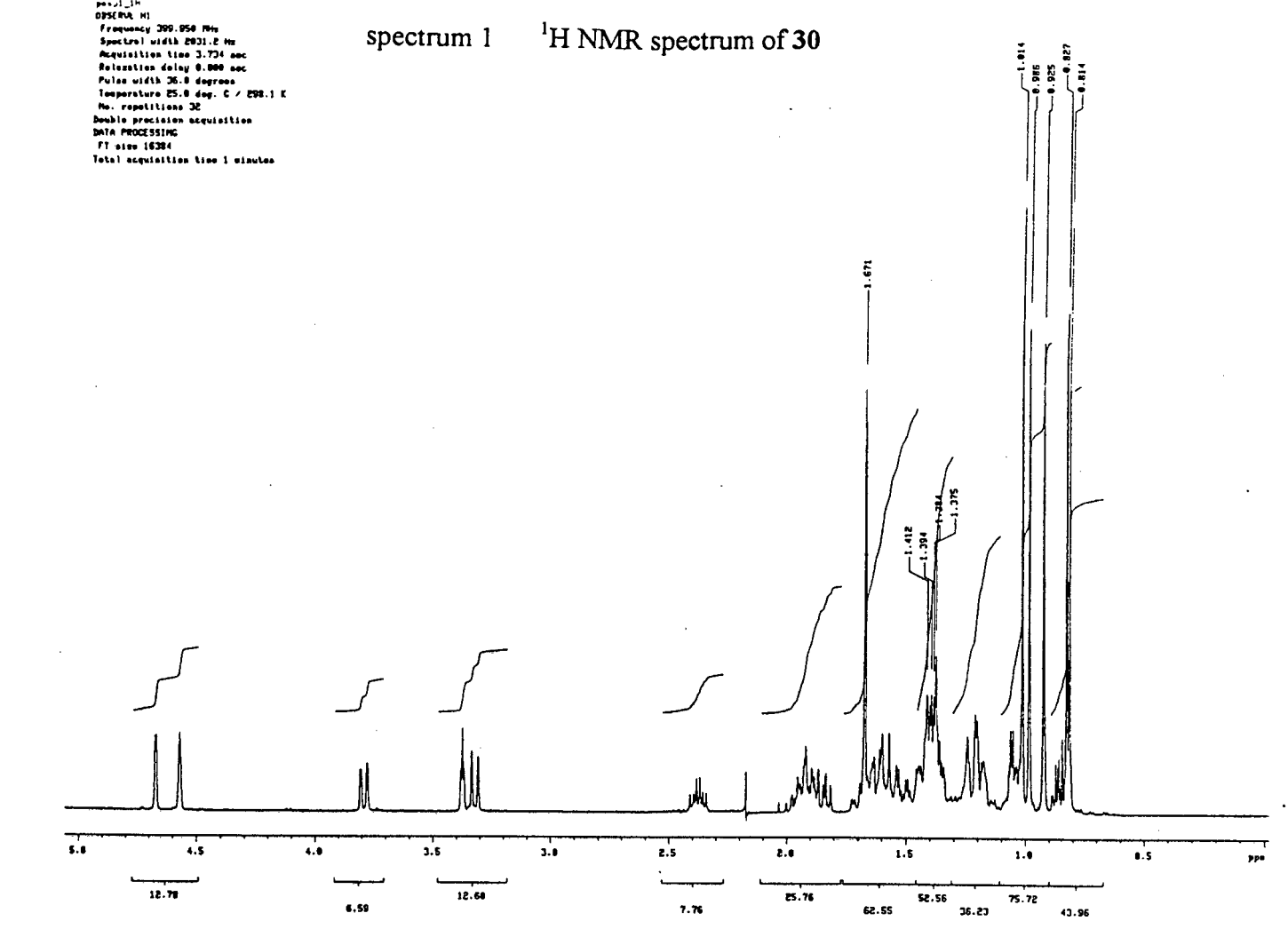

spectrum 2 ^{13}C NMR spectrum of **30**

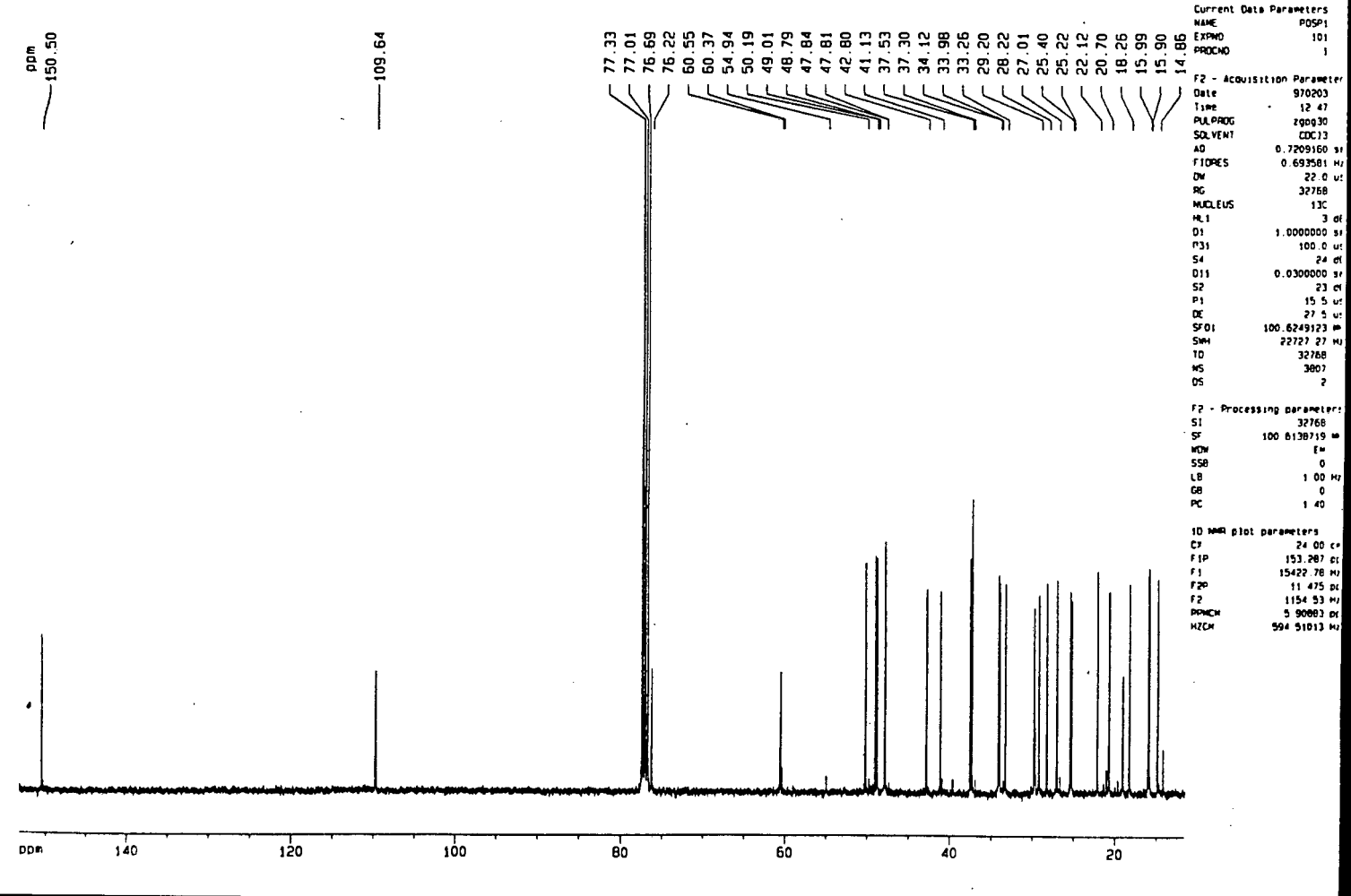

spectrum 3 DETP spectrum of **30**

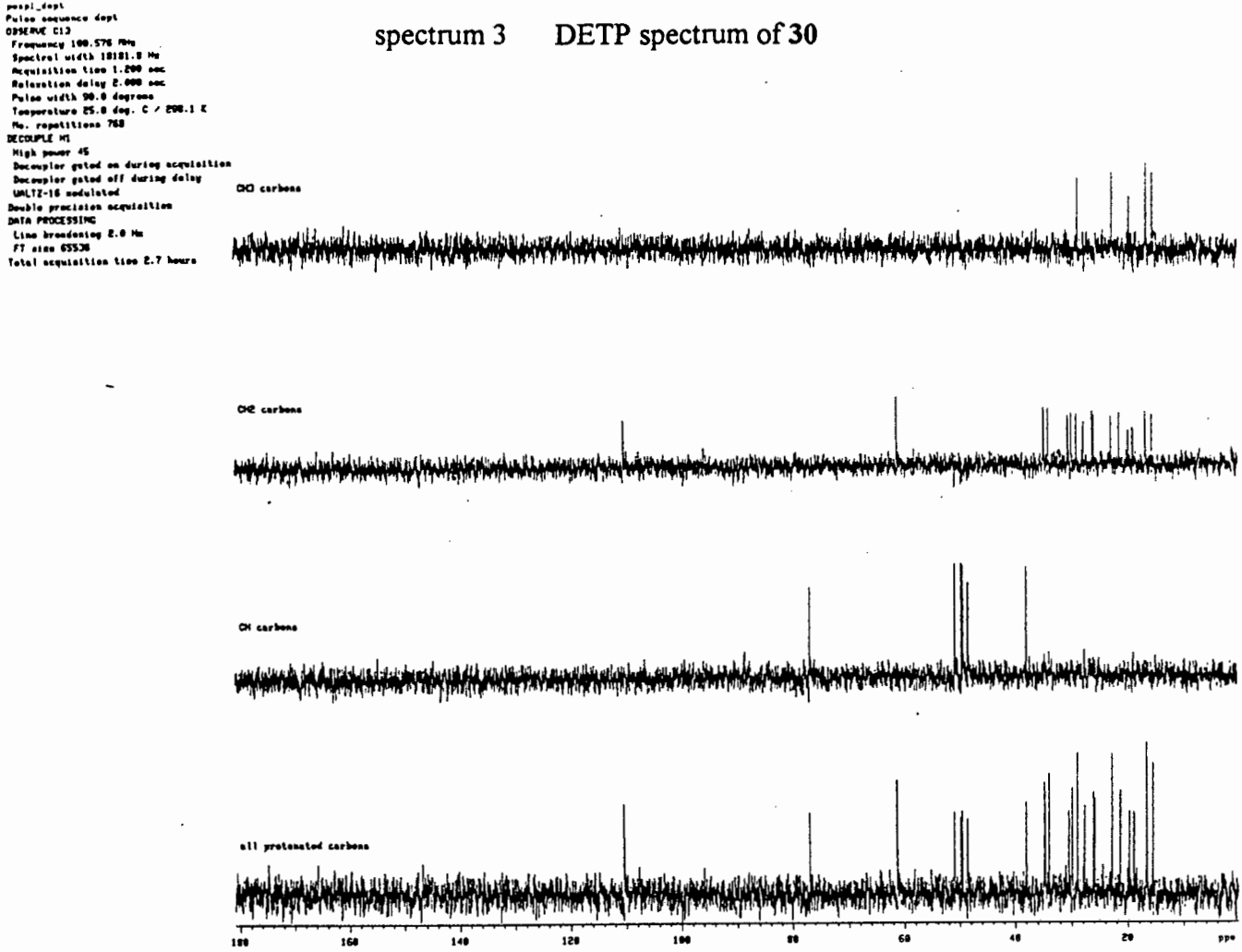

spectrum 4 COSY spectrum of **30**

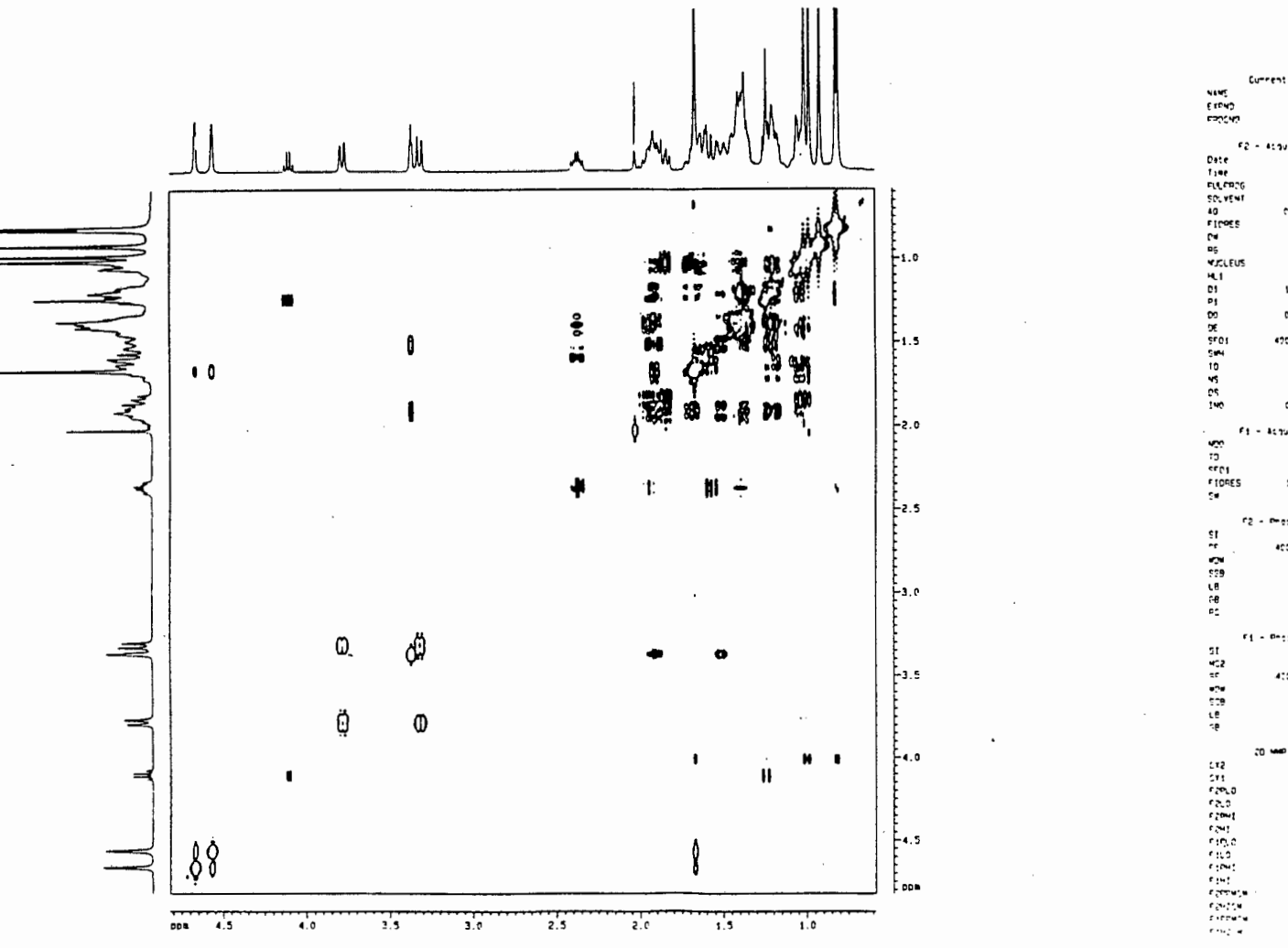

spectrum 5 HMQC spectrum of **30**

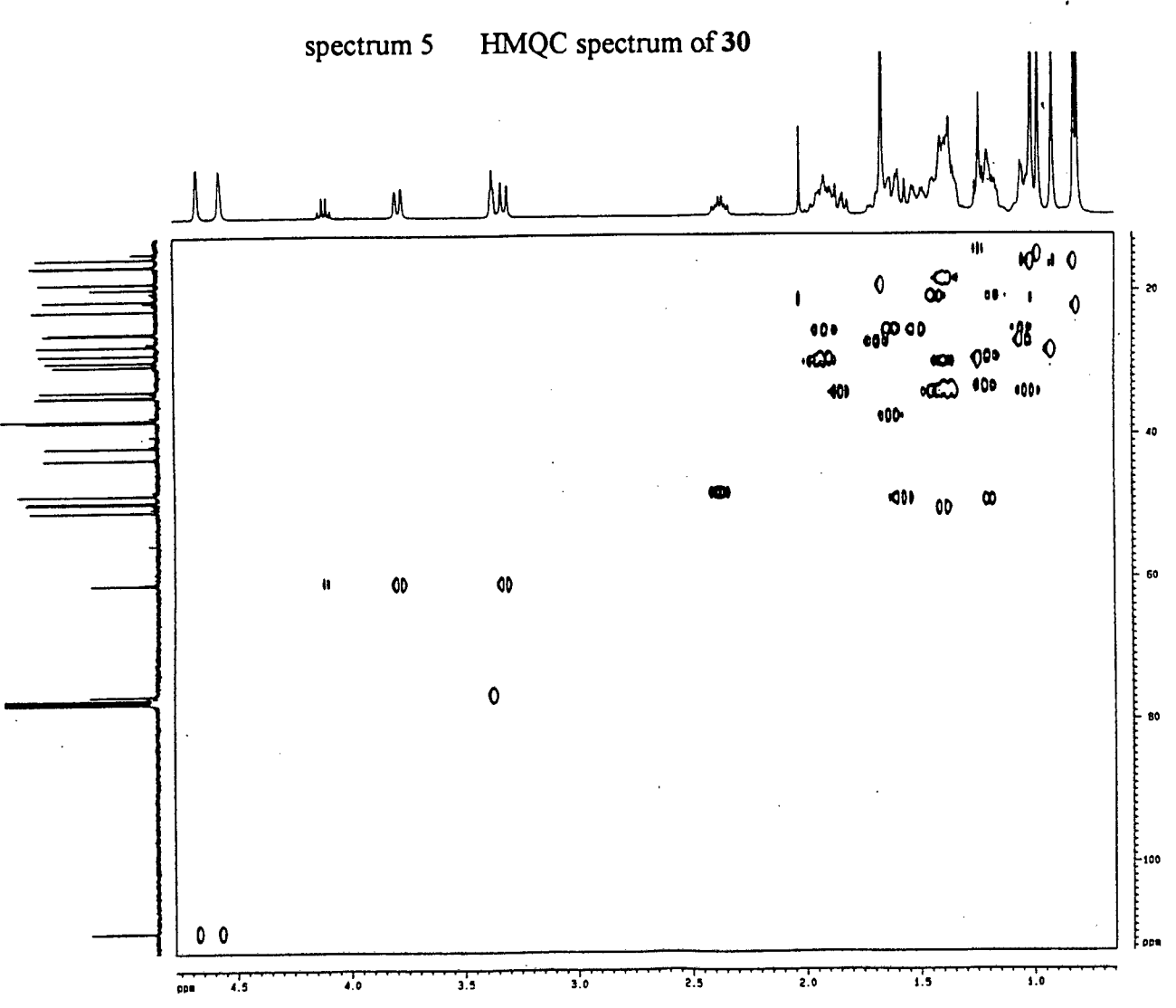

spectrum 6 HMBC spectrum of **30**

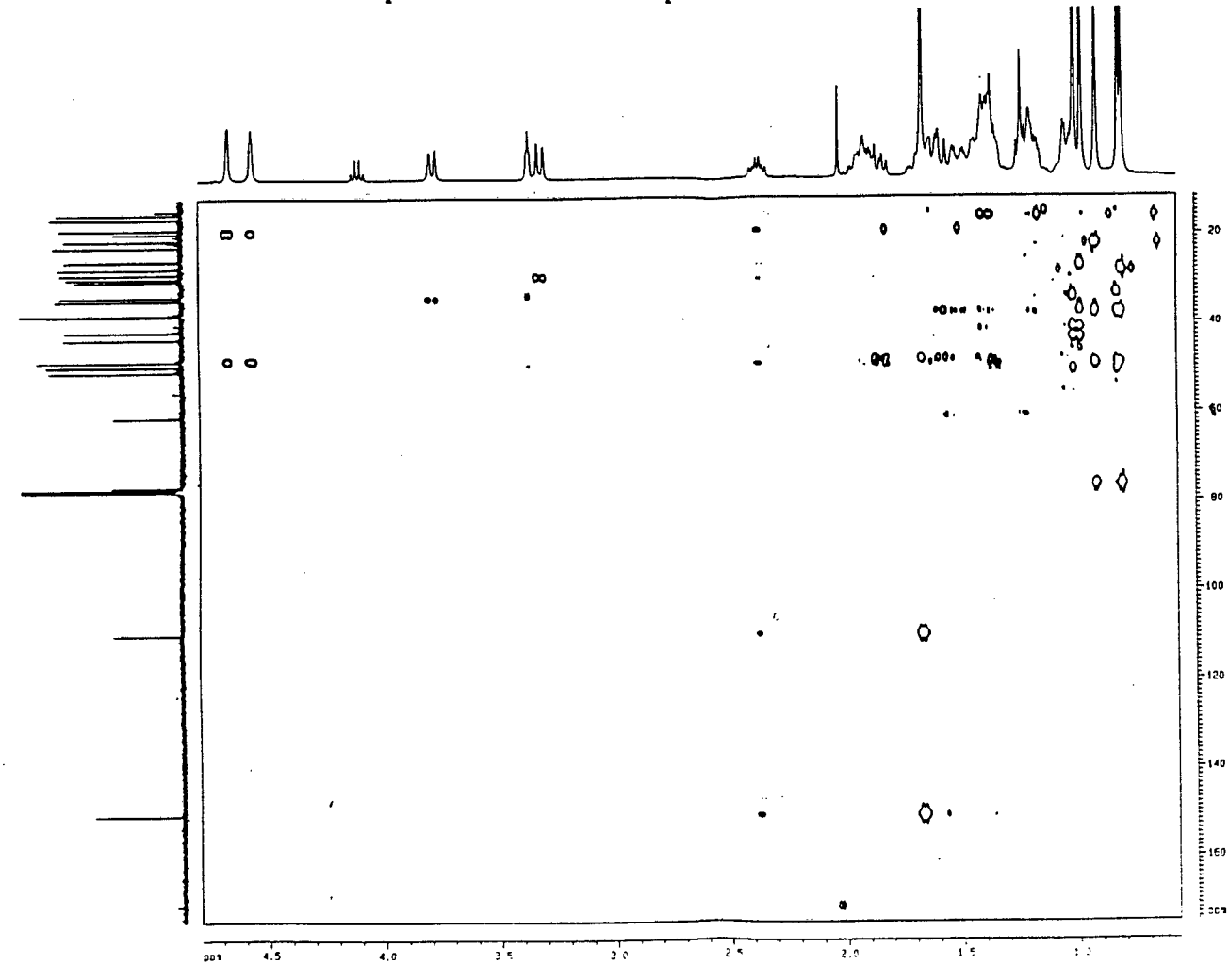

spectrum 7 NOESY spectrum of 30

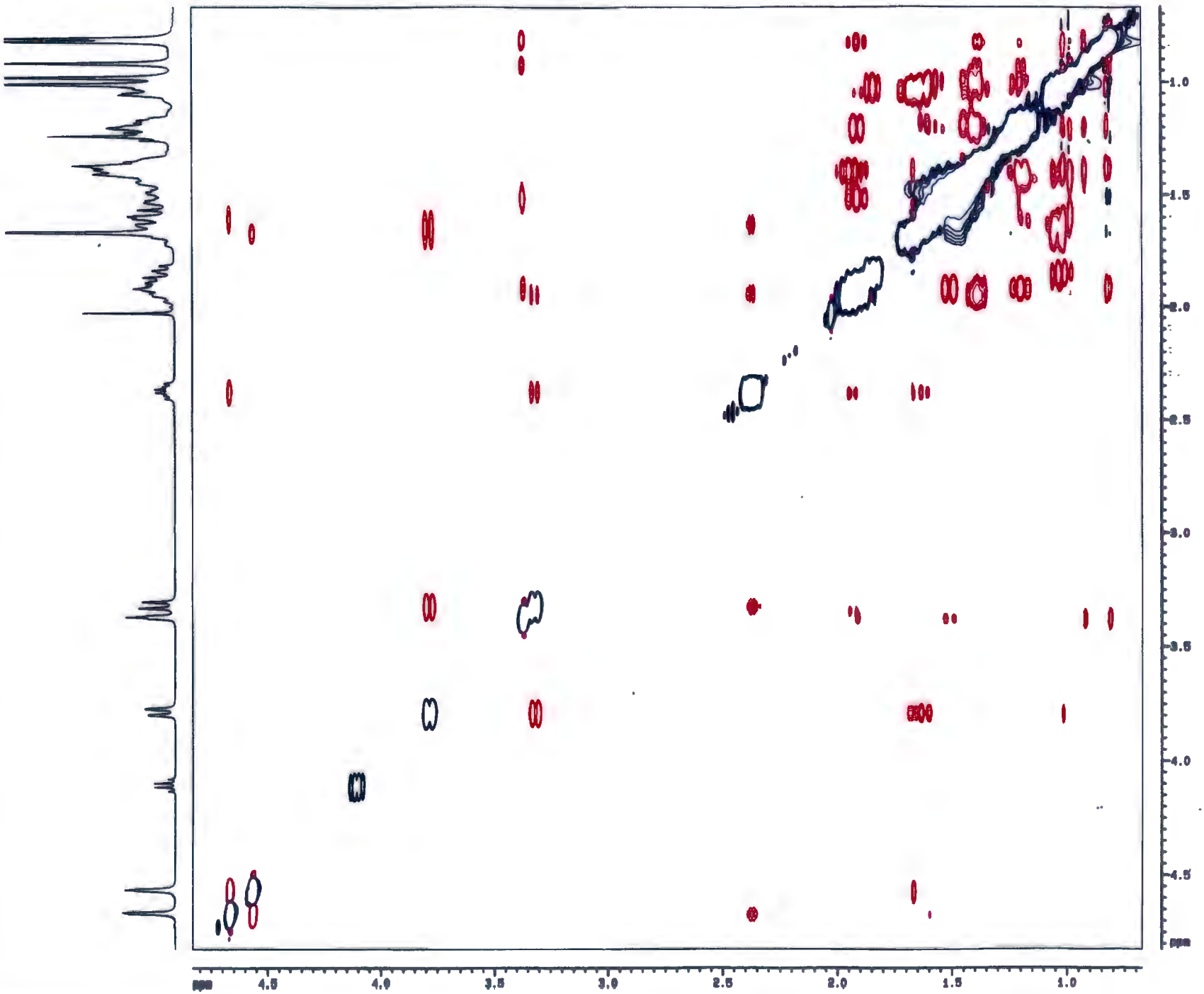

Current Data Parameters

NAME	POSP1
EXPNO	106
PROCNO	1

F2 - Acquisition Parameters

Date	970310
Time	22.27
PULPROG	noesytp
SOLVENT	CDCl3
AQ	0.3195080 sec
FIDRES	1.565004 Hz
DW	156.0 usec
RG	64
NUCLEUS	1H
HL1	1 dB
D1	2.0000000 sec
P1	13.4 usec
D0	0.0000030 sec
D8	0.8000000 sec
DE	222.9 usec
SFO1	400.1360000 MHz
SWH	3205.13 Hz
TD	2048
NS	48
DS	4
INO	0.0001562 sec

F1 - Acquisition parameters

NDO	2
TD	256
SFO1	400.136 MHz
FIDRES	12.504250 Hz
SW	8.000 ppm

F2 - Processing parameters

SI	2048
SF	400.1343970 MHz
WDW	QSINE
SSB	2
LB	0.00 Hz
GB	0
PC	1.40

F1 - Processing parameters

SI	1024
MC2	TPPI
SF	400.1343951 MHz
WDW	QSINE
SSB	2
LB	0.00 Hz
GB	0

2D NMR plot parameters

CX2	25.00 cm
CX1	25.00 cm
F2PLO	4.831 ppm
F2LO	1933.16 Hz
F2PHI	0.674 ppm
F2HI	269.58 Hz
F1PLO	4.823 ppm
F1LO	1930.05 Hz
F1PHI	0.667 ppm
F1HI	266.98 Hz
F2PPMCM	0.16630 ppm/cm
F2HZCM	66.54398 Hz/cm
F1PPMCM	0.16625 ppm/cm
F1HZCM	66.52251 Hz/cm

spectrum 8 ^{1}H NMR spectrum of **32**

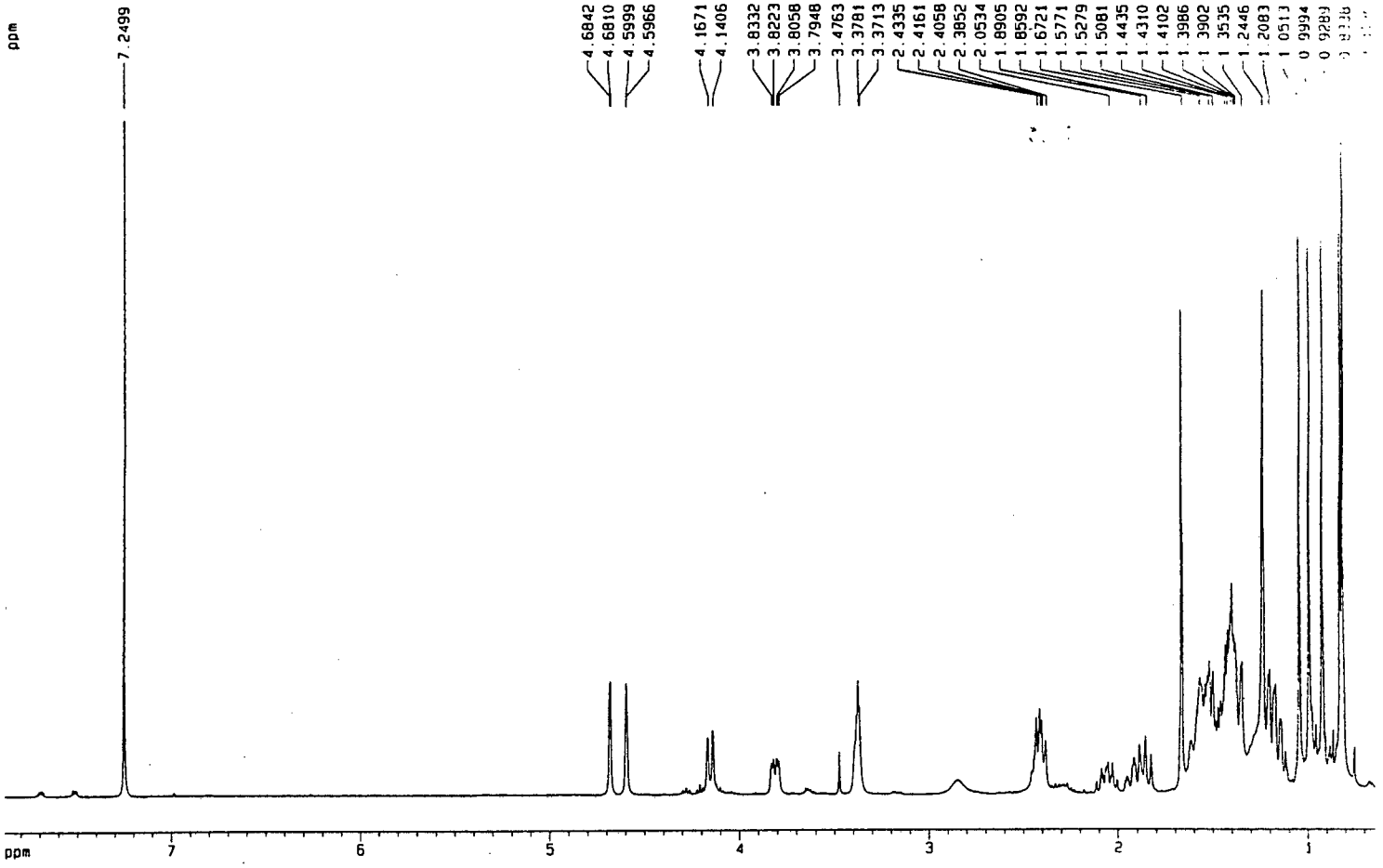

spectrum 9 ^{13}C NMR spectrum of **32**

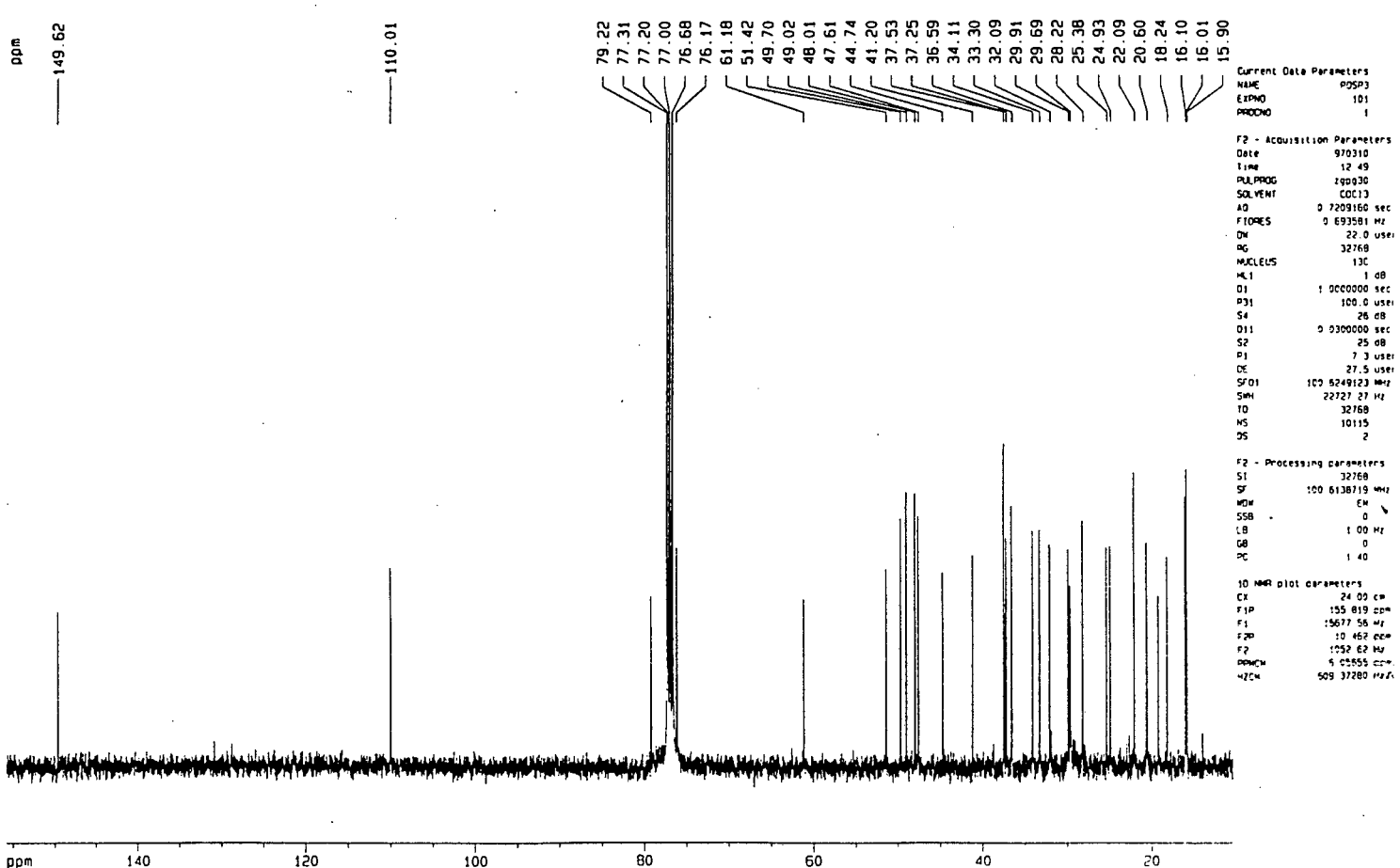

spectrum 10 DEPT spectrum of **32**

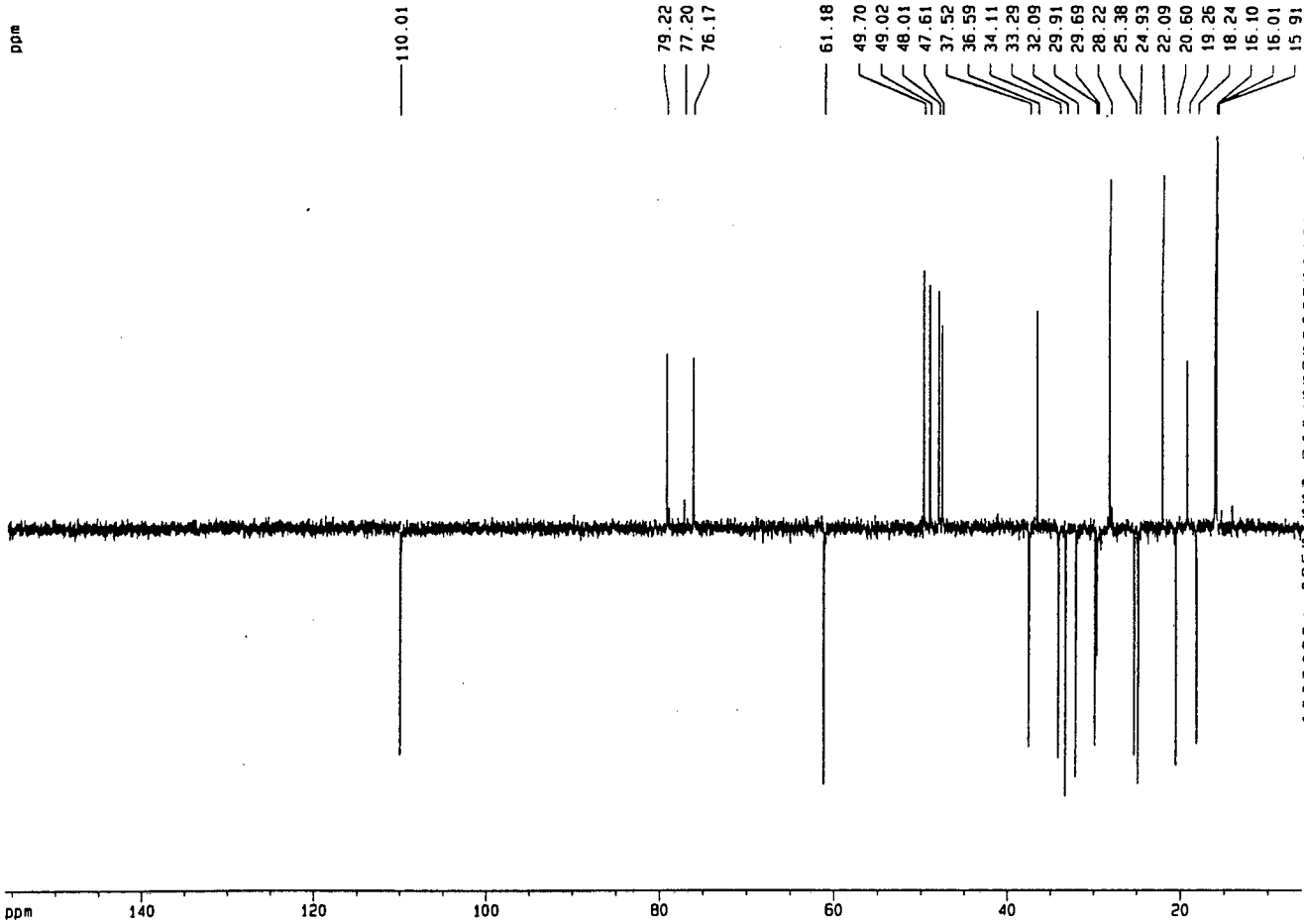

spectrum 11 COSY spectrum of **32**

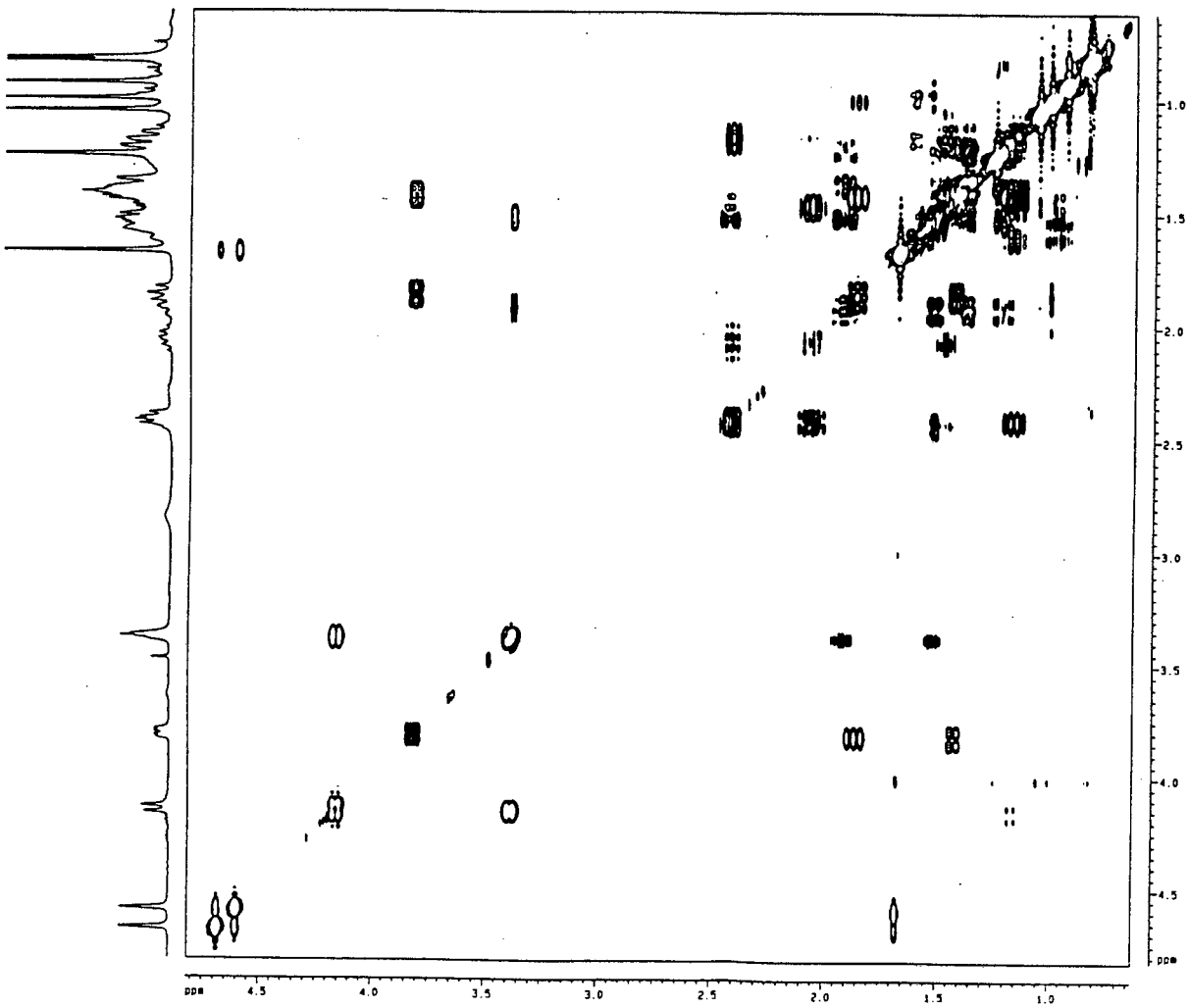

spectrum 12 HMQC spectrum of **32**

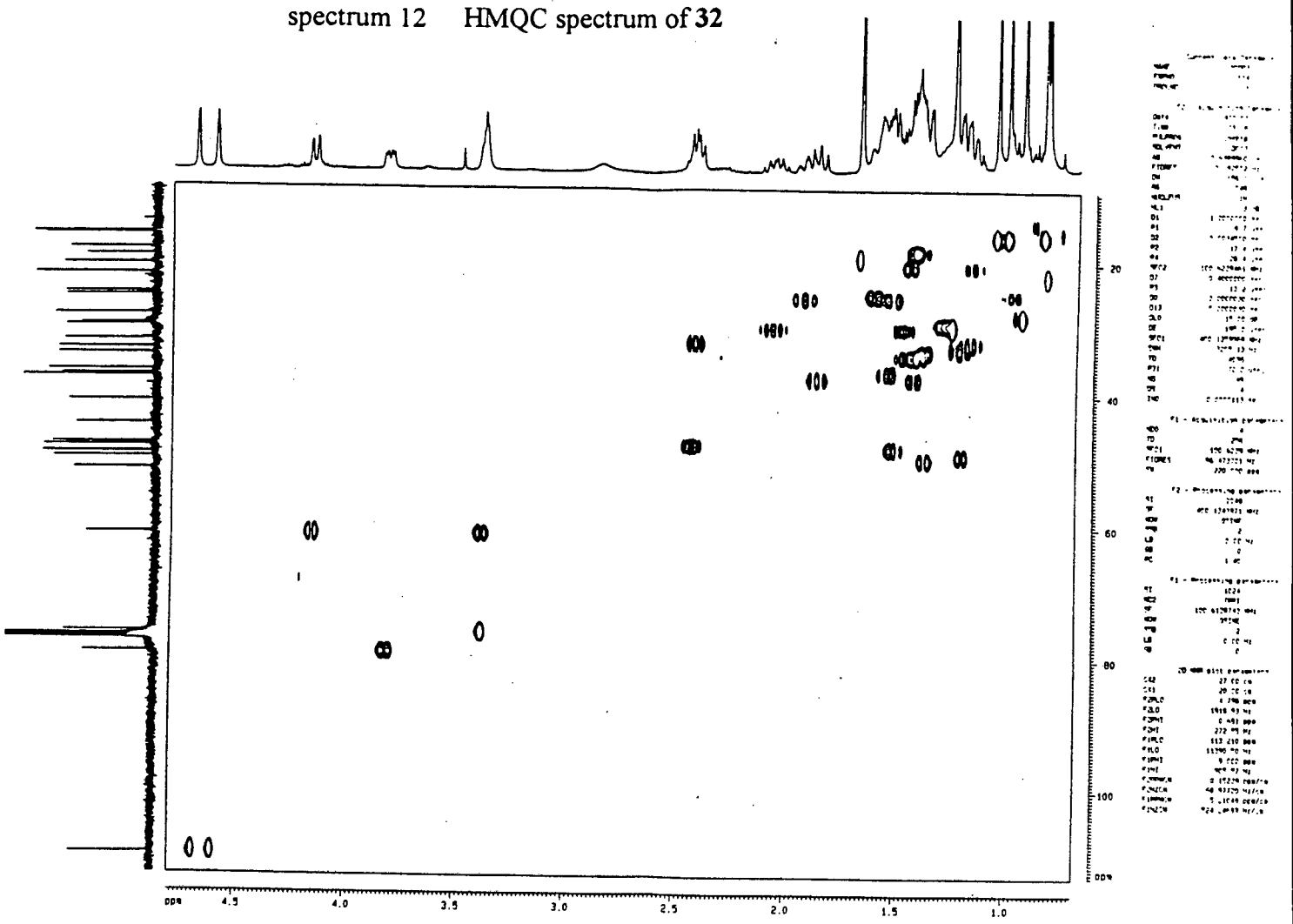

spectrum 13 HMBC spectrum of **32**

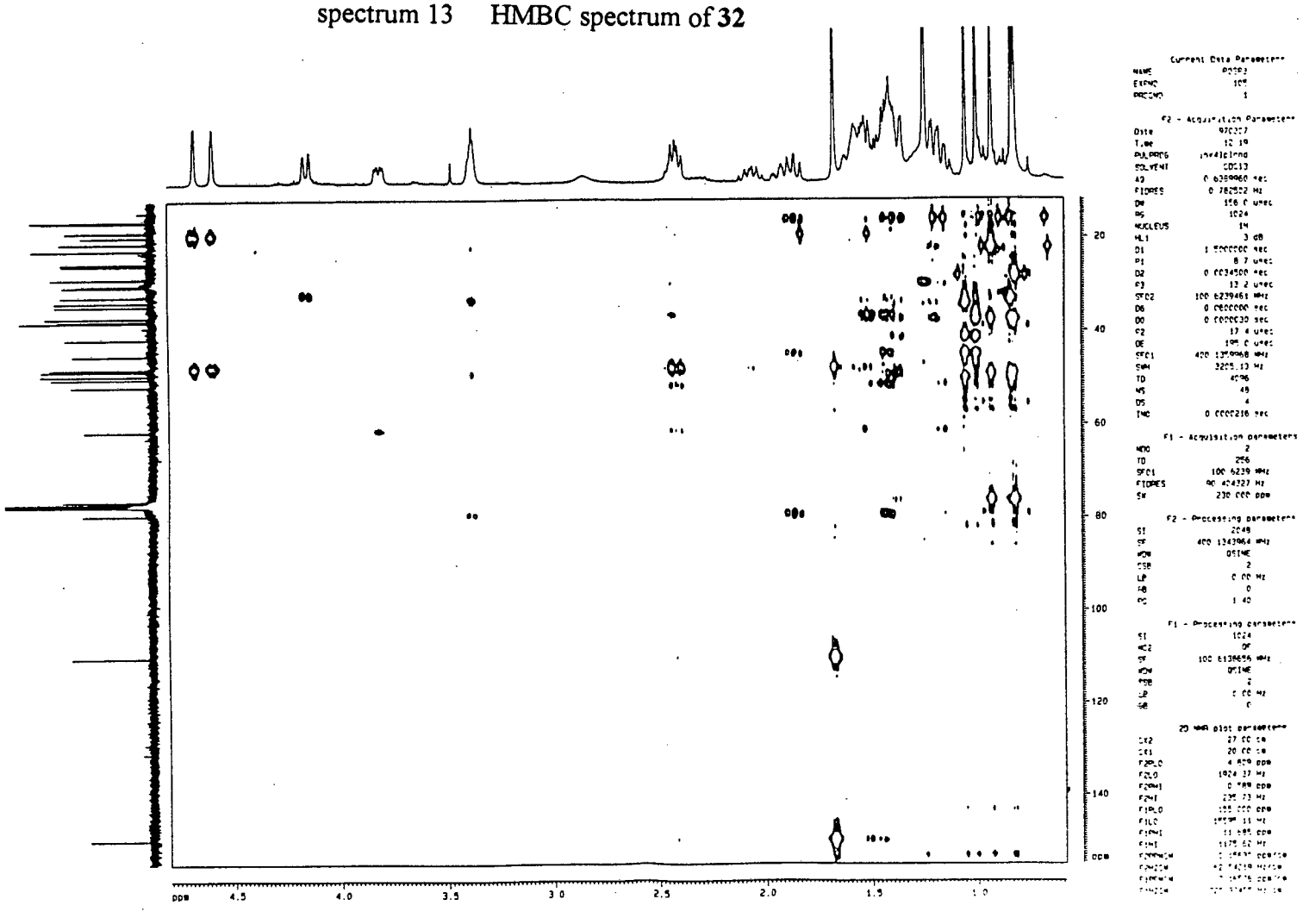

spectrum 14 NOESY spectrum of 32

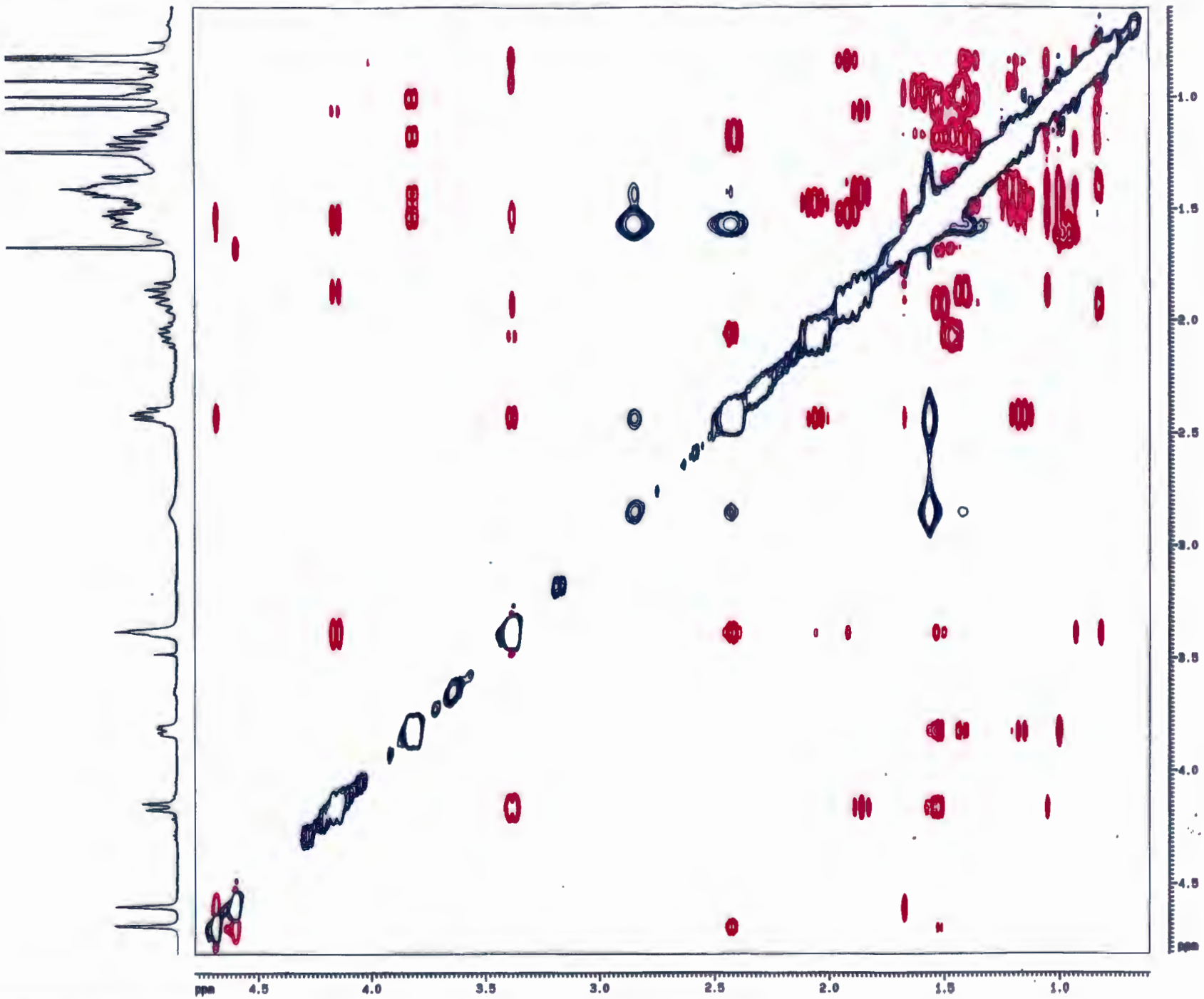

Current Data Parameters

NAME	POSP3
EXPNO	106
PROCNO	1

F2 - Acquisition Parameters

Date	970407
Time	11.51
PULPROG	noesytp
SOLVENT	CDCl3
AQ	0.2826440 sec
FIDRES	1.769135 Hz
DW	138.0 usec
RG	256
NUCLEUS	1H
NL1	3 dB
D1	1.5000000 sec
P1	8.8 usec
D0	0.0000030 sec
DB	0.8000000 sec
DE	197.1 usec
SFO1	400.1360000 MHz
SWH	3623.19 Hz
TD	2048
NS	32
DS	4
IN0	0.0001380 sec

F1 - Acquisition parameters

ND0	2
TD	256
SFO1	400.136 MHz
FIDRES	14.153091 Hz
SW	9.055 ppm

F2 - Processing parameters

SI	2048
SF	400.1343970 MHz
WDW	QSINE
SSB	2
LB	0.00 Hz
GB	0
PC	1.00

F1 - Processing parameters

SI	1024
MC2	TPPI
SF	400.1343948 MHz
WDW	QSINE
SSB	2
LB	0.00 Hz
GB	0

2D NMR plot parameters

CX2	25.00 cm
CX1	25.00 cm
F2PL0	4.780 ppm
F2L0	1912.59 Hz
F2PHI	0.611 ppm
F2HI	244.29 Hz
F1PL0	4.807 ppm
F1L0	1923.61 Hz
F1PHI	0.598 ppm
F1HI	239.40 Hz
F2PPMCM	0.16677 ppm/cm
F2HZCM	66.73177 Hz/cm
F1PPMCM	0.16837 ppm/cm
F1HZCM	67.36872 Hz/cm

spectrum 15 ^{1}H NMR spectrum of **42**

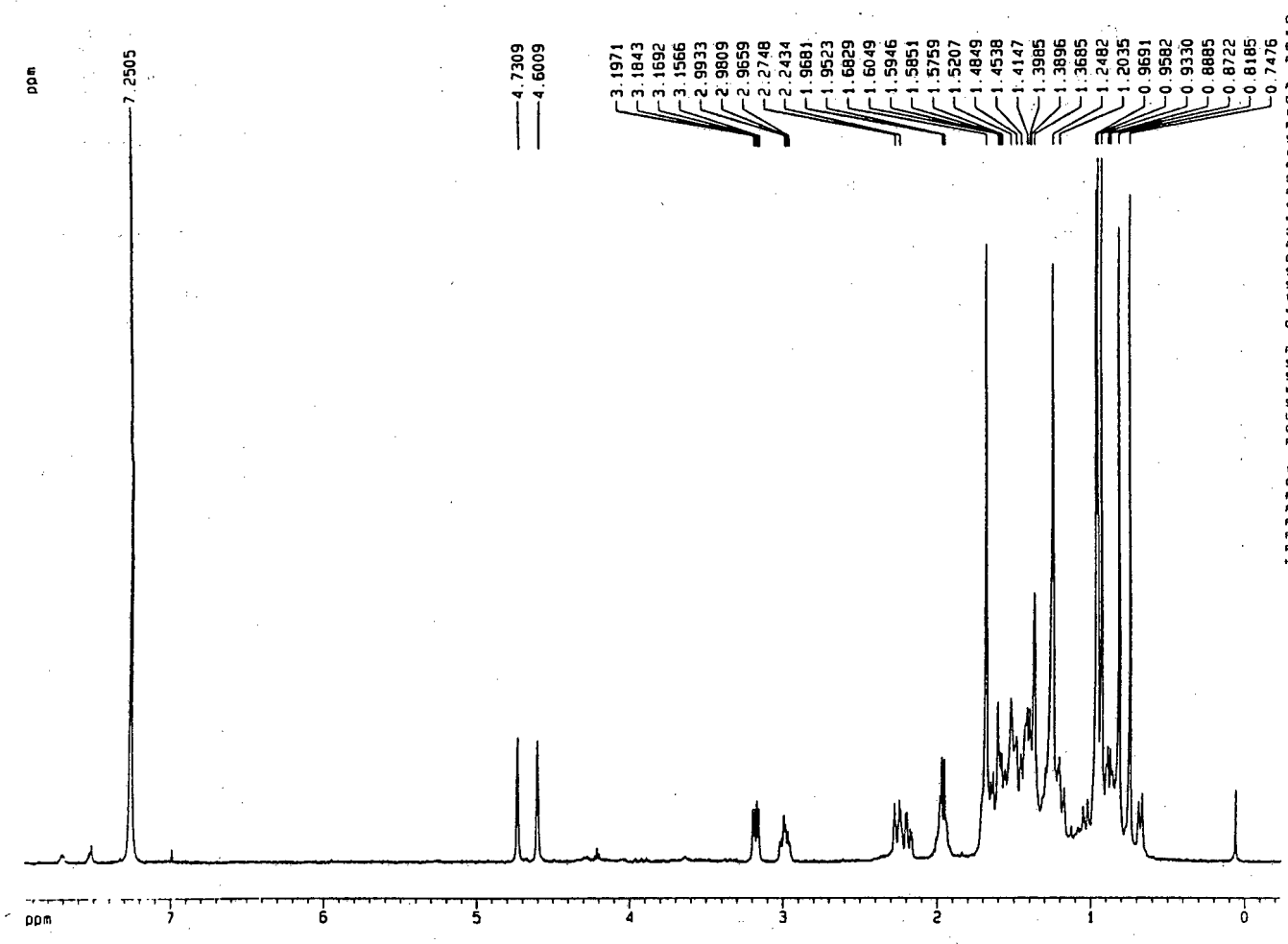

spectrum 16 ^{13}C NMR spectrum of **42**

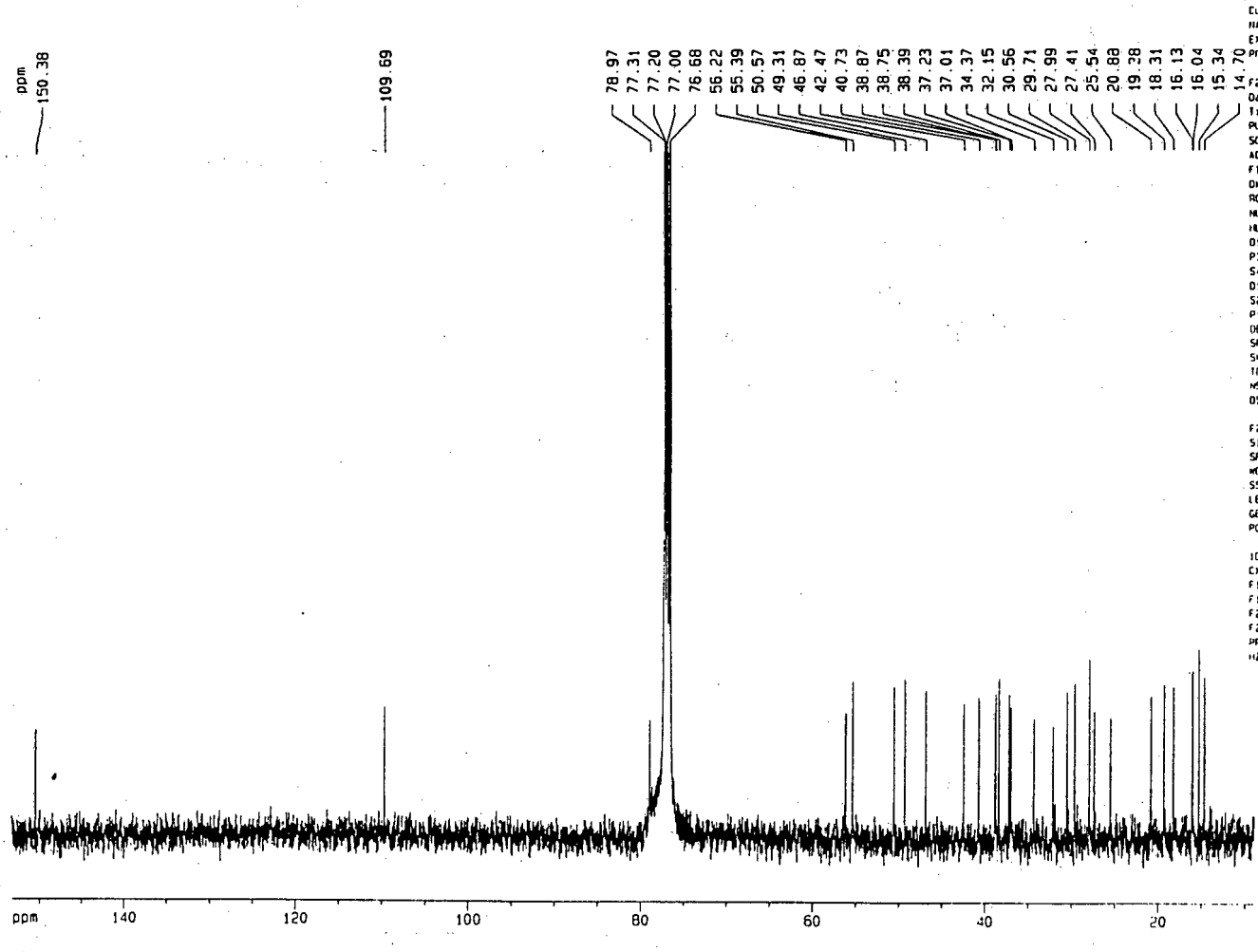

spectrum 17 COSY spectrum of **42**

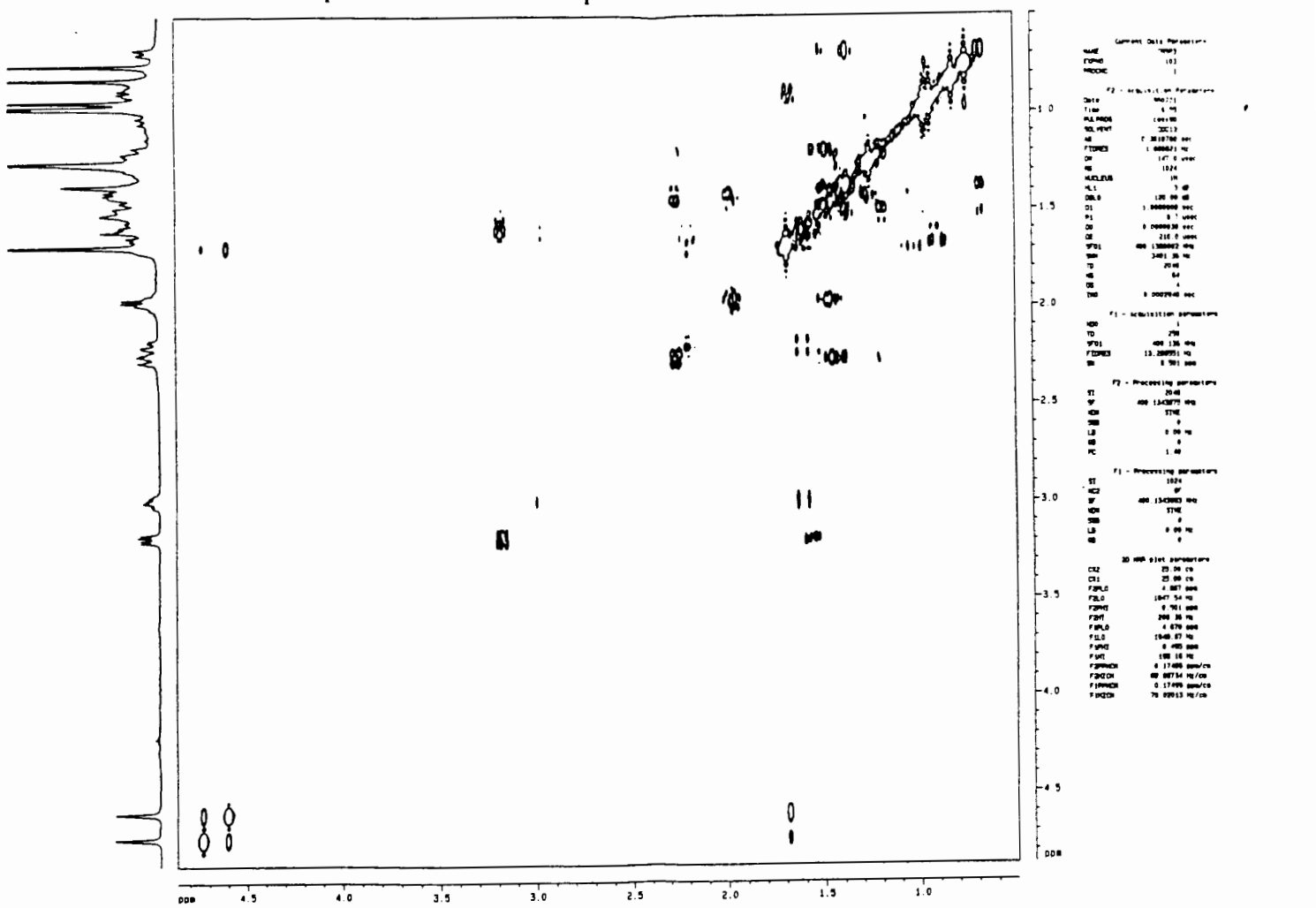

spectrum 18 HMQC spectrum of **42**

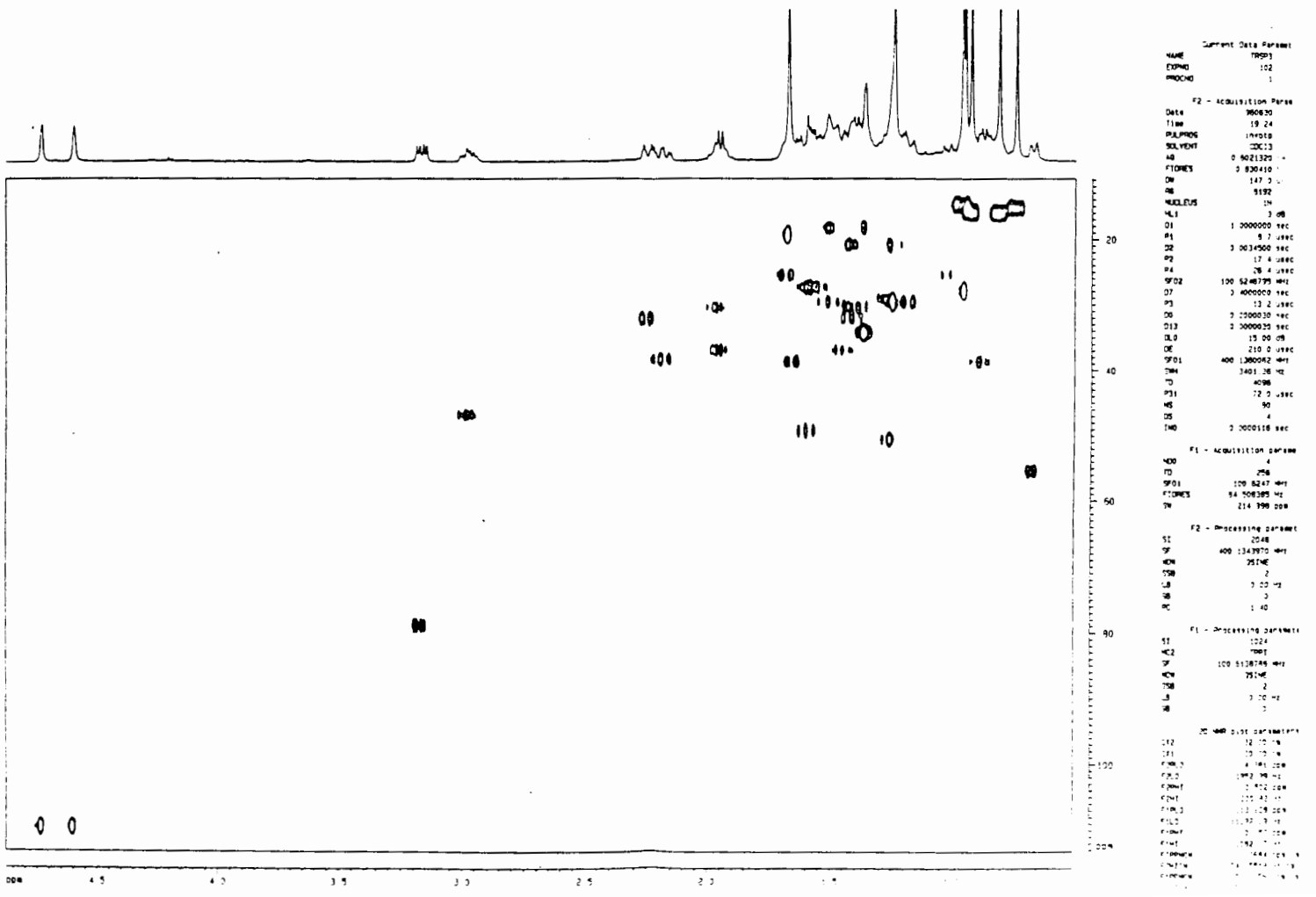

spectrum 19 HMBC spectrum of **42**

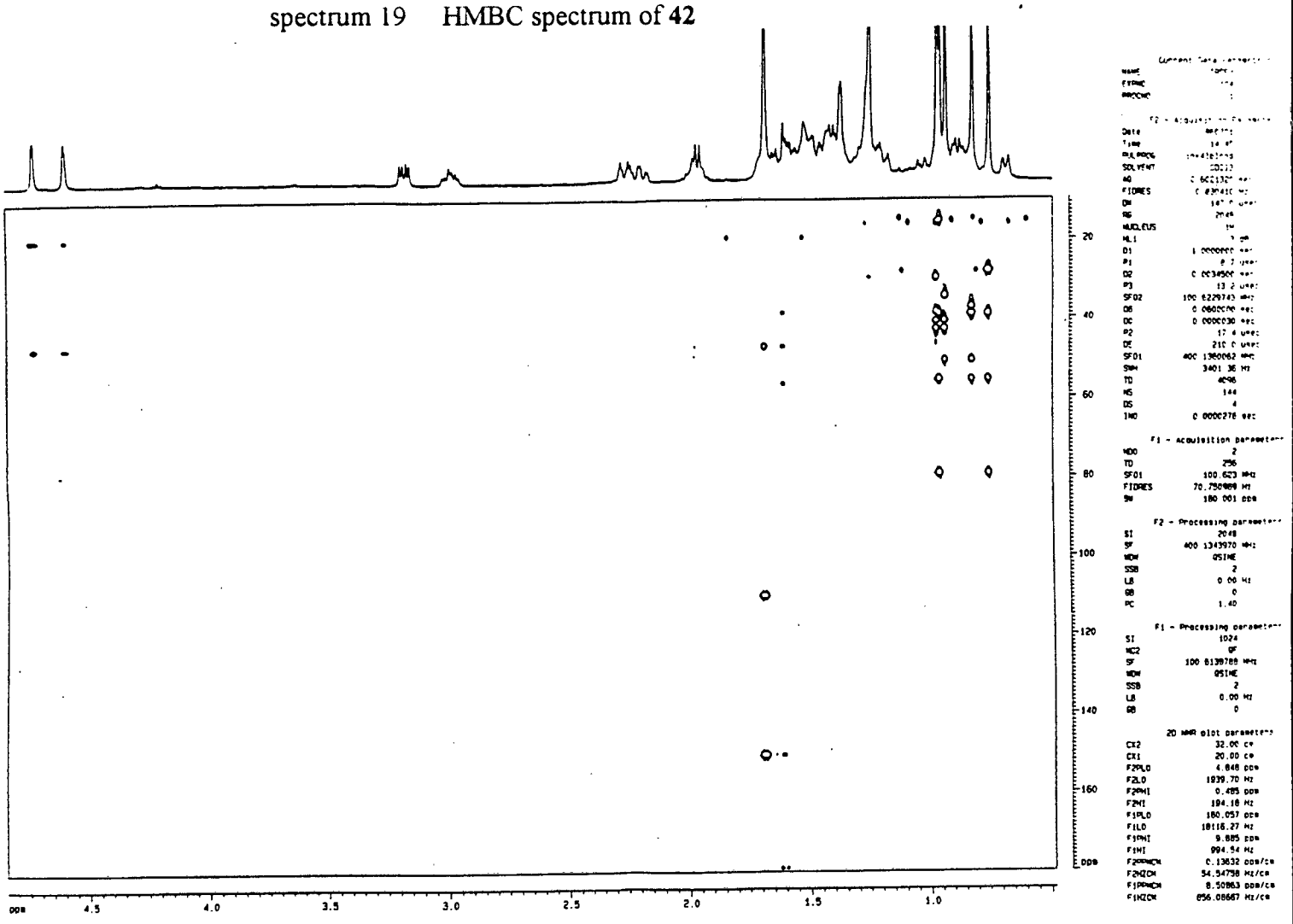

spectrum 20 ^{1}H NMR spectrum of **44**

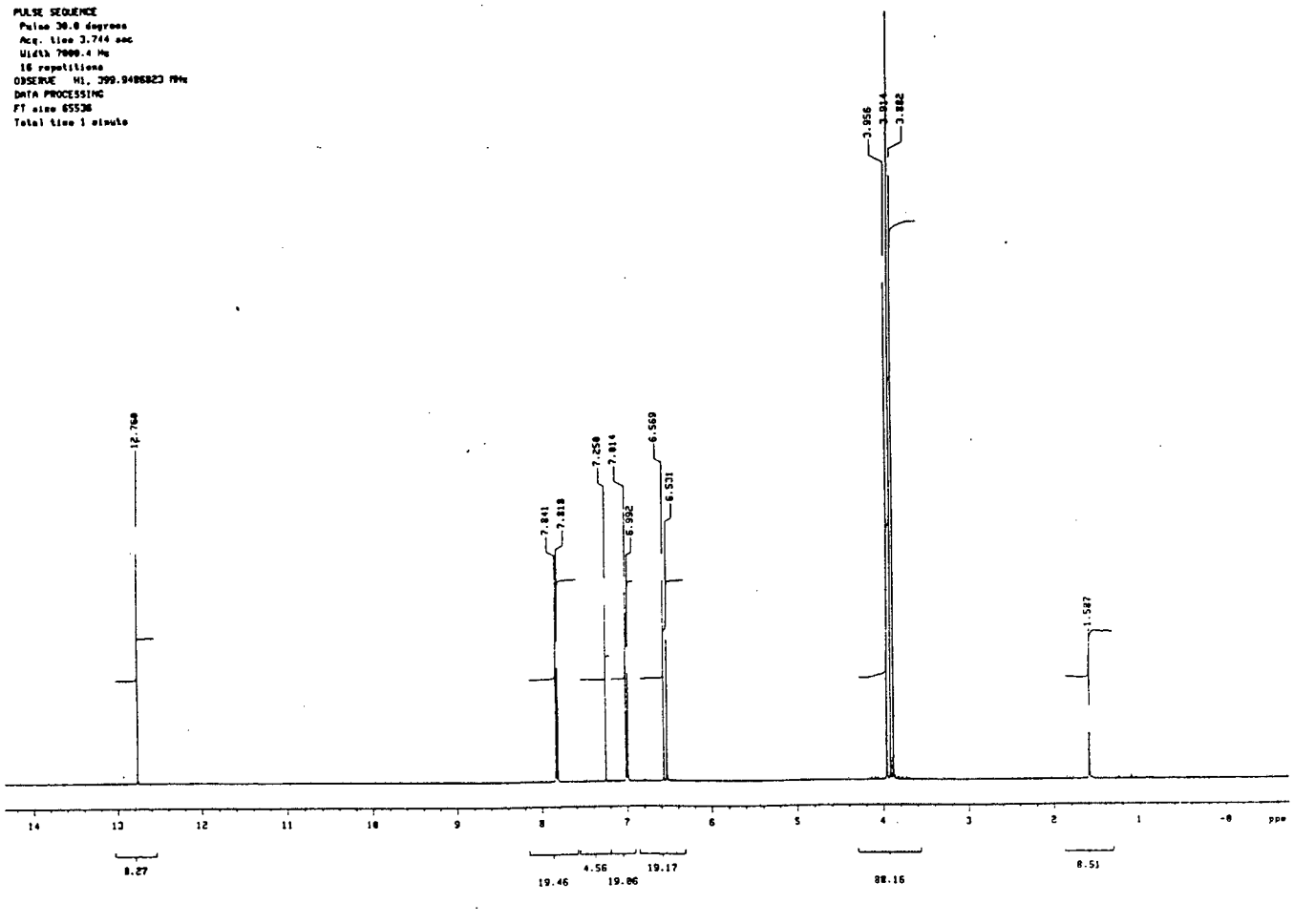

spectrum 21 ^{13}C NMR spectrum of **44**

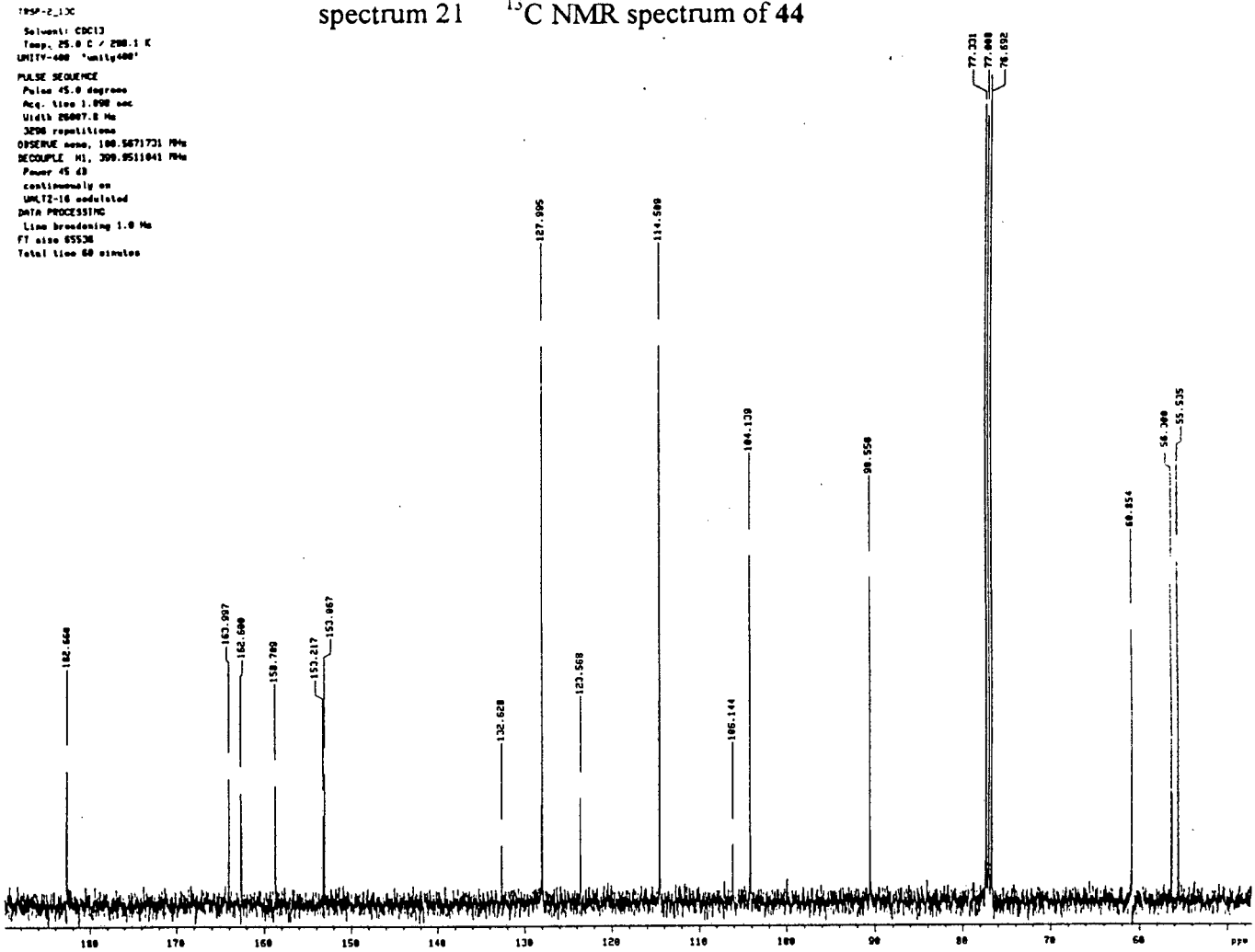

spectrum 22 COSY spectrum of **44**

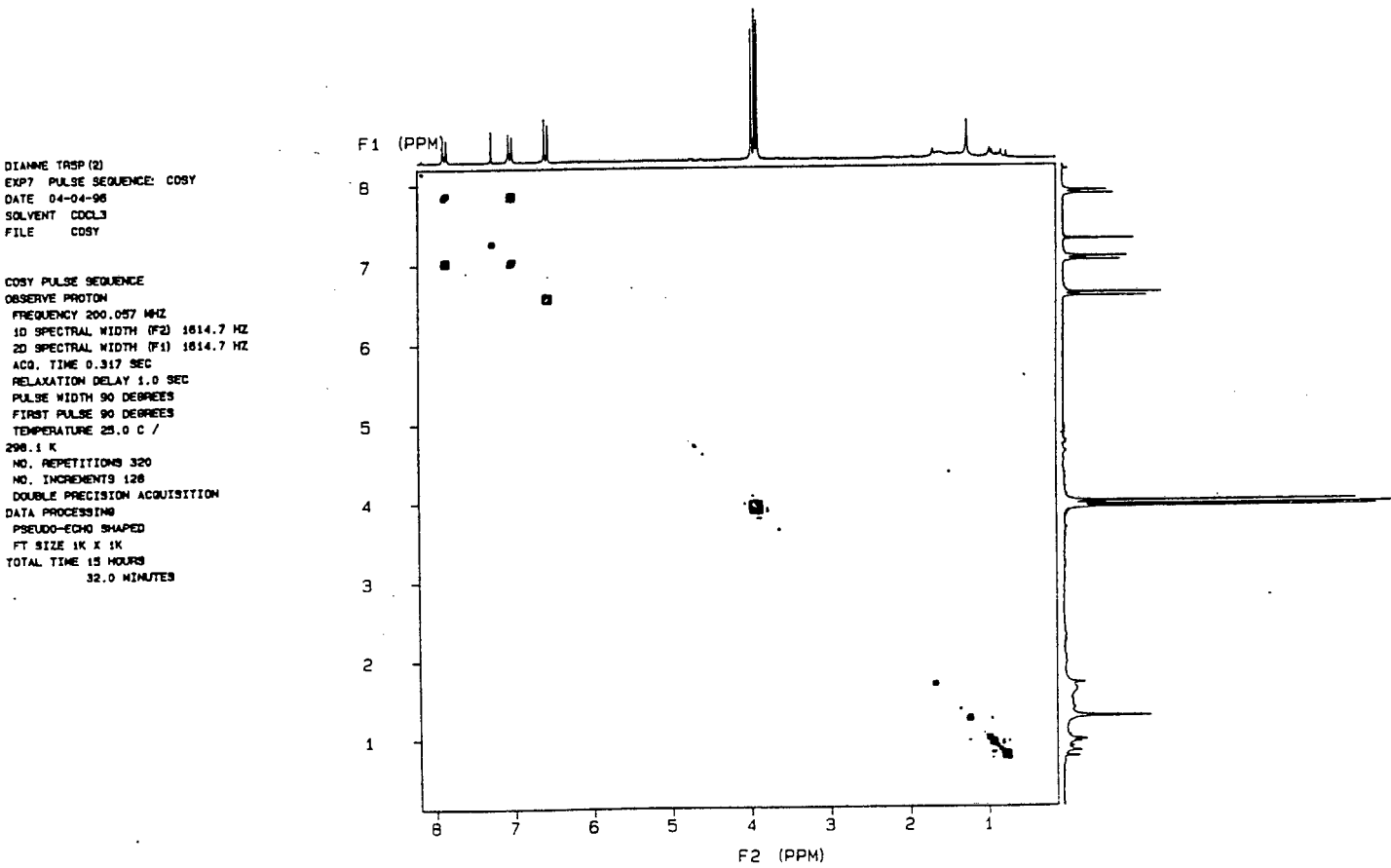

spectrum 23 HETCOR spectrum of **44**

```
TRSP_hetcor
  Solvent: CDCl3
  Temp. 25.0 C / 298.1 K
UNITY-400  'unity400'
PULSE SEQUENCE: hetcor
  Relax. delay 1.000 sec
  Acq. time 0.068 sec
  Width    15083.0 Hz
  2D Width 5027.7 Hz
  320 repetitions
  128 increments
OBSERVE nano, 100.5671718 MHz
DECOUPLE  H1, 399.9515371 MHz
  Power 45 dB
  on during acquisition
  off during delay
  WALTZ-16 modulated
DATA PROCESSING
  Sine bell 0.034 sec
F1 DATA PROCESSING
  Sine bell 0.018 sec
FT size 2048 x 1024
Total time 12.3 hours
```

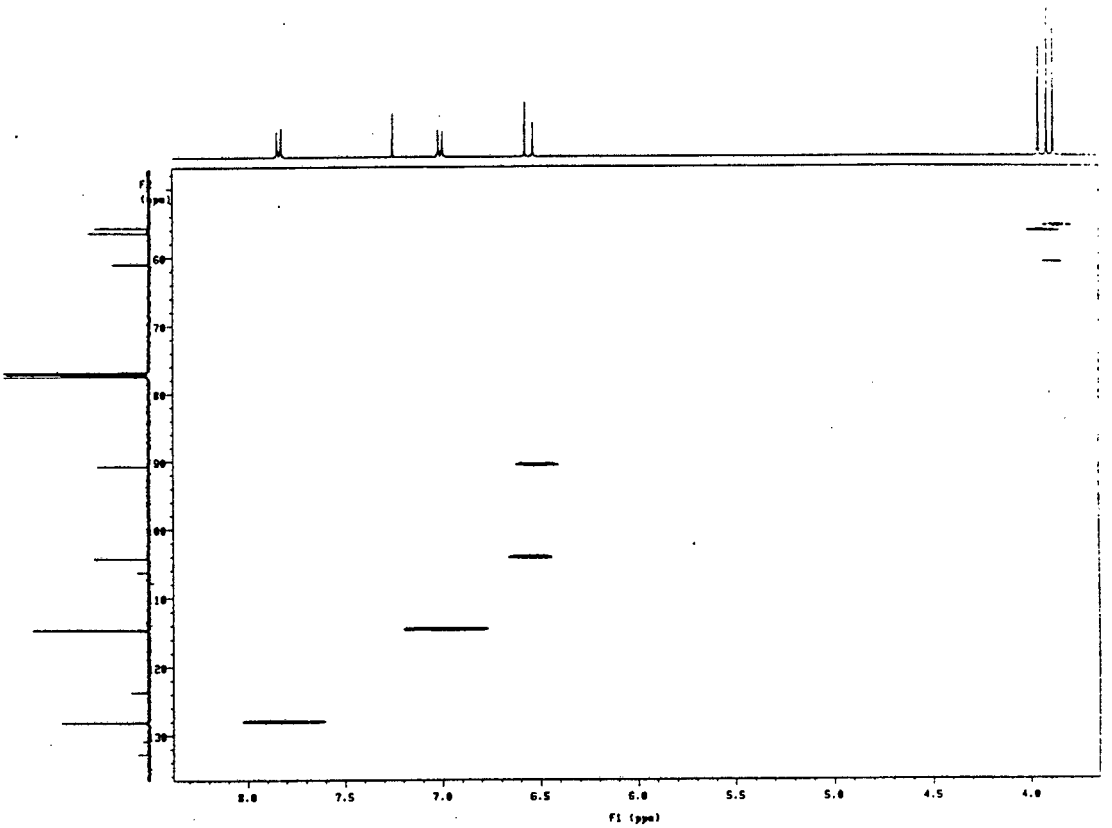

spectrum 24 NOESY spectrum of **44**

```
TRSP2_noesy
  Solvent: CDCl3
  Temp. 25.0 C / 298.1 K
UNITY-400  'unity400'
PULSE SEQUENCE: noesy
  Relax. delay 2.000 sec
  Mixing 0.200 sec
  Acq. time 0.245 sec
  Width    4175.4 Hz
  2D Width 4173.6 Hz
  8 repetitions
  2 x 128 increments
OBSERVE   H1, 399.9486772 MHz
DATA PROCESSING
  Line broadening 2.6 Hz
  Gauss window 0.089 sec
    center at 0.006 sec
  Sine bell 0.043 sec
    Shifted by -0.043 sec
F1 DATA PROCESSING
  Line broadening 4.5 Hz
  Gauss apodization 0.056 sec
  Sq. sine bell 0.012 sec
    Shifted by -0.012 sec
FT size 1024 x 1024
Total time 84 minutes
```

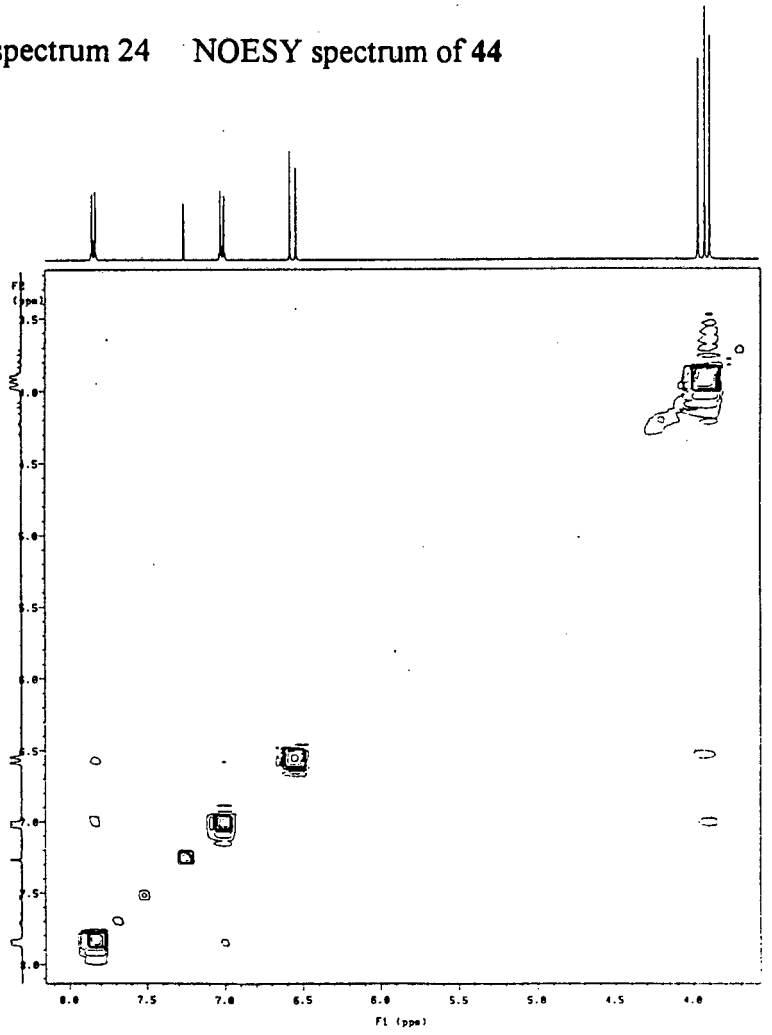

spectrum 25 ^{1}H NMR spectrum of **45**

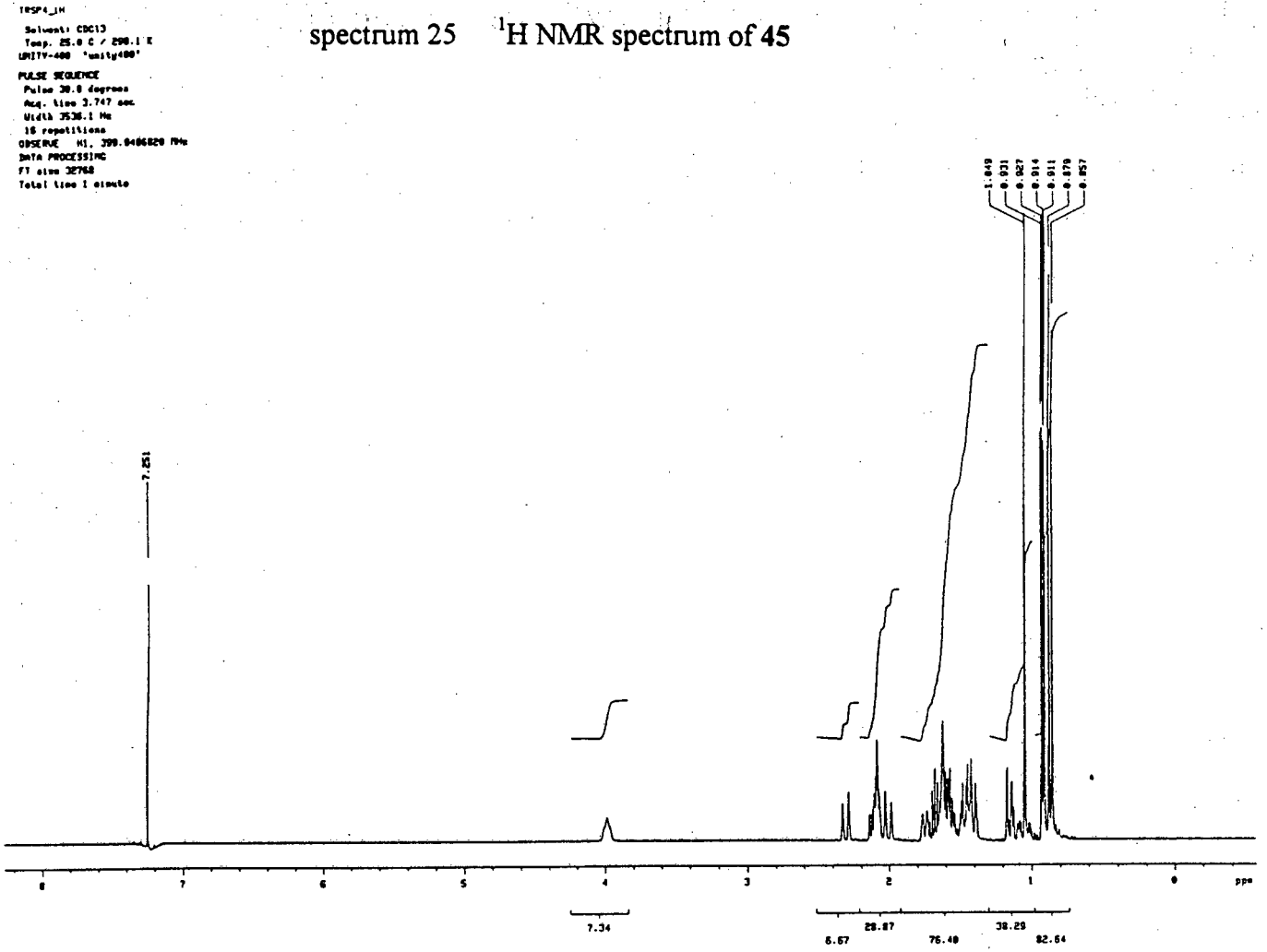

spectrum 26 ^{13}C NMR spectrum of **45**

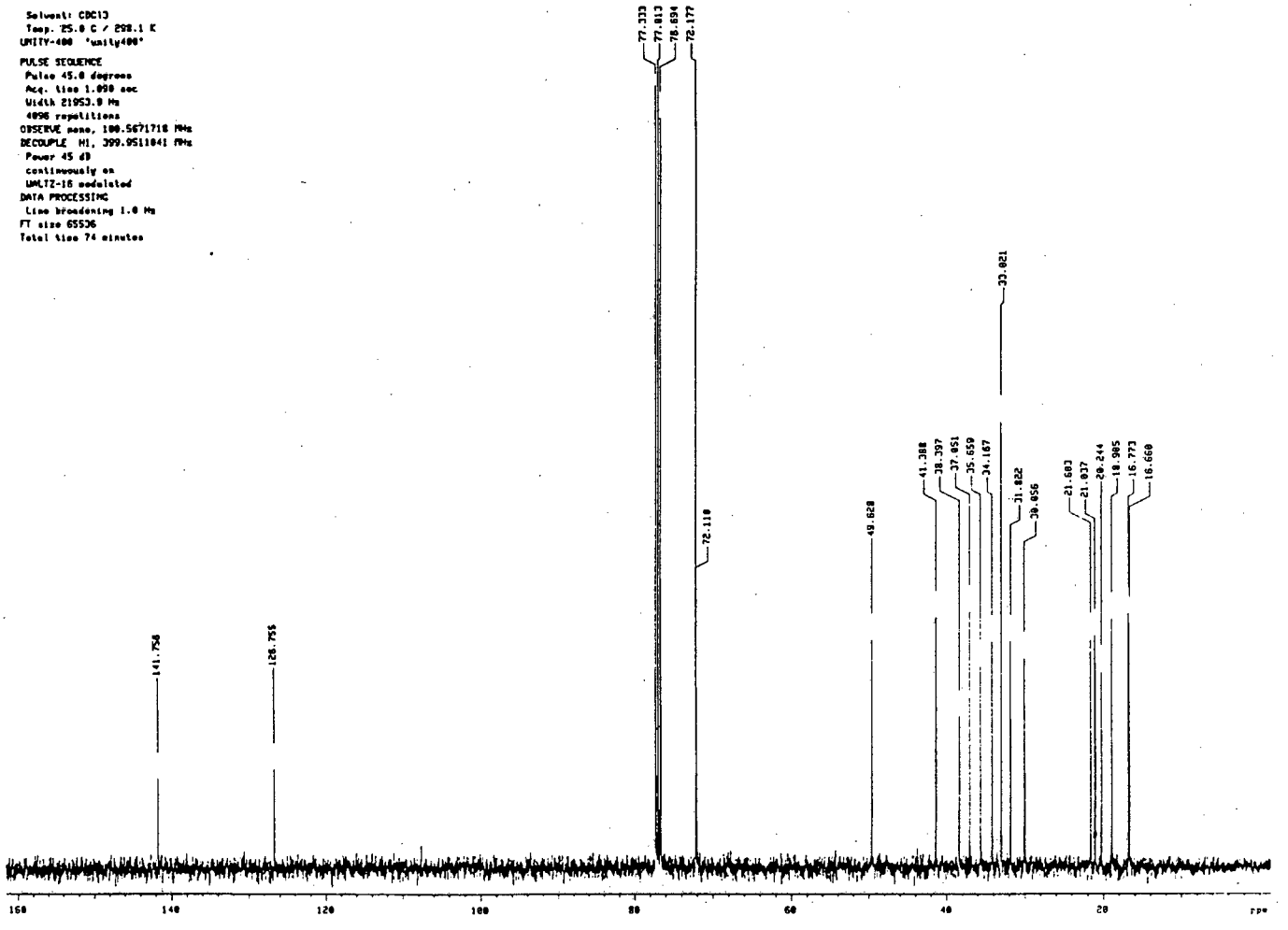

spectrum 27 HMQC spectrum of **45**

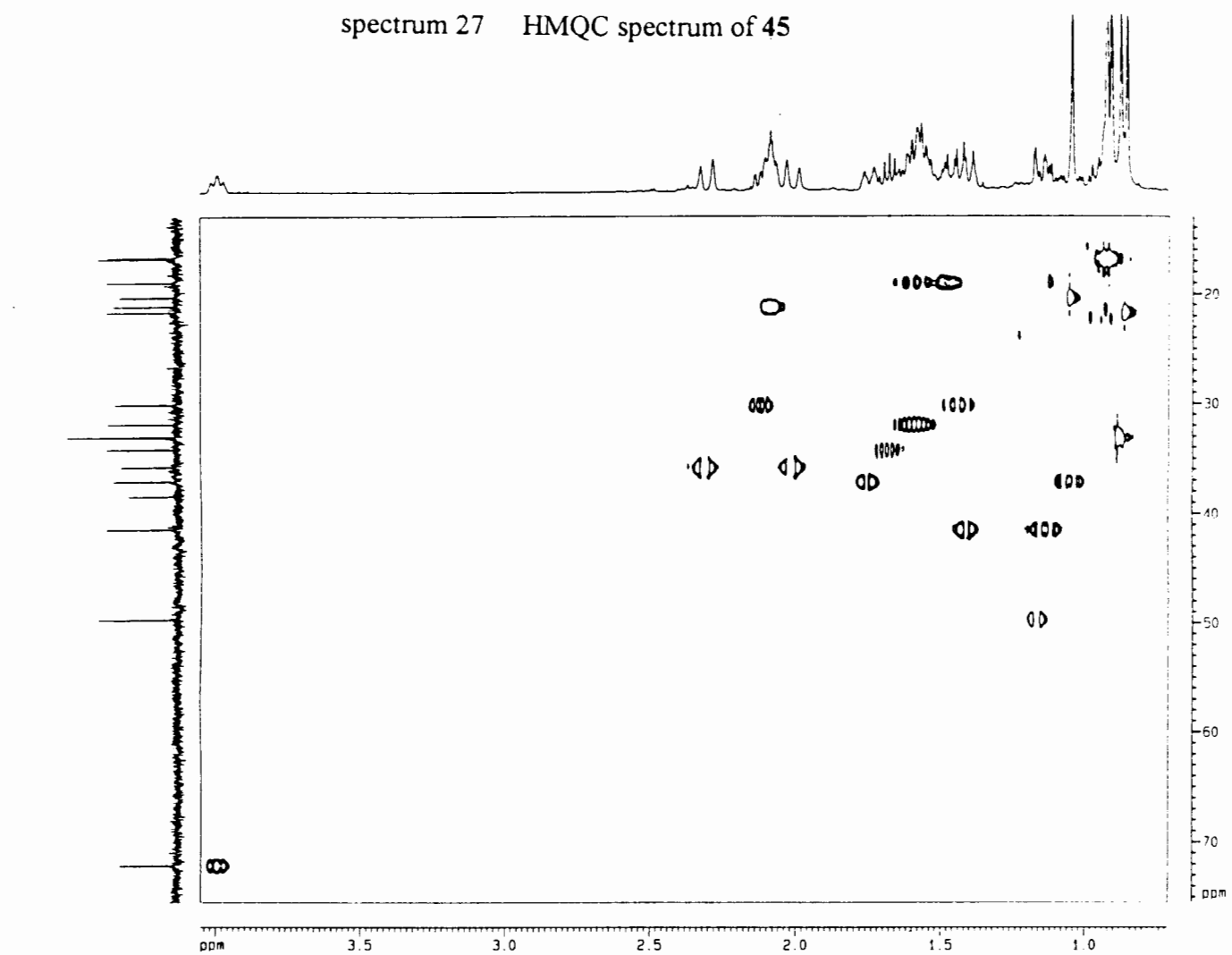

spectrum 28 HMBC spectrum of **45**

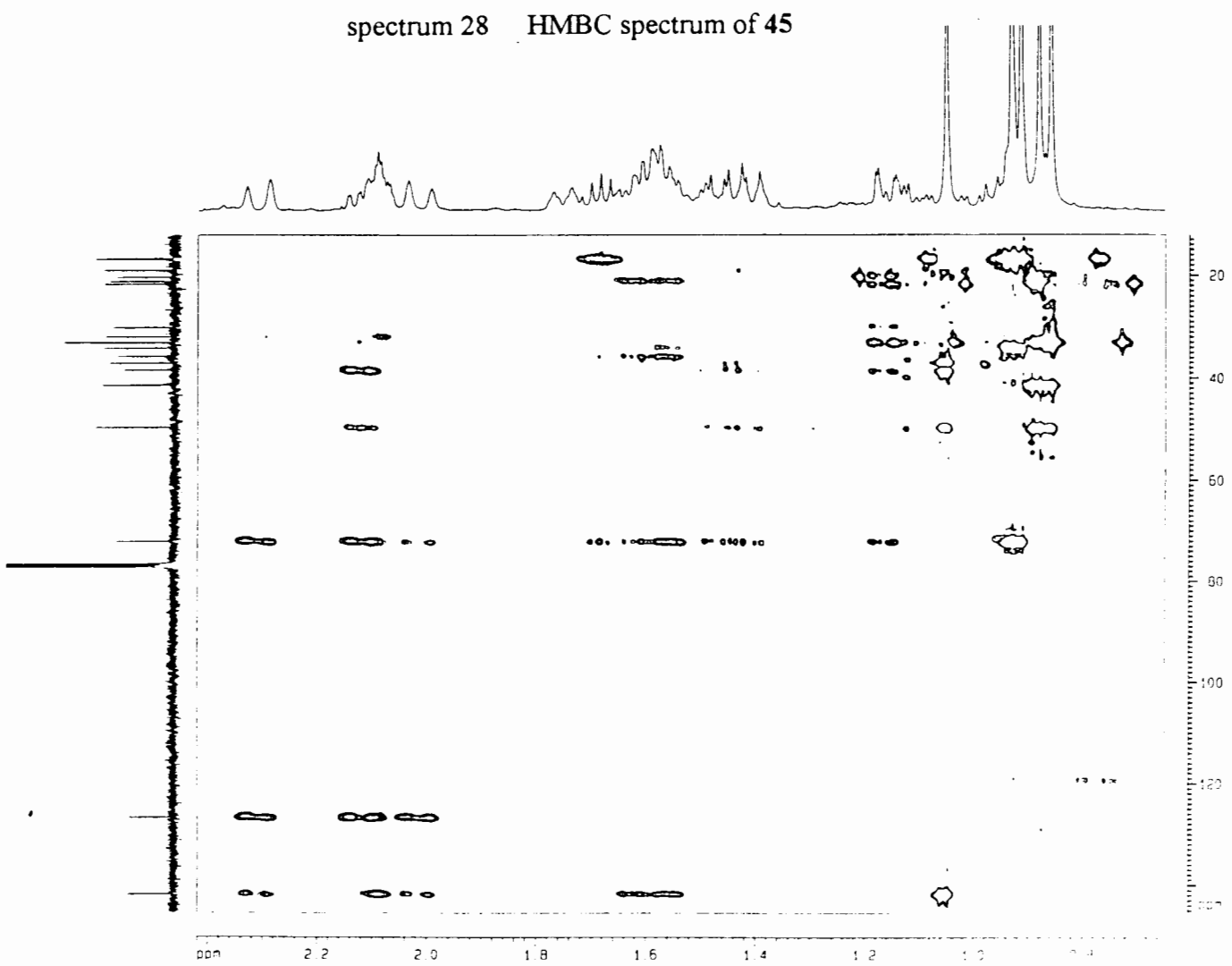

spectrum 29 ^{1}H NMR spectrum of **51**

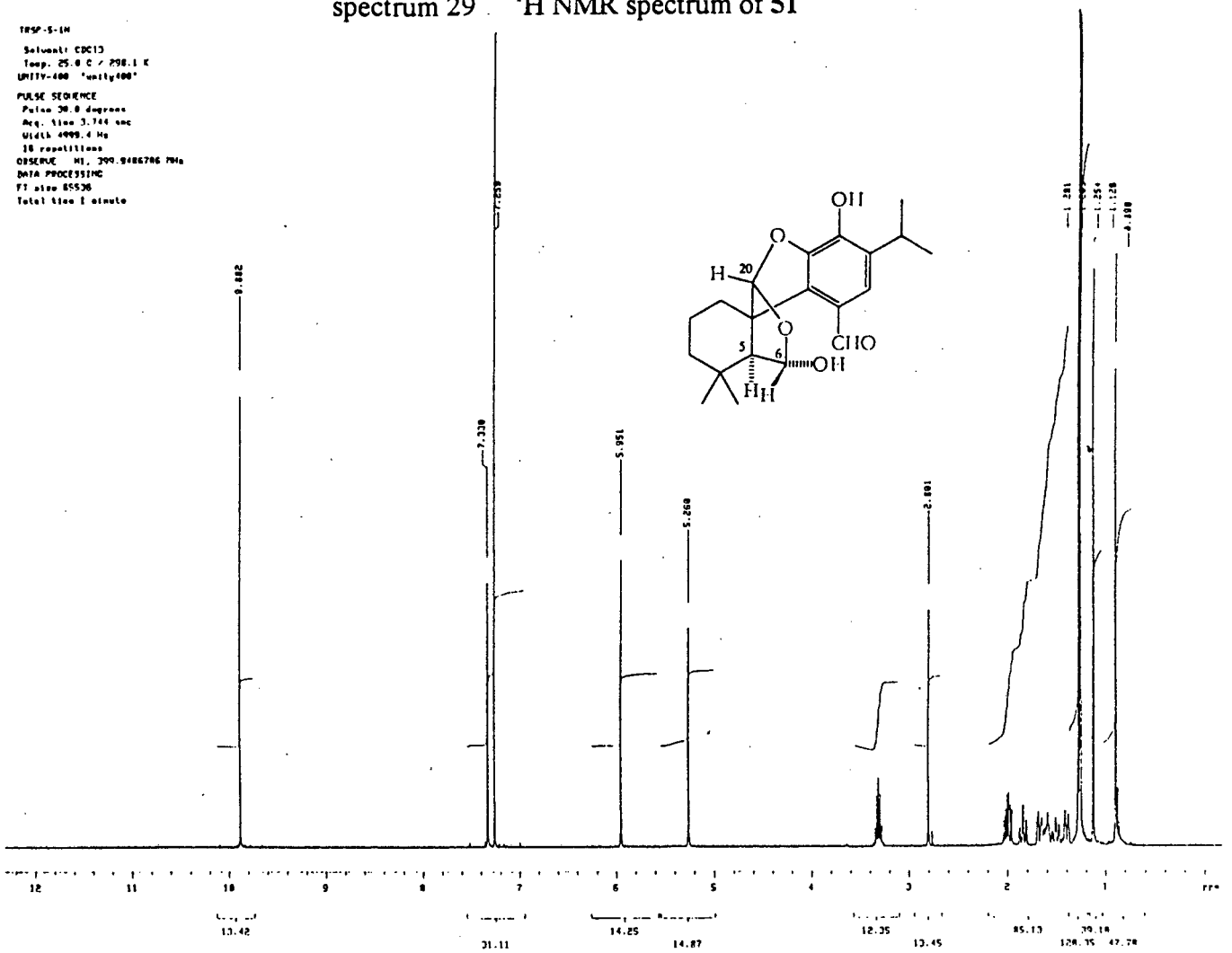

spectrum 30 ^{13}C NMR spectrum of **51**

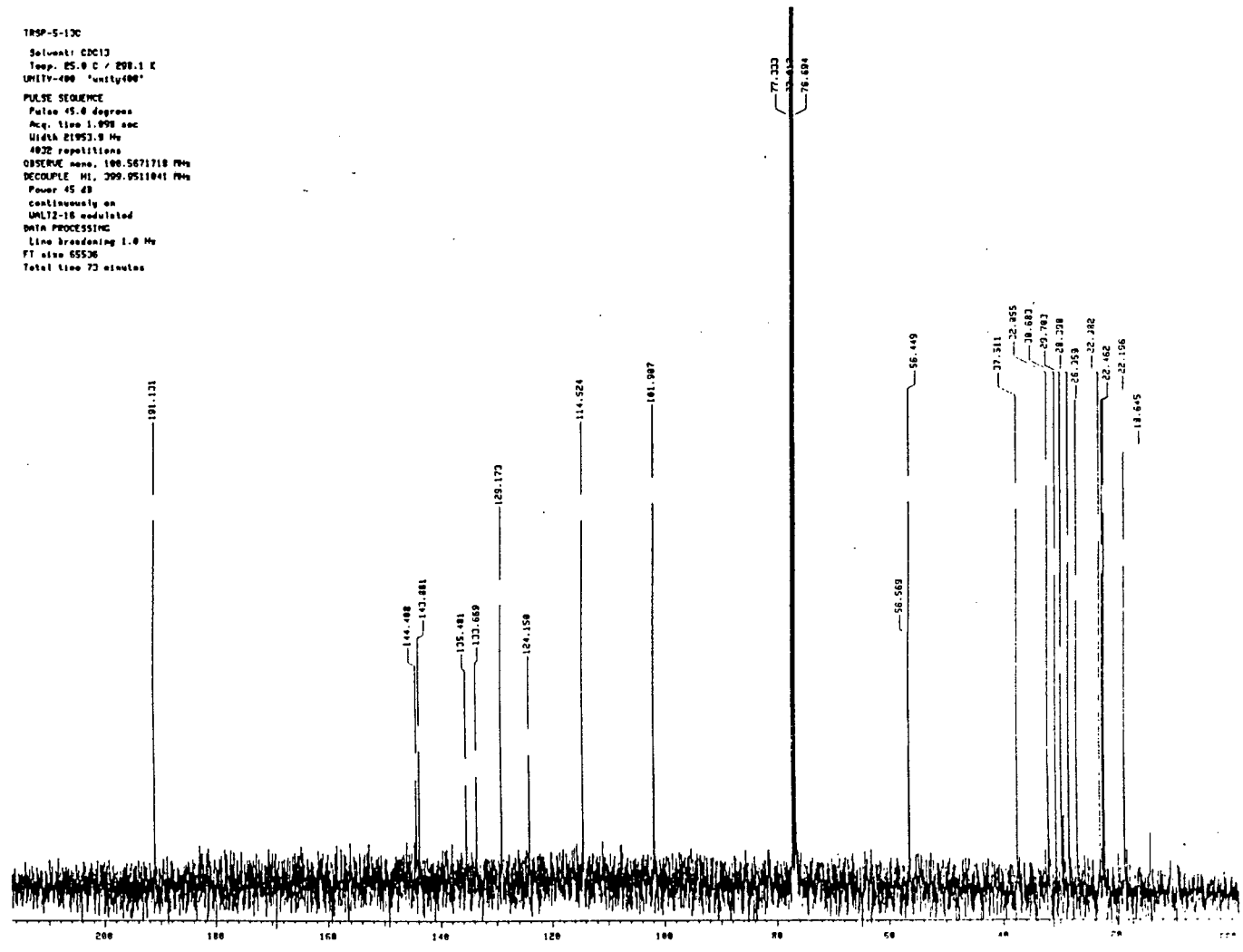

spectrum 31 DEPT spectrum of **51**

index	frequency	ppm	intensity
1 D	17423.6	191.331	19.120
2 D	12991.3	189.166	25.310
3 D	11518.6	114.524	12.060
4 T			4.575
5 D	10249.0	101.901	18.580
6 Q			4.575
7 D	5677.6	56.449	27.940
8 D	3772.7	37.511	28.130
9 T			21.081
10 D	3224.8	32.055	47.112
11 D	2987.5	29.703	16.720
12 T			11.965
13 D	2815.2	27.998	35.210
14 D	2711.2	26.964	13.580
15 D			
16 Q	2312.1	22.989	53.702
17 Q	2258.5	22.456	46.842
18 D	2232.4	22.196	47.305
19 D	1875.3	18.645	26.320
20 T			22.081

Number of protonated carbons: 20
CH : 10
CH2: 5
CH3: 5

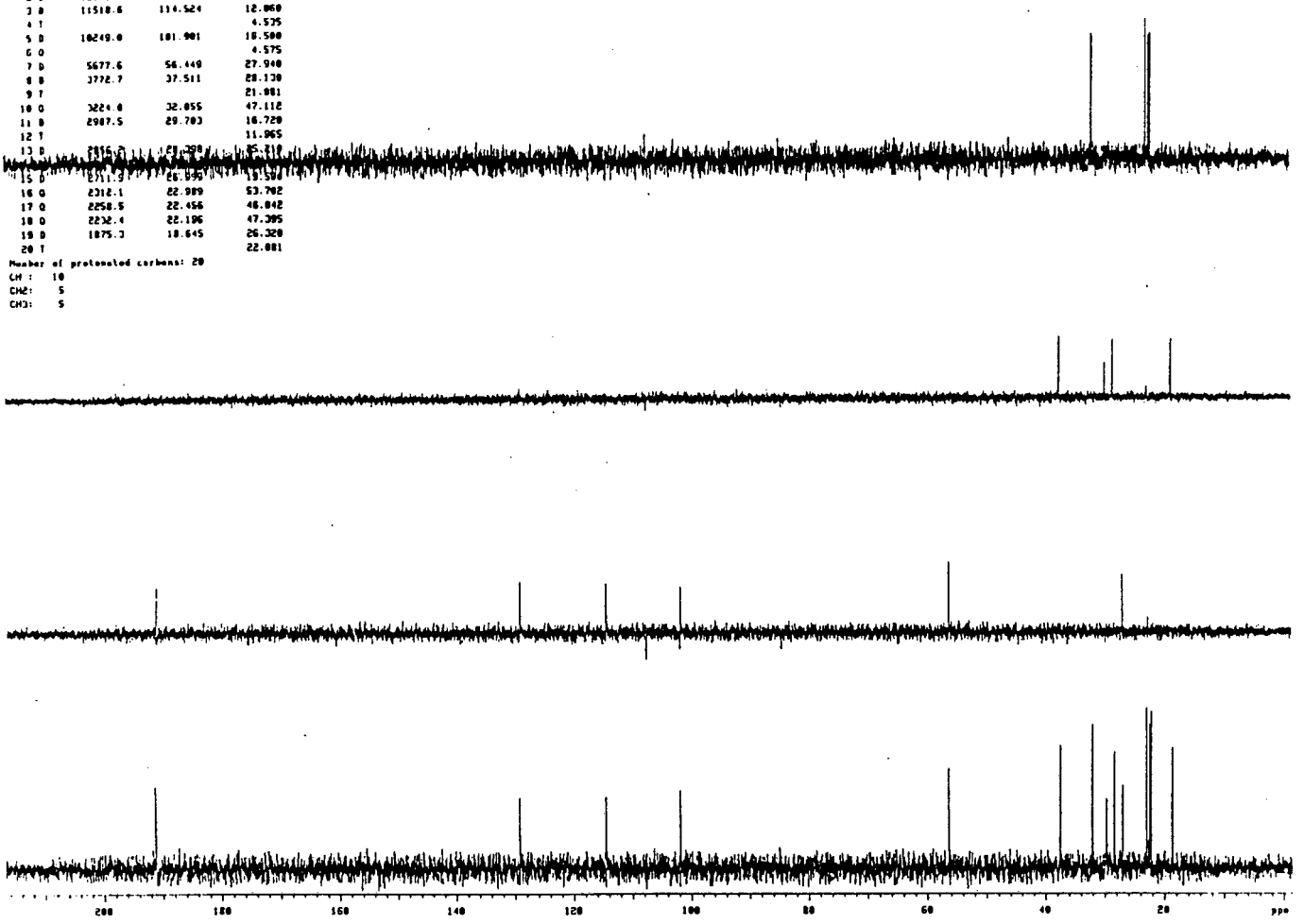

spectrum 32 COSY spectrum of **51**

TRSP-S-1H

Solvent: CDCl3
Temp. 25.0 C / 298.1 K
UNITY-400 'unity400'

PULSE SEQUENCE: relayh
Relax. delay 1.000 sec
COSY 90-45
Acq. time 0.247 sec
Width 4140.8 Hz
2D Width 4140.8 Hz
32 repetitions
320 increments
OBSERVE H1, 399.9486788 MHz
DATA PROCESSING
Line broadening 1.4 Hz
Gauss window 0.102 sec
center at 0.226 sec
Sine bell 0.203 sec
Shifted by -0.012 sec
F1 DATA PROCESSING
Line broadening 1.4 Hz
Gauss window 0.229 sec
center at 0.242 sec
Sine bell 0.119 sec
Shifted by -0.001 sec
FT size 2048 x 2048
Total time 3.7 hours

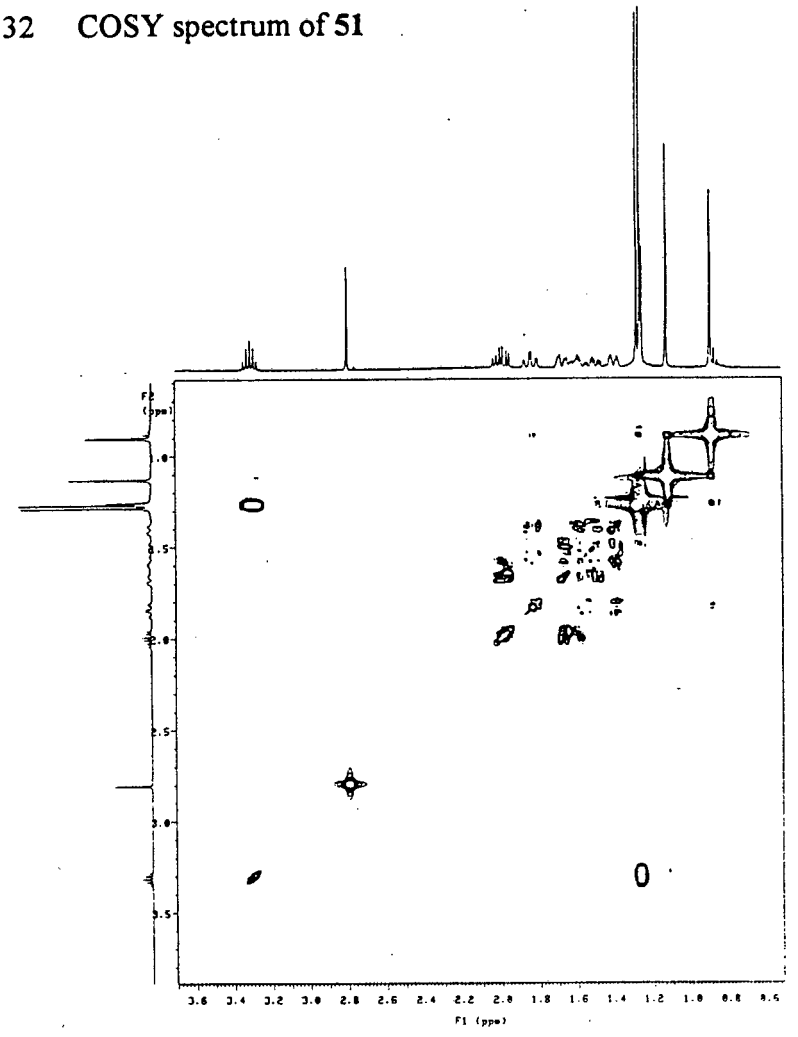

spectrum 33 HMQC spectrum of **51**

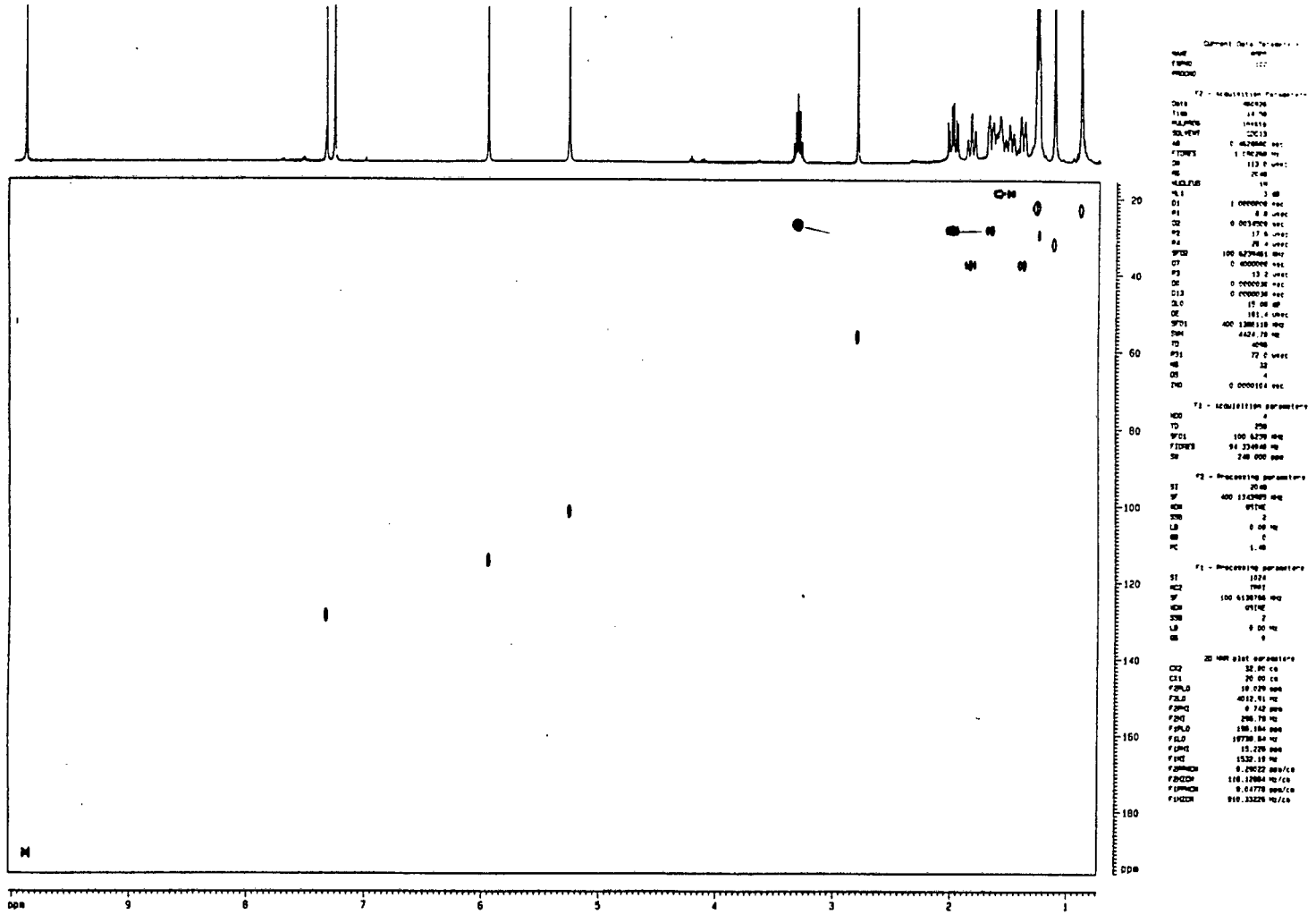

spectrum 34 HMBC spectrum of **51**

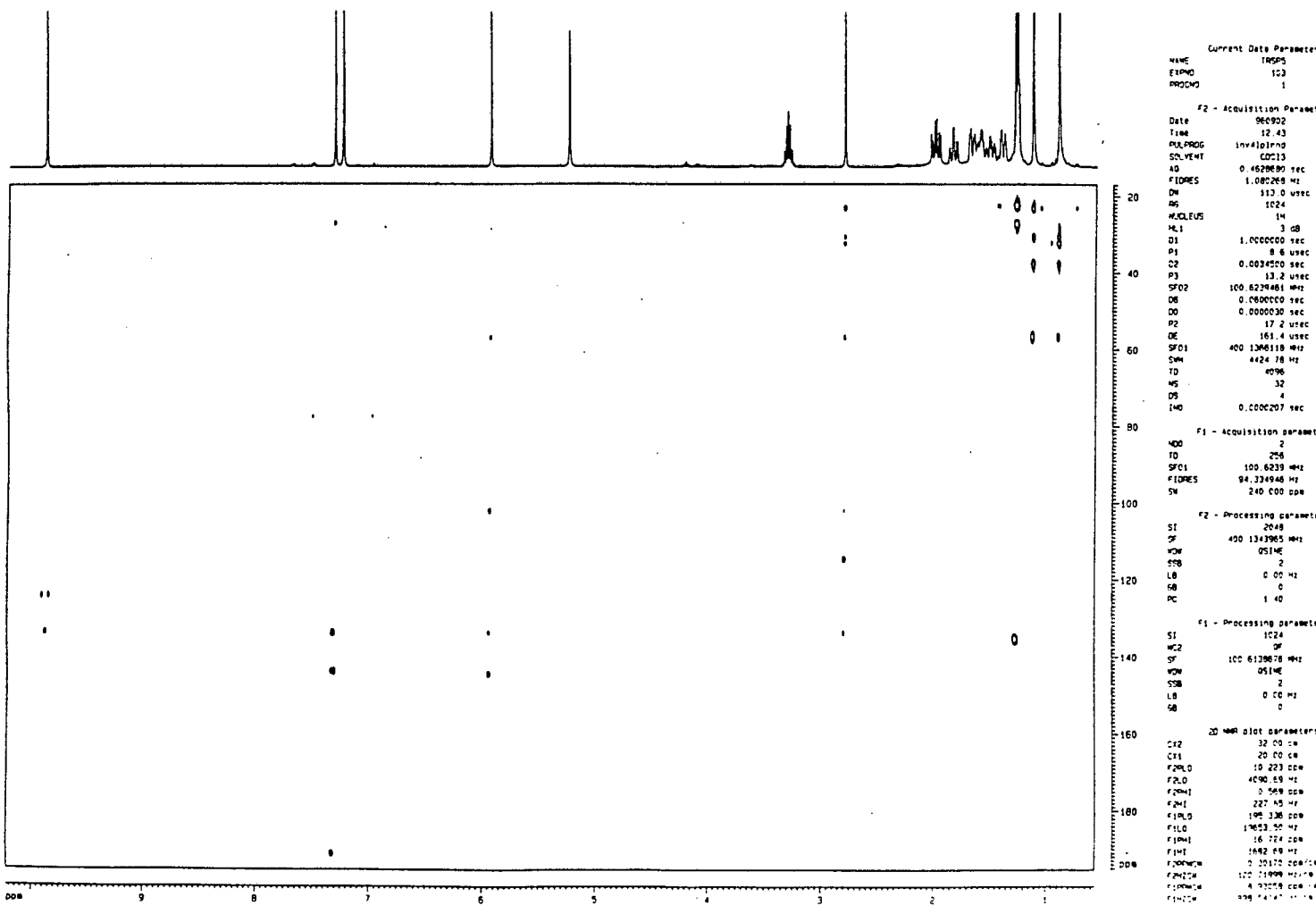

spectrum 35 ^{1}H NMR spectrum of **61**

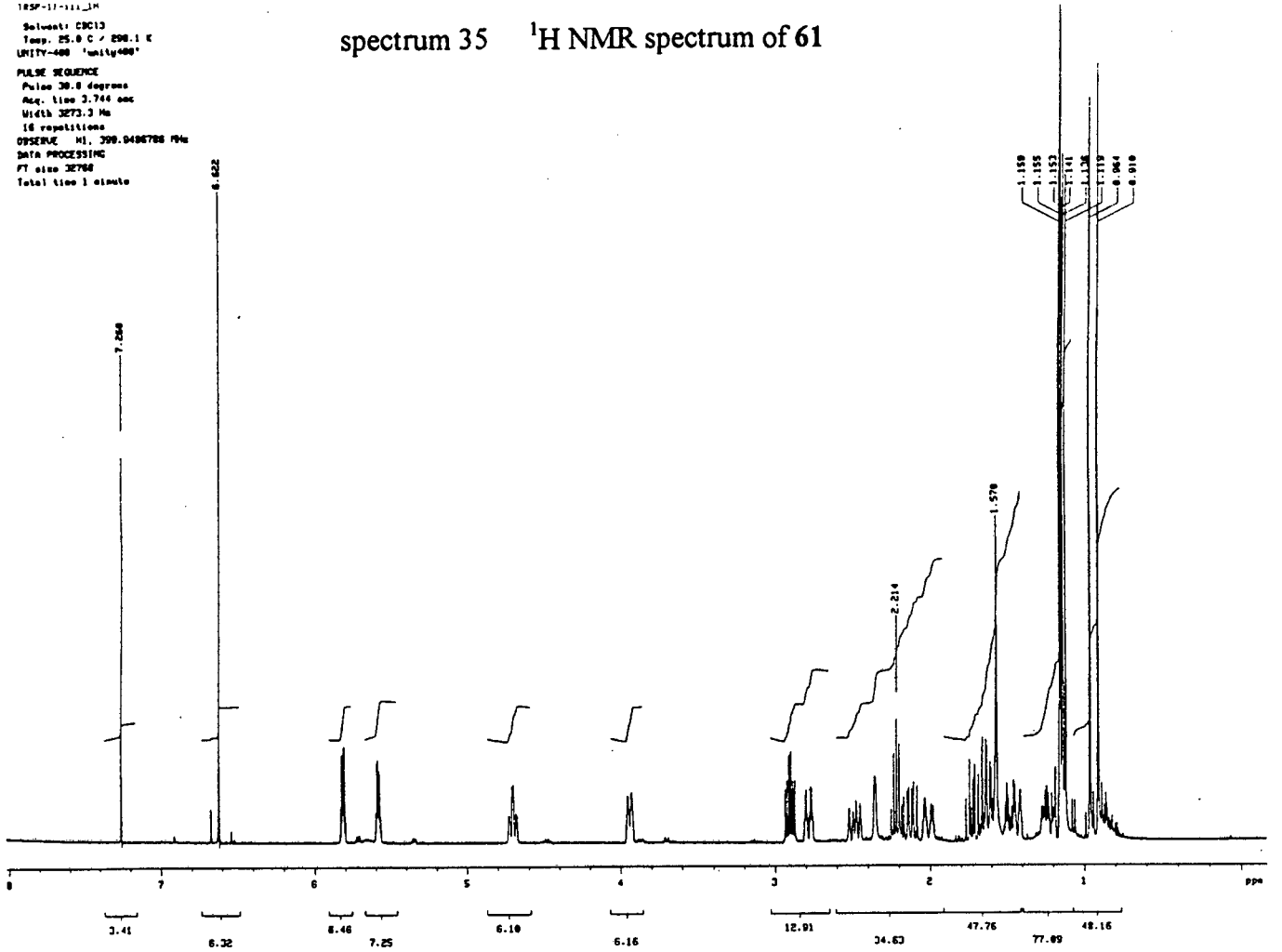

spectrum 36 D_2O wash ^{1}H NMR spectrum of **61**

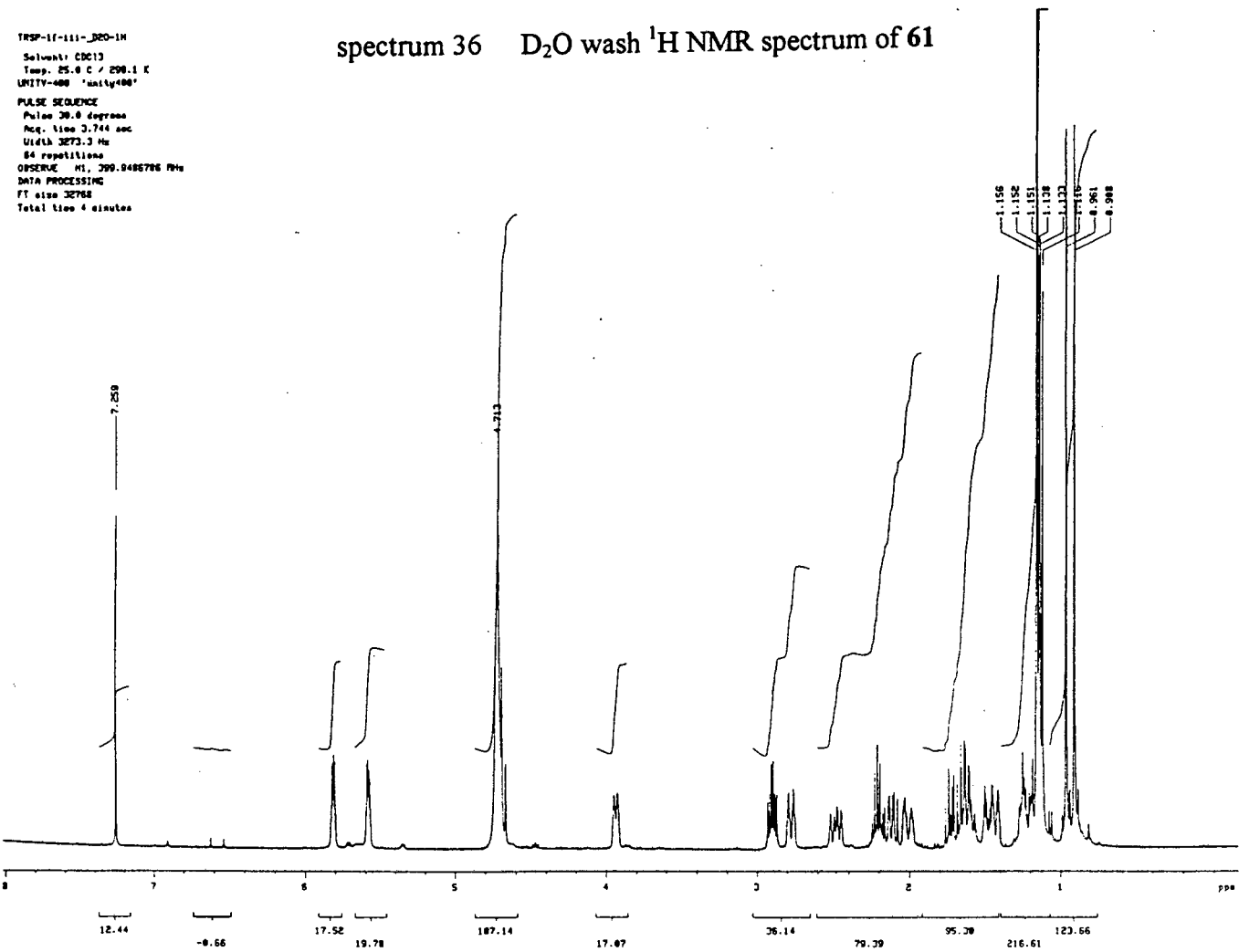

spectrum 37 ^{13}C NMR spectrum of **61**

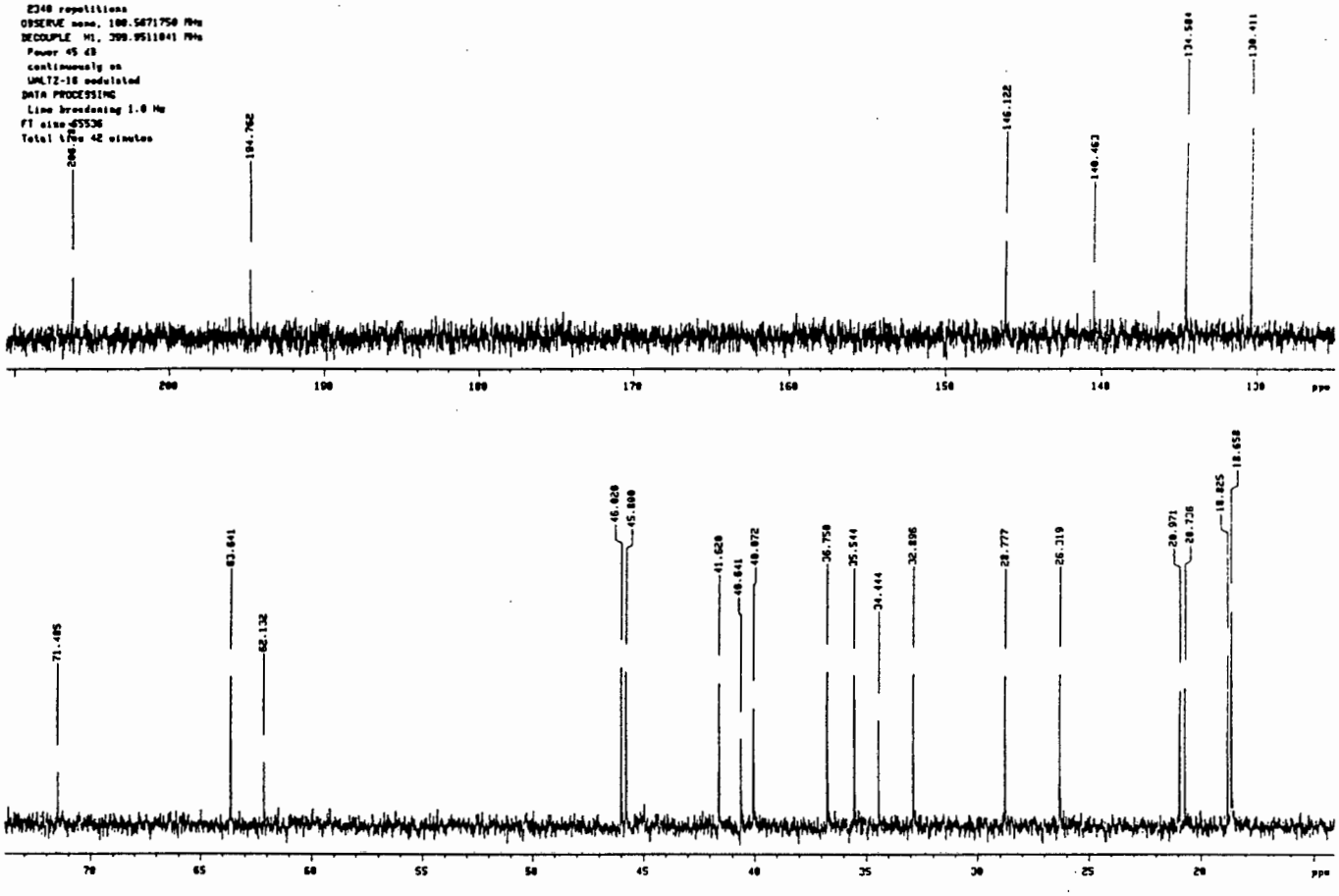

spectrum 38 COSY spectrum of **61**

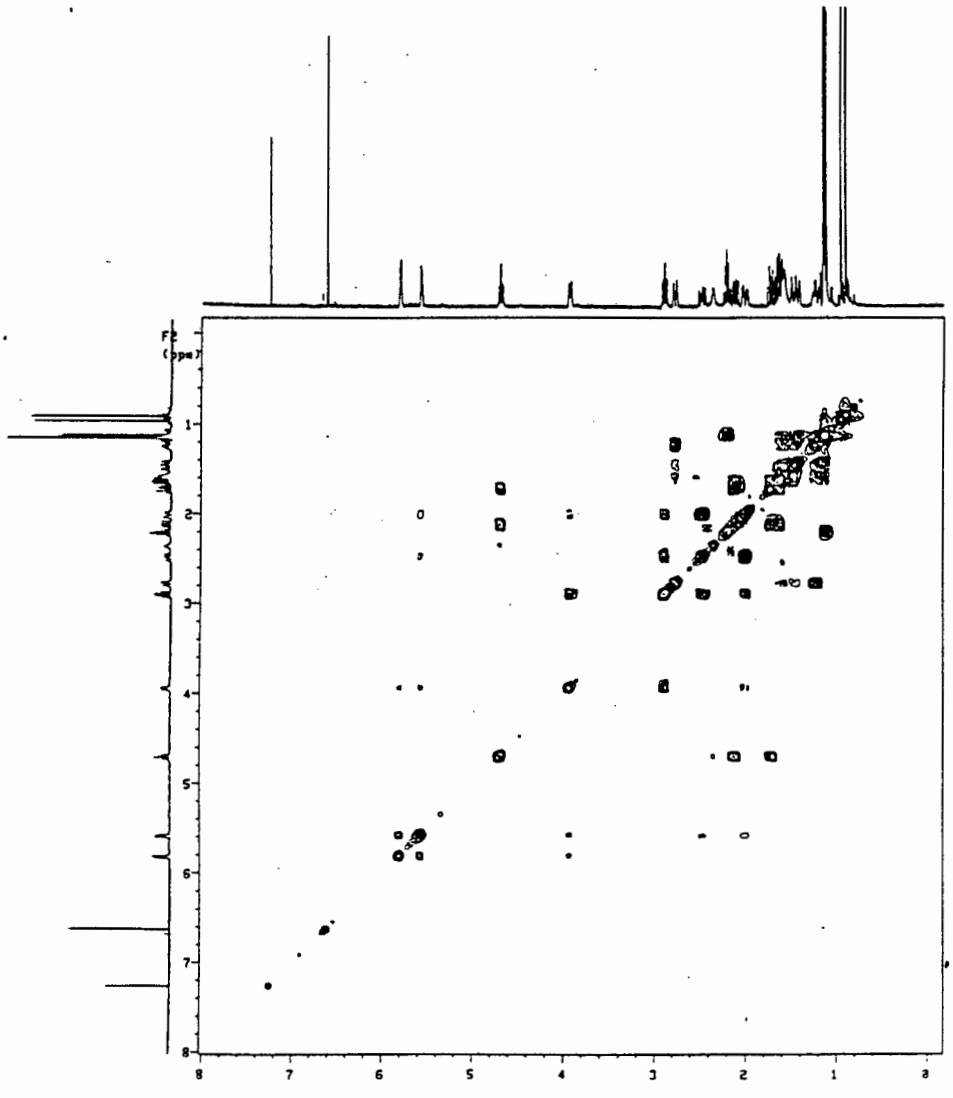

spectrum 39 HMQC spectrum of **61**

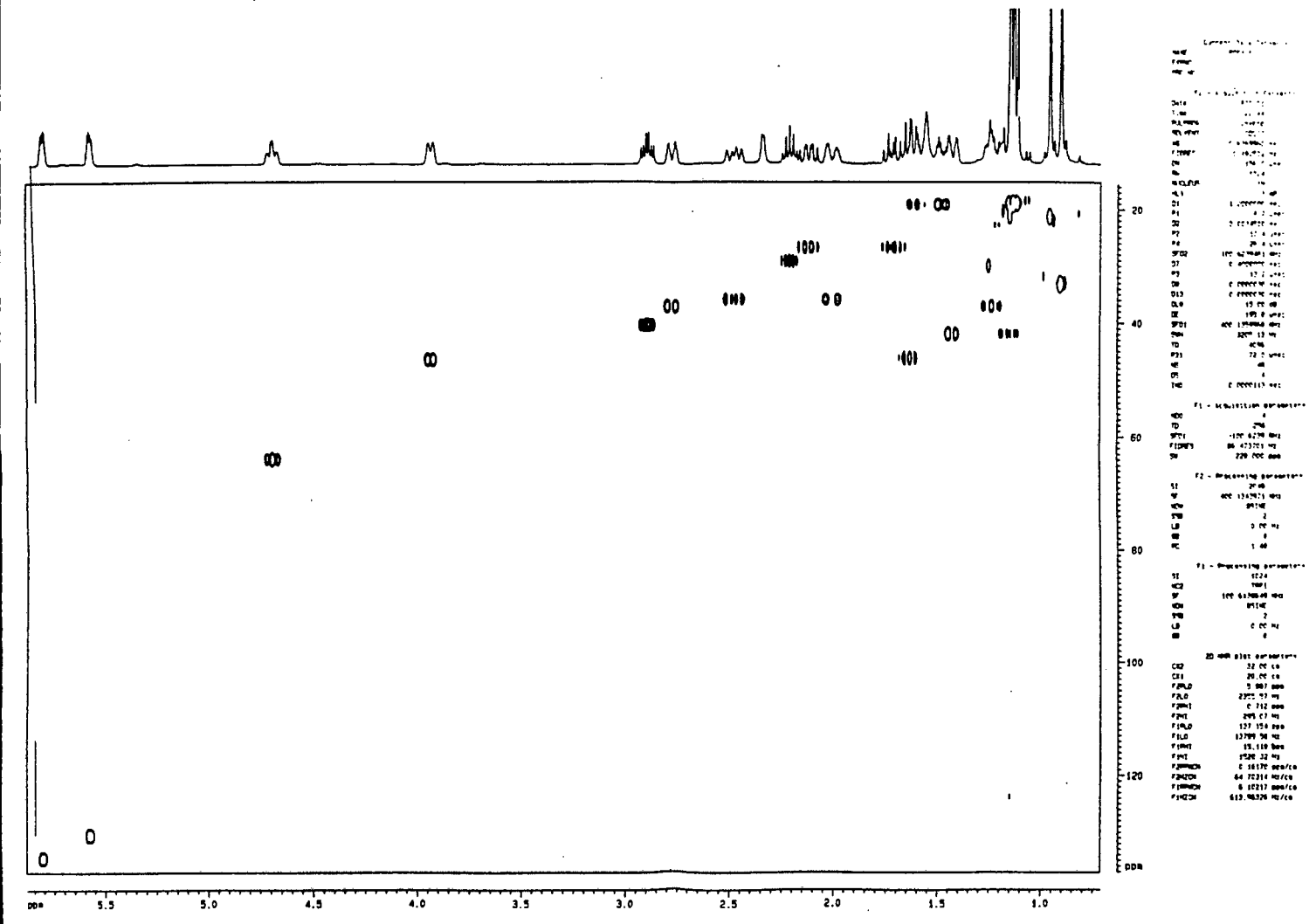

spectrum 40 HMBC spectrum of **61**

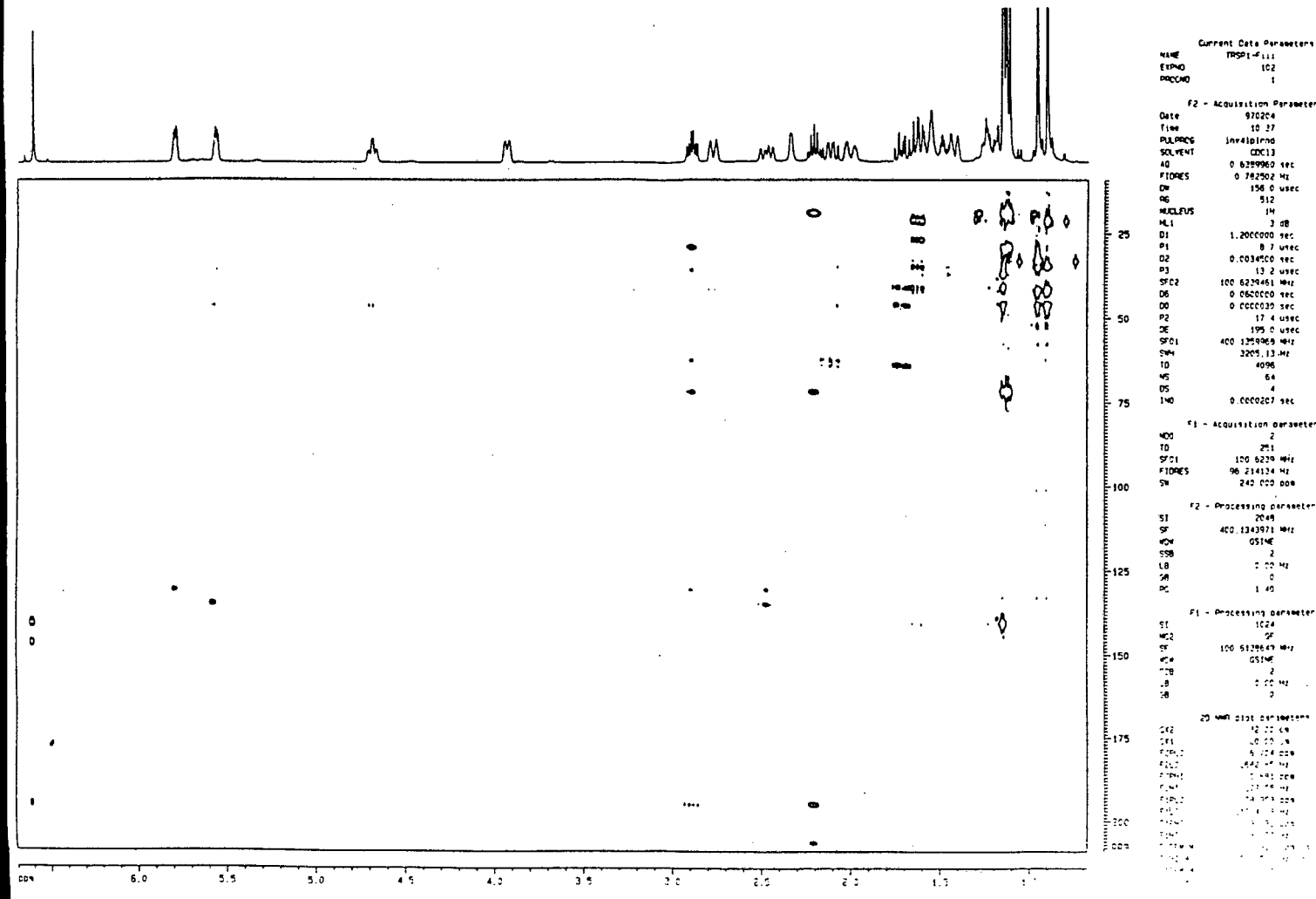

spectrum 41 NOESY spectrum of 61

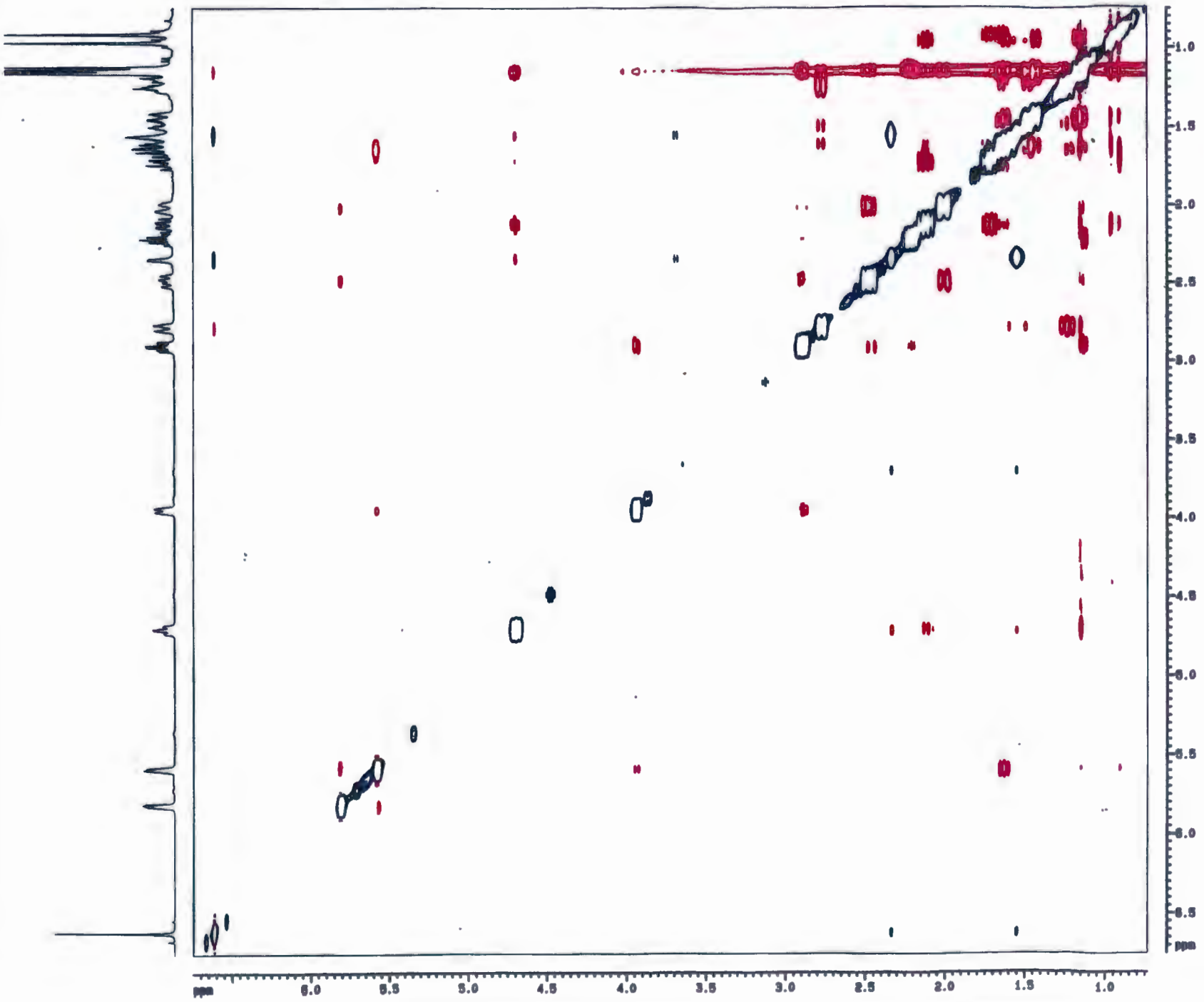

Current Data Parameters

NAME	TRSP1-F111
EXPNO	103
PROCNO	1

F2 - Acquisition Parameters

Date	970311
Time	10.53
PULPROG	noesytp
SOLVENT	CDCl3
AQ	0.2826440 sec
FIDRES	1.769135 Hz
DW	138.0 usec
RG	256
NUCLEUS	1H
HL1	1 dB
D1	1.5000000 sec
P1	13.4 usec
D0	0.0000030 sec
D8	0.8000000 sec
DE	197.1 usec
SFO1	400.1360000 MHz
SWH	3623.19 Hz
TD	2048
NS	32
DS	4
INO	0.0001380 sec

F1 - Acquisition parameters

NDO	2
TD	256
SFO1	400.136 MHz
FIDRES	14.153091 Hz
SW	9.055 ppm

F2 - Processing parameters

SI	2048
SF	400.1343970 MHz
WDW	QSINE
SSB	2
LB	0.00 Hz
GB	0
PC	1.00

F1 - Processing parameters

SI	1024
MC2	TPPI
SF	400.1343961 MHz
WDW	QSINE
SSB	2
LB	0.00 Hz
GB	0

2D NMR plot parameters

CX2	25.00 cm
CX1	25.00 cm
F2PLO	6.747 ppm
F2LO	2699.85 Hz
F2PHI	0.734 ppm
F2HI	293.83 Hz
F1PLO	6.750 ppm
F1LO	2700.75 Hz
F1PHI	0.737 ppm
F1HI	294.72 Hz
F2PPMCM	0.24052 ppm/cm
F2HZCM	96.24094 Hz/cm
F1PPMCM	0.24052 ppm/cm
	96.24103 Hz/cm

spectrum 42 ^{1}H NMR spectrum of **62**

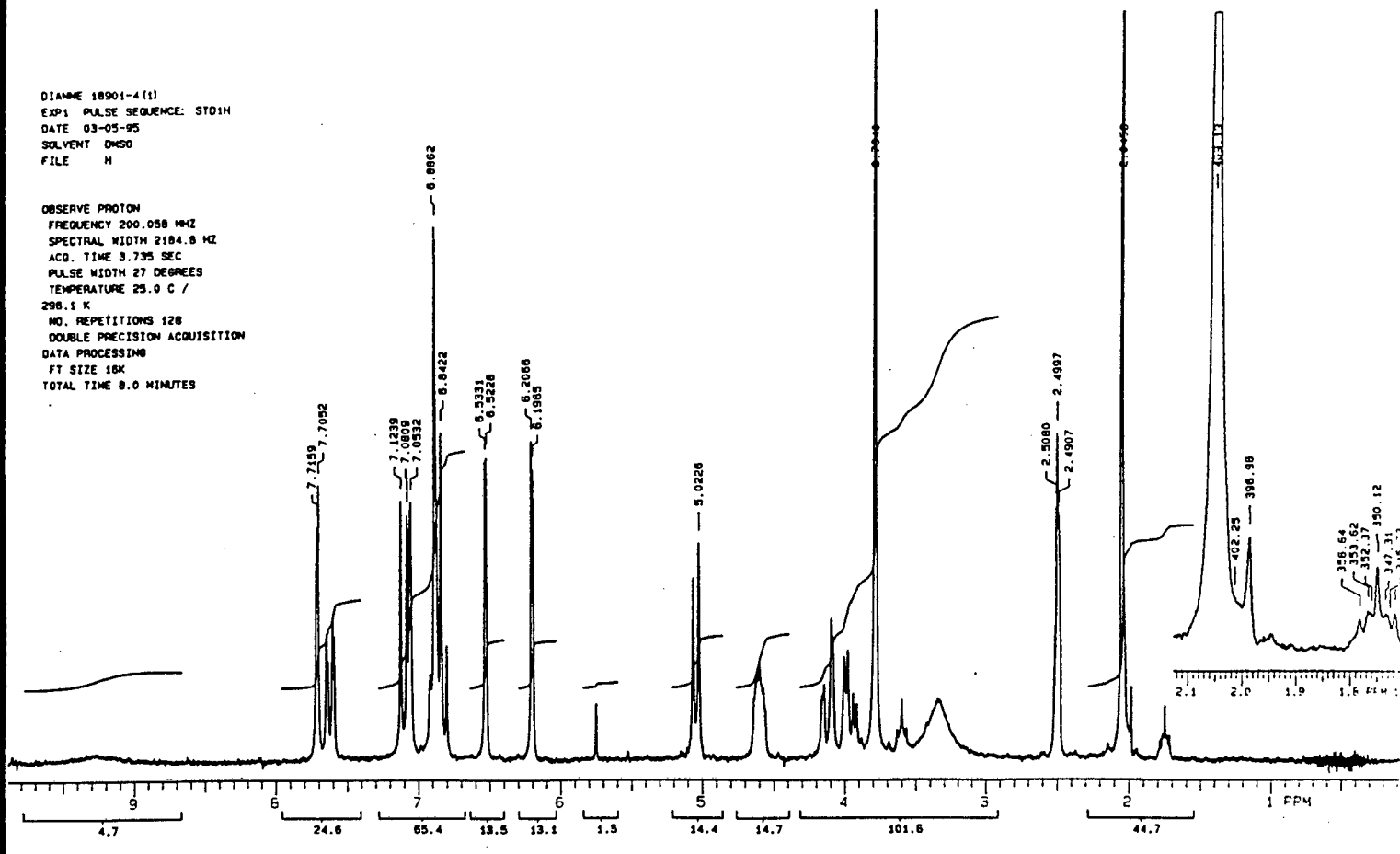

spectrum 43 ^{13}C NMR spectrum of **62**

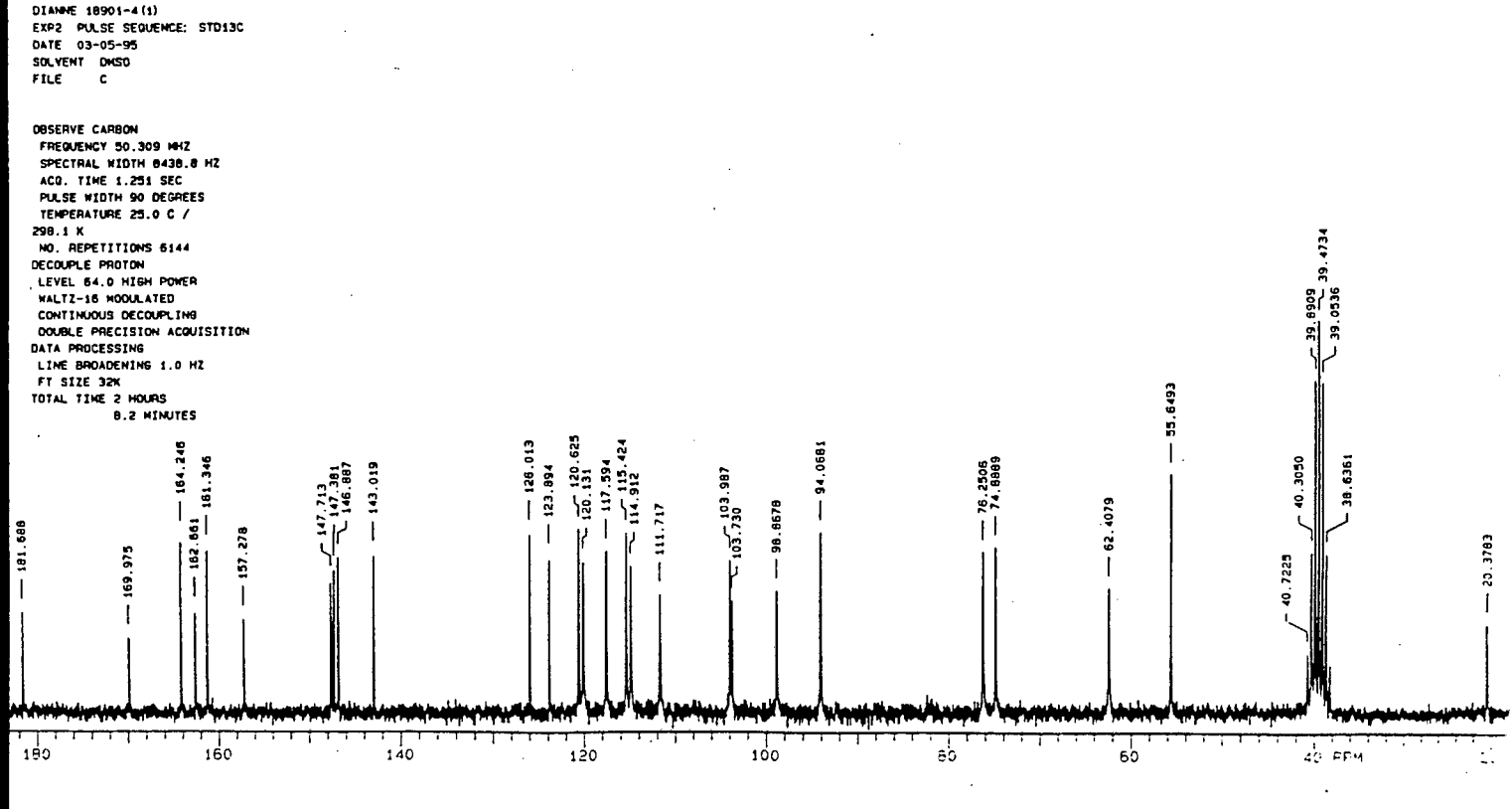

spectrum 44 DEPT spectrum of **62**

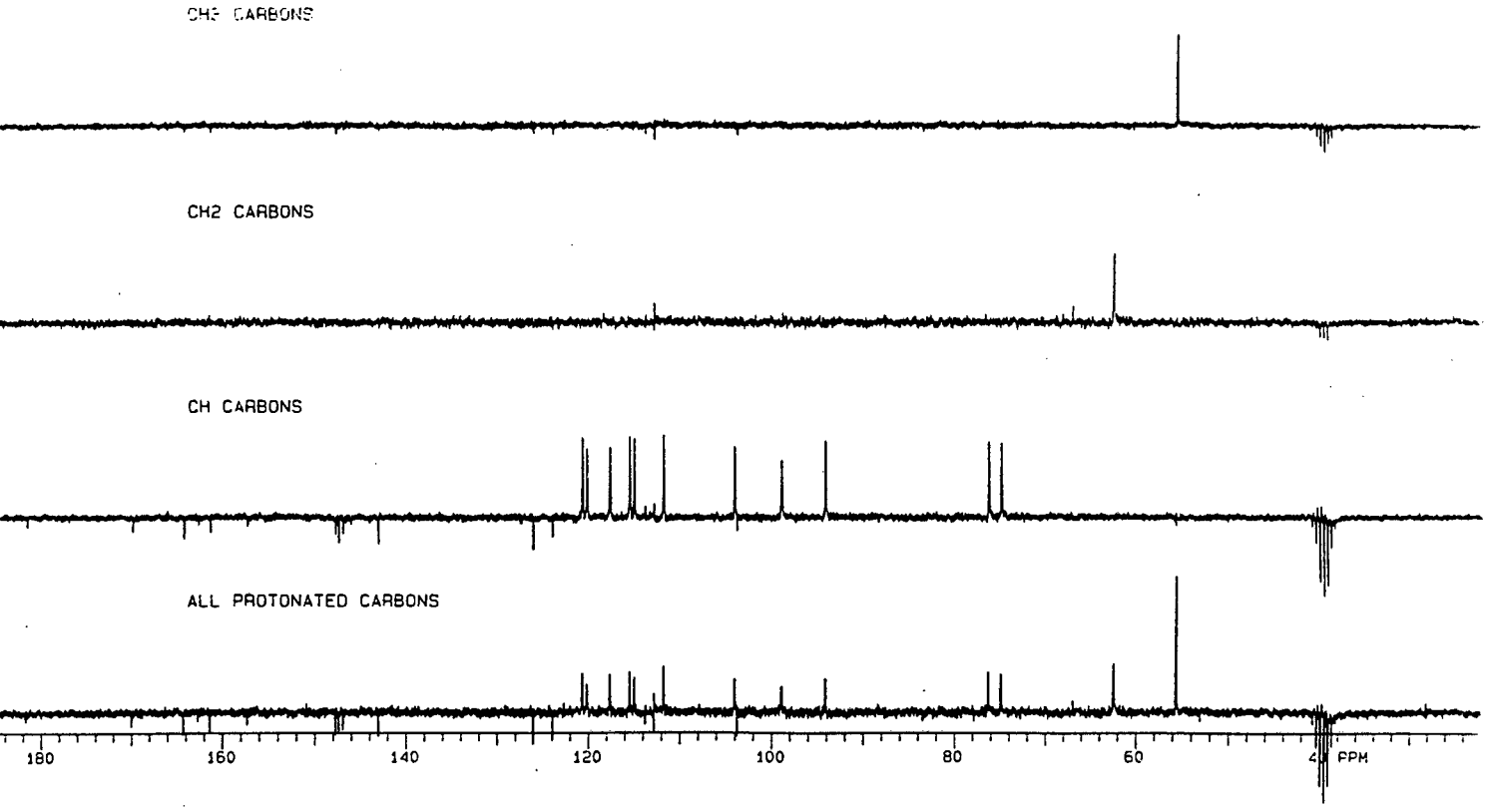

13.250	50	1.250	-381.1	32	---	---	DEPT	
8438.8	300	NNY	2	1.000	---	---	DIANNE 18901-4(1)	
1.251	2.000	CCS	9900	8438.3	854.0	25.0		03-05
13.0	2825	14.1	58.0			DMSO		VXR

spectrum 45 COSY spectrum of **62**

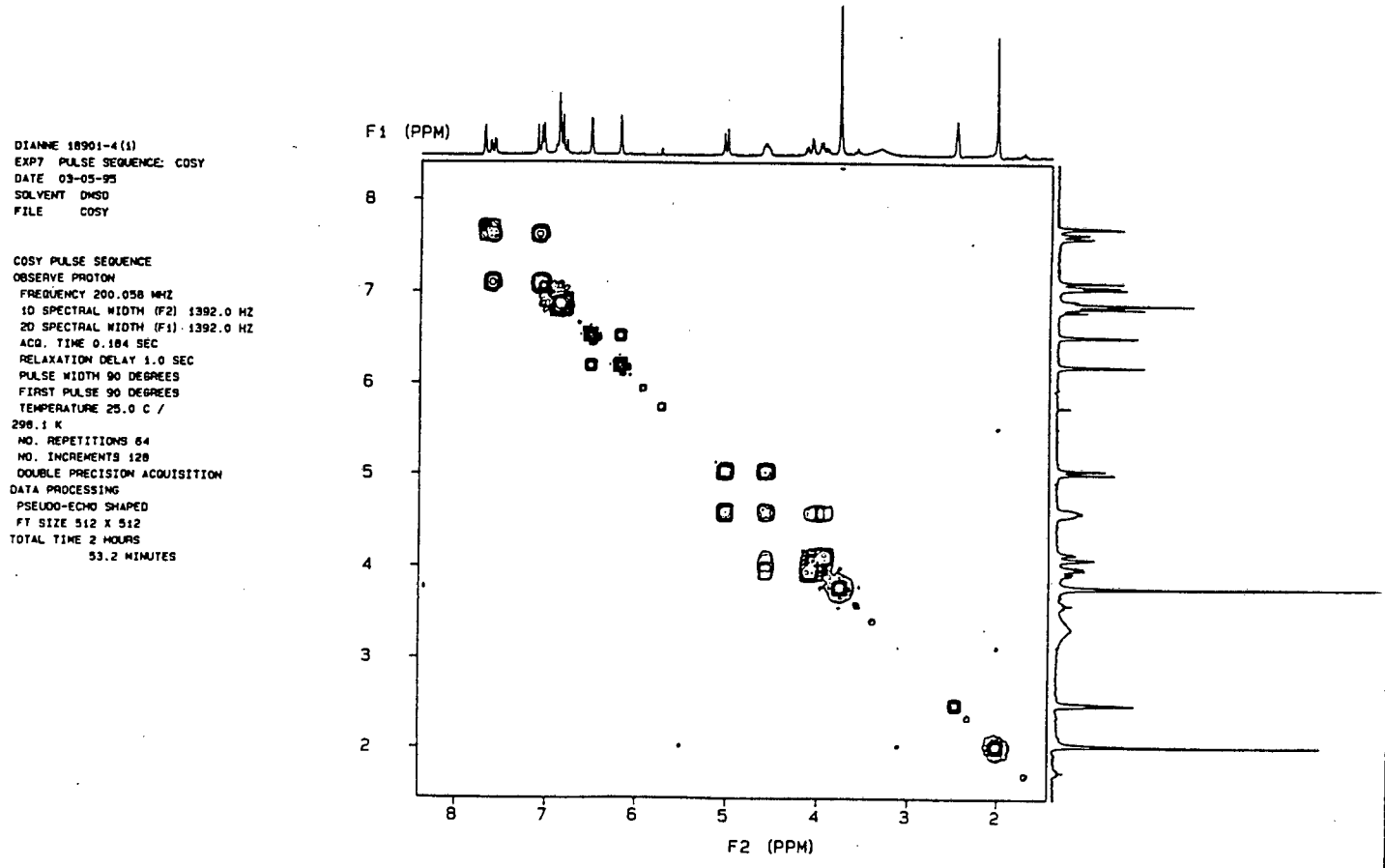

spectrum 46 HETCOR spectrum of **62**

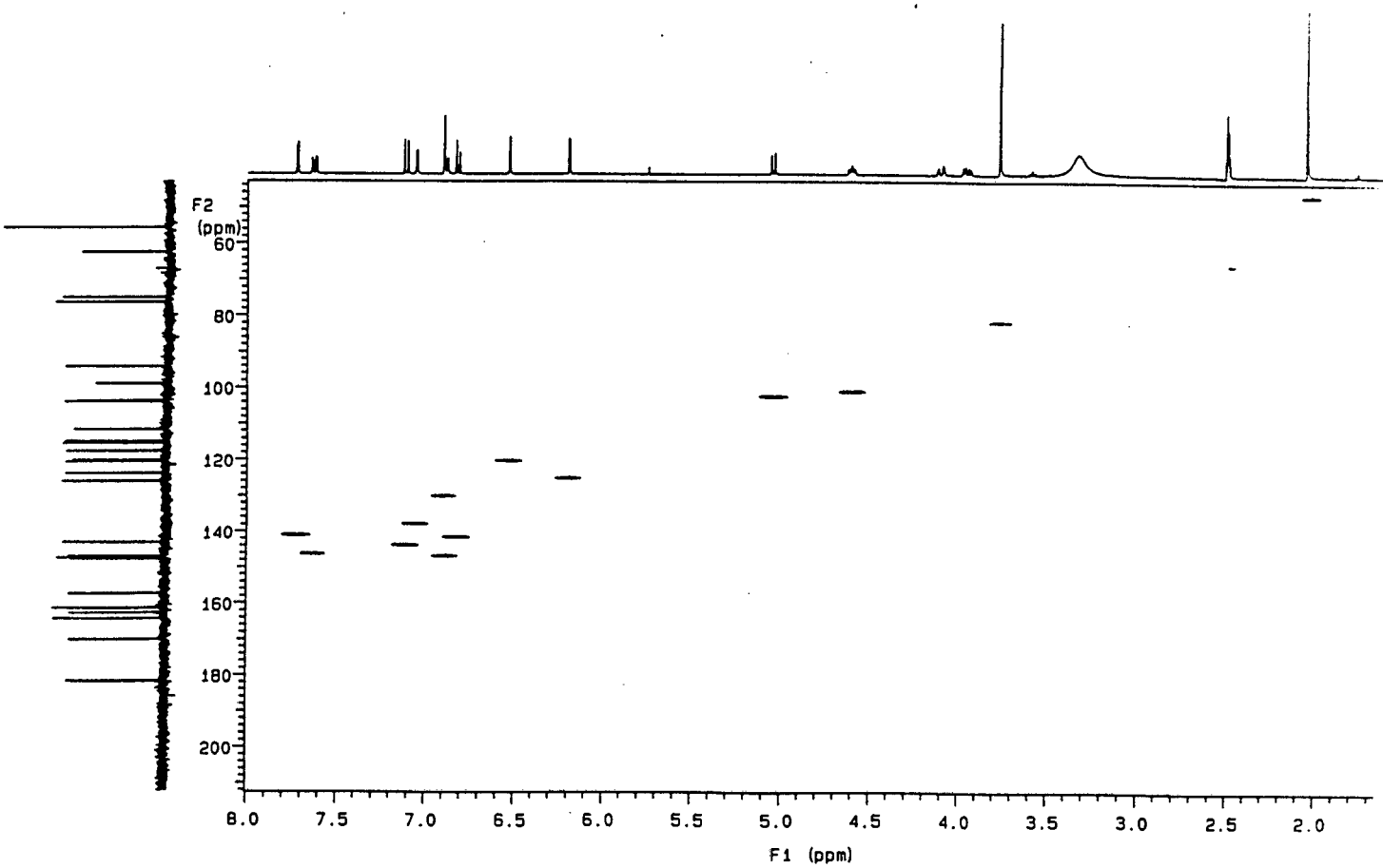

spectrum 47 HMBC spectrum of **62**

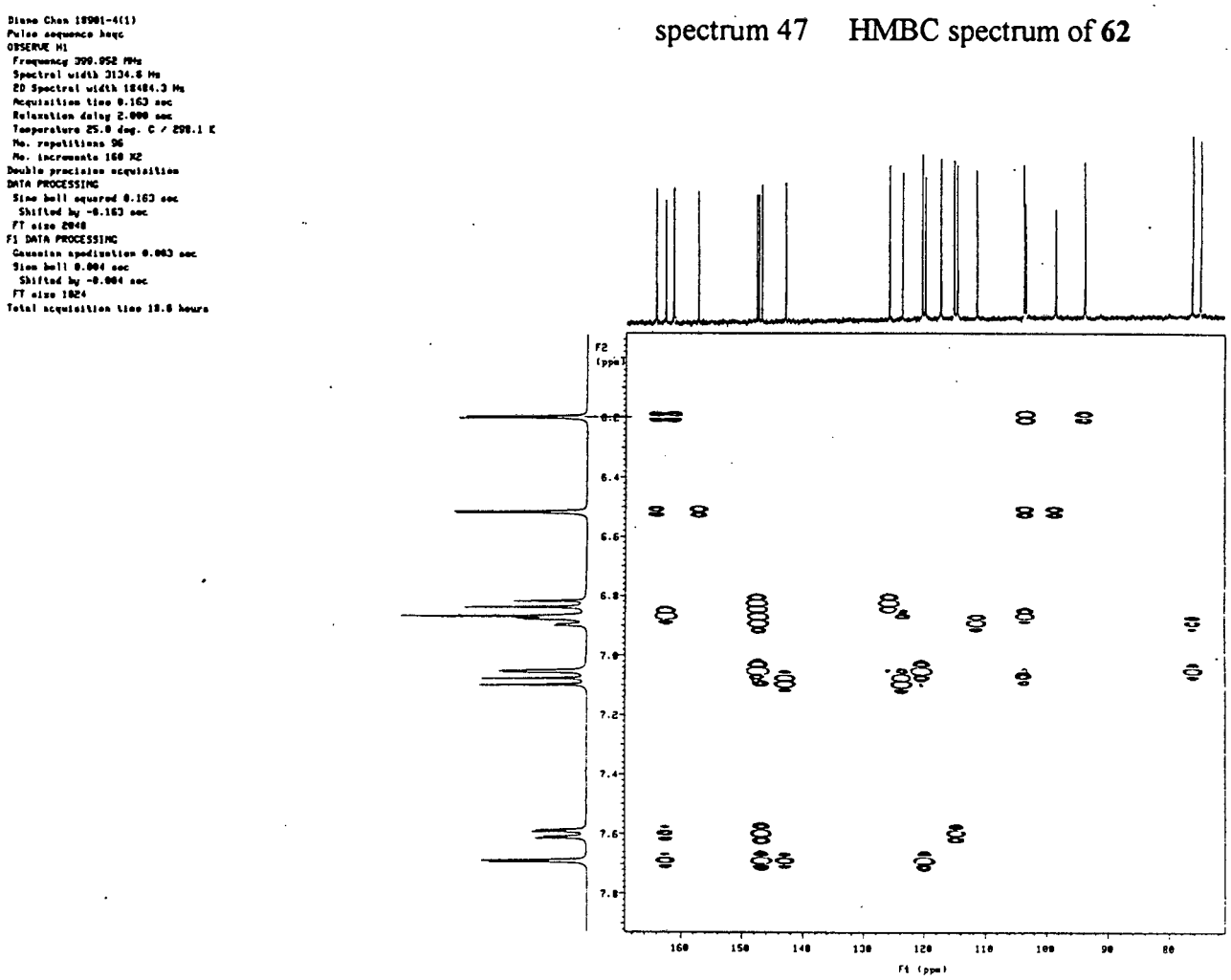

spectrum 48 ^{1}H NMR spectrum of **63**

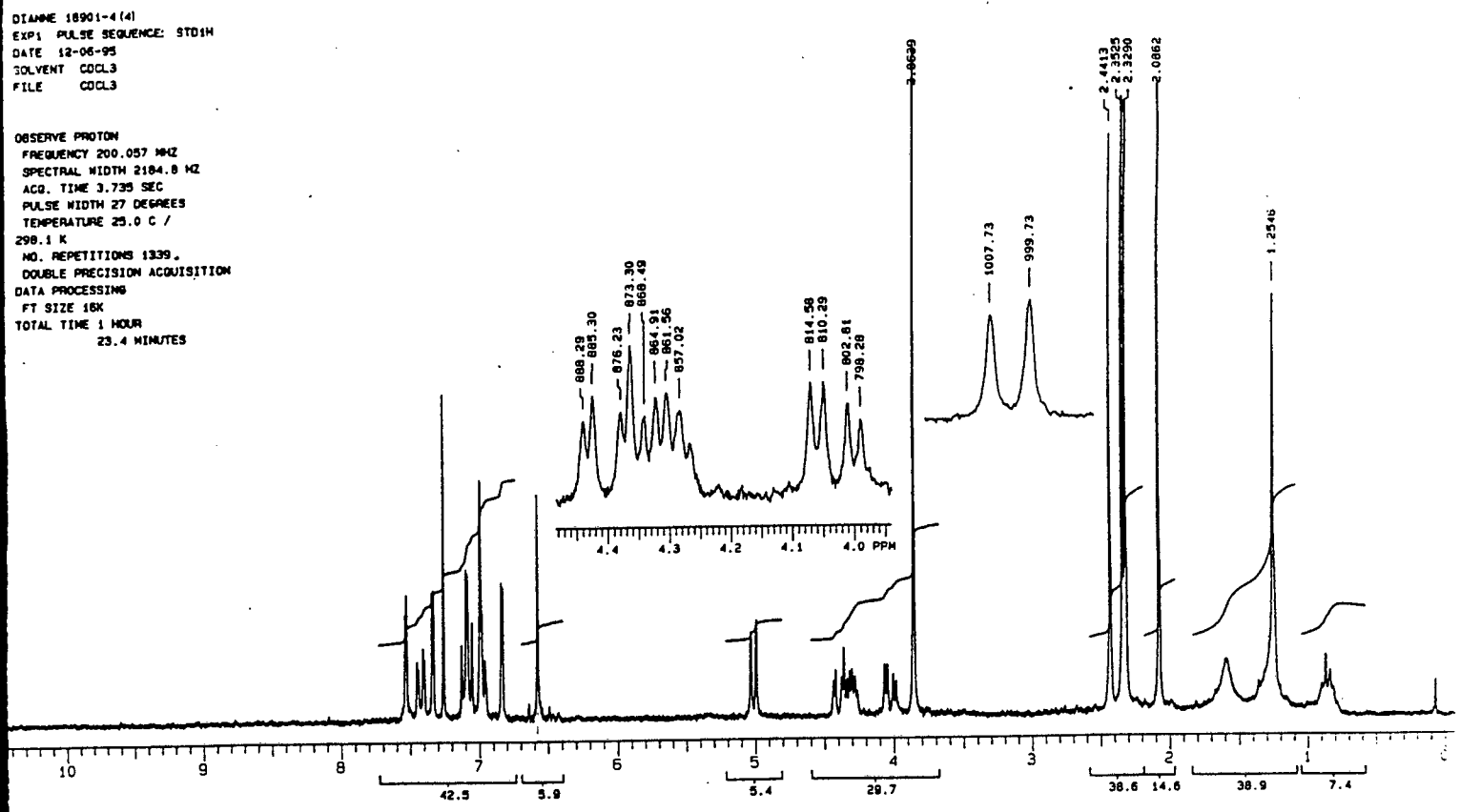

spectrum 49 ^{13}C NMR spectrum of **64**